AD_____

Award Number: W81XWH-12-1-0041

TITLE: Understanding and Targeting Epigenetic Alterations in Acquired Bone Marrow Failure

PRINCIPAL INVESTIGATOR: Omar Abdel-Wahab

CONTRACTING ORGANIZATION: Memorial Sloan-Kettering Cancer Center
New York, NY 10065

REPORT DATE: May 2013

TYPE OF REPORT: Annual Summary

PREPARED FOR: U.S. Army Medical Research and Materiel Command
                         Fort Detrick, Maryland 21702-5012

REPORT DOCUMENTATION PAGE

Form Approved
OMB No. 0704-0188

Public reporting burden for this collection of information is estimated to average 1 hour per response, including the time for reviewing instructions, searching existing data sources, gathering and maintaining the data needed, and completing and reviewing this collection of information. Send comments regarding this burden estimate or any other aspect of this collection of information, including suggestions for reducing this burden to Department of Defense, Washington Headquarters Services, Directorate for Information Operations and Reports (0704-0188), 1215 Jefferson Davis Highway, Suite 1204, Arlington, VA 22202-4302. Respondents should be aware that notwithstanding any other provision of law, no person shall be subject to any penalty for failing to comply with a collection of information if it does not display a currently valid OMB control number. **PLEASE DO NOT RETURN YOUR FORM TO THE ABOVE ADDRESS.**

1. REPORT DATE	2. REPORT TYPE	3. DATES COVERED
May 2013	Annual Summary	1 May 2012 – 30 April 2013

4. TITLE AND SUBTITLE

Understanding and Targeting Epigenetic Alterations in Acquired Bone Marrow Failure

5a. CONTRACT NUMBER
W81XWH-12-1-0041

5b. GRANT NUMBER
K , %LK < !%&!%$$(%

5c. PROGRAM ELEMENT NUMBER

6. AUTHOR(S)

Omar Abdel-Wahab

E-Mail: abdelwao@mskcc.org

5d. PROJECT NUMBER

5e. TASK NUMBER

5f. WORK UNIT NUMBER

7. PERFORMING ORGANIZATION NAME(S) AND ADDRESS(ES)

Memorial Sloan-Kettering Cancer Center,
1275 York Ave,
New York, NY 10065

8. PERFORMING ORGANIZATION REPORT NUMBER

9. SPONSORING / MONITORING AGENCY NAME(S) AND ADDRESS(ES)

U.S. Army Medical Research and Materiel Command
Fort Detrick, Maryland 21702-5012

10. SPONSOR/MONITOR'S ACRONYM(S)

11. SPONSOR/MONITOR'S REPORT NUMBER(S)

12. DISTRIBUTION / AVAILABILITY STATEMENT

Approved for Public Release; Distribution Unlimited

13. SUPPLEMENTARY NOTES

14. ABSTRACT

Systematic genomic discovery efforts in patients with bone marrow failure due to myelodysplastic syndrome (MDS) has led to the rapid discovery of recurrent somatic genetic alterations underlying these disorders. Remarkably, a large number of these mutations occur in genes whose function is known, or suspected, to be involved in epigenetic regulation of gene transcription. This includes mutations in *ASXL1, TET2,* and *EZH2.* The goals of our proposal were to (1) perform functional genetic characterization of these alterations, (2) determine if these alterations are therapeutically targetable, and (3) perform detailed genomic analysis of specific subsets of MDS patients with no known genetic alterations and with severe bone marrow failure to discover additional genetic alterations contributing to MDS pathogenesis. Since funding of this award we have made major progress in (1) understanding the impact of *ASXL1* mutations and loss on chromatin (Abdel-Wahab, *et al. Cancer Cell* 2012), (2) identifying the *in vivo* biological effects of deletion of *Asxl1* and *Tet2* alone and in combination with one another (Abdel-Wahab, *et al. J Exp Med* 2013 (in press)), and (3) identified the genome-wide effects of Asxl1 on transcription (Abdel-Wahab, *et al. J Exp Med* 2013 (in press) and *Abdel-Wahab, O,* et al. *Leukemia* 2013).

15. SUBJECT TERMS

ASXL1; Bone marrow failure; Myelodysplastic Syndrome; TET2

16. SECURITY CLASSIFICATION OF:			17. LIMITATION OF ABSTRACT	18. NUMBER OF PAGES	19a. NAME OF RESPONSIBLE PERSON USAMRMC
a. REPORT	**b. ABSTRACT**	**c. THIS PAGE**	UU	67	**19b. TELEPHONE NUMBER** (include area code)
U	U	U			

Table of Contents

Introduction

Increasing use of genomic discovery efforts in patients with bone marrow failure due to myelodysplastic syndrome (MDS) has led to the rapid discovery of a series of recurrent genetic abnormalities underlying these disorders. Remarkably, a large number of these alterations appear to be in genes whose function is known, or suspected, to be involved in epigenetic regulation of gene transcription. In the last 3 years alone, mutations in the genes *TET2*, *ASXL1*, *DNMT3a*, and *EZH2* have all been found to be frequent mutations amongst patients with MDS. Mutations in several of these genes have proven to be important markers of disease outcome with *ASXL1* and *EZH2* mutations recurrently being identified as adverse prognosticators in MDS patients. Identification of frequent mutations in epigenetic modifiers has also highlighted the fact that a number of these genes encode enzymes and/or result in alterations in enzymatic alterations which may represent novel, tractable therapeutic targets for MDS patients. In this proposal, we originally aimed to identify (a) if mice with genetically engineered deletion of epigenetic modifiers mutated in MDS would serve as valuable murine models of MDS, (b) if mutations in epigenetic modifiers may specifically impact DNA methylation and/or histone post-translational modifications in a manner that is therapeutically targetable, and (c) if additional mutations must exist in patients with specific subsets of MDS with the worst clinical outcome. Since awarding of the proposal, we have made major insights into the epigenomic function of ASXL1 as well as the biological impact of conditional deletion of *Asxl1* alone and in combination with other genetic alterations including *Tet2* deletions and NRasG12D overexpression. This work has resulted in several publications, multiple oral presentations at national meetings, and has been used as the basis for a proposal recently awarded to me as a Damon Runyon Clinical Investigator Award.

Body

Task 1. "Obtain DoD ACURO approval for the use of animals in the experiments outlined below in Tasks 2 to 4."

We received approval on 6/27/2013 for initial experiments to generate *Asxl1, Tet2,* and *Ezh2* single and compound knockout mice.

Task 2. "Complete characterization of mice with conditional deletion of Asxl1 alone and Asxl1 combined with Tet2 (Months 1-24) at the work performance site of Memorial Sloan-Kettering Cancer Center."

We have recently completed generation of mice with deletion of *Asxl1, Tet2,* or both using multiple differe Cre recombinases. This work has just been accepted for publication in the *Journal of Experimental Medicine* (**Abdel-Wahab, O**, Gao, J, Adli, MM, Dey, A, Trimarchi, T, Chung, YR, Kuscu, C, Hricik, T, Ndiaye-Lobry, D, La Fave, LM, Koche, R, Shih, AH, Guryanova, OA, Kim, E, Pandey, S, Shin, JY, Liu, J, Bhatt, PK, Monette, S, Zhao, X, Park, CY, Bernstein, BE, Aifantis, I, Levine, RL. Deletion of Asxl1 Results in Myelodysplasia and Severe Developmental Defects in Vivo. *J Exp Med* 2013 (in press)) (please see **Appendix 2**). In brief, we identified the following (please see **Appendix 2** for all experimental details and comprehensive data):
-Constitutive loss of *Asxl1* results in developmental abnormalities including anopthalmia, microcephaly, cleft palates, and mandibular malformations.

-Hematopoietic-specific deletion of *Asxl1* results in progressive, multilineage cytopenias and dysplasia in the context of increased numbers of hematopoietic stem/progenitor cells (HSPCs), characteristic features of human MDS.
-Serial transplantation of *Asxl1*-null hematopoietic cells results in a lethal myeloid disorder at a shorter latency than primary *Asxl1* knockout mice.
-*Asxl1* deletion reduces hematopoietic stem-cell self-renewal, which is restored by concomitant deletion of *Tet2*, a gene commonly co-mutated with *ASXL1* in MDS patients.
-Compound *Asxl1/Tet2* deletion results in an MDS phenotype with hastened death compared to single-gene knockout mice.

Task 3. Continue development of mice with Ezh2 deletion alone and characterize mice with compound deletion of Ezh2/Tet2 and Ezh2/Asxl1 (Months 1-24) at the work performance site of Memorial Sloan-Kettering Cancer Center.

We have recently generated mice with Ezh2 deletion in the postnatal compartment (*Mx1-cre Ezh2fl/fl*) mice and mice with compound deletion of *Ezh2* and *Asxl1.* We are just now beginning to characterize these mice.

Task 4. Determine the epigenetic contribution of Asxl1 and Ezh2 loss to bone marrow failure through Chromatin immunoprecipitation (ChIP) of histone H3 lysine 27 trimethyl (H3K27me3) followed by next-generation sequencing in primary murine hematopoietic cells (Months 1-24) at the work performance site of Memorial Sloan-Kettering Cancer Center.

We have recently completed detailed characterization of the effects of *ASXL1* mutations and loss using cell lines (see **Appendix 1**) and primary cells from knockout mice (see **Appendix 2**). These results which have been published now in 2 papers (again shown in **Appendix 1** and **2)** identified the following:

-*ASXL1* mutations result in loss of PRC2-mediated histone H3 lysine 27 (H3K27) tri-methylation.
-Through integration of microarray data with genome-wide histone modification ChIP-Seq data we identified targets of ASXL1 repression including the posterior *HOXA* cluster that is known to contribute to myeloid transformation.
-We demonstrated that *ASXL1* associates with the Polycomb repressive complex 2 (PRC2), and that loss of ASXL1 *in vivo* collaborates with *NRASG12D* to promote myeloid leukemogenesis.
-*Asxl1* loss *in vivo* results in a global reduction of H3K27 trimethylation and dysregulated expression of known regulators of hematopoiesis.
-Combining RNA-seq/ChIP-seq analyses of Asxl1 in hematopoietic cells identified a subset of differentially expressed genes as direct targets of Asxl1.

These findings underscore the importance of Asxl1 in Polycomb-group function, development, and hematopoiesis.

Task 5: Determine the effect of Tet2, Asxl1, and Ezh2 loss to a panel of currently clinically utilized compounds in patients with MDS. Drug panel will include decitabine, 5-azacytidine, lenalidomide, cytarabine, daunorubicin, HDACi (vorinostat, romidepsin, panobinostat, AR-42, trichostatin A), HSP-90 inhibitors (AUY-922, PUH-71), and

parthenolide (Months 1-24) at the work performance site of Memorial Sloan-Kettering Cancer Center.

This work is just now underway.

Task 5: Perform candidate gene and exome sequencing on DNA samples from 20 MDS patients with *ASXL1* mutations alone (Months 1-6) at the work performance site of Memorial Sloan-Kettering Cancer Center.

This work is just now underway.

Task 6: Perform candidate gene and exome sequencing on DNA samples from 40 patients with MDS accompanied by moderate to severe bone marrow fibrosis (Months 1-6) at the work performance site of Memorial Sloan-Kettering Cancer Center.

This work is just now underway.

Task 7: Present findings at national meetings and publish in peer-reviewed journals (Month 6-36).

I have given 5 presentations at national meetings on the work performed with funding from this award in the last year (see list of presentations in **Reportable Outcomes** below).

Key Research Accomplishments

- Developed and published the first conditional knockout mouse for *Asxl1* as well as the first murine model with combined *Asxl1* and *Tet2* deletion. We believe these models are valuable genetically-accurate murine models of acquired bone marrow failure.
- Confirmed important development functions for Asxl1 with observations that germline deletion of *Asxl1* including anopthalmia, microcephaly, cleft palates, and mandibular malformations. This matches human data identifying critical functions for Asxl1 germline mutations in developmental disorder Bohring-Opitz syndrome.
- Identified that hematopoietic-specific deletion of *Asxl1* results in progressive, multilineage cytopenias and dysplasia in the context of increased numbers of hematopoietic stem/progenitor cells (HSPCs), characteristic features of human MDS.
- Identified that serial transplantation of *Asxl1*-null hematopoietic cells results in a lethal myeloid disorder at a shorter latency than primary *Asxl1* knockout mice.
- Identified that *Asxl1* deletion reduces hematopoietic stem-cell self-renewal, which is restored by concomitant deletion of *Tet2*, a gene commonly co-mutated with *ASXL1* in MDS patients.
- Identified that compound *Asxl1/Tet2* deletion results in an MDS phenotype with hastened death compared to single-gene knockout mice.
- Identified *ASXL1* mutations result in loss of PRC2-mediated histone H3 lysine 27 (H3K27) tri-methylation.

- Through integration of microarray data with genome-wide histone modification ChIP-Seq data we identified targets of ASXL1 repression including the posterior *HOXA* cluster that is known to contribute to myeloid transformation.
- Demonstrated that *ASXL1* associates with the Polycomb repressive complex 2 (PRC2), and that loss of ASXL1 *in vivo* collaborates with *NRASG12D* to promote myeloid leukemogenesis.
- Combined RNA-seq/ChIP-seq analyses of Asxl1 in hematopoietic cells to identify a subset of differentially expressed genes as direct targets of Asxl1.

Reportable Outcomes

Manuscripts:

Abdel-Wahab, O, Gao, J, Adli, MM, Dey, A, Trimarchi, T, Chung, YR, Kuscu, C, Hricik, T, Ndiaye-Lobry, D, La Fave, LM, Koche, R, Shih, AH, Guryanova, OA, Kim, E, Pandey, S, Shin, JY, Liu, J, Bhatt, PK, Monette, S, Zhao, X, Park, CY, Bernstein, BE, Aifantis, I, Levine, RL. Deletion of Asxl1 Results in Myelodysplasia and Severe Developmental Defects in Vivo. *J Exp Med* 2013 (in press)

Abdel-Wahab O, Dey A. The ASXL-BAP1 axis: new factors in myelopoiesis, cancer and epigenetics. Leukemia. 2013 Jan;27(1):10-5. doi: 10.1038/leu.2012.288. Epub 2012 Oct 9. Review. PubMed PMID: 23147254.

Abdel-Wahab O, Figueroa ME. Interpreting new molecular genetics in myelodysplastic syndromes. Hematology Am Soc Hematol Educ Program. 2012;2012:56-64. doi: 10.1182/asheducation-2012.1.56. Review. PubMed PMID: 23233561.

Shih AH, **Abdel-Wahab O (co-first author),** Patel JP, Levine RL. The role of mutations in epigenetic regulators in myeloid malignancies. Nat Rev Cancer. 2012 Sep;12(9):599-612. doi: 10.1038/nrc3343. Epub 2012 Aug 17. Review. PubMed PMID: 22898539.

Abdel-Wahab O, Adli M, LaFave LM, Gao J, Hricik T, Shih AH, Pandey S, Patel JP, Chung YR, Koche R, Perna F, Zhao X, Taylor JE, Park CY, Carroll M, Melnick A, Nimer SD, Jaffe JD, Aifantis I, Bernstein BE, Levine RL. ASXL1 mutations promote myeloid transformation through loss of PRC2-mediated gene repression. Cancer Cell. 2012 Aug 14;22(2):180-93. doi: 10.1016/j.ccr.2012.06.032. PubMed PMID: 22897849; PubMed Central PMCID: PMC3422511.

Abstracts:

Abdel-Wahab, O, Gao, J, Adli, MM, Chung, YR, Koche, R, Shih, AH, Pandey, S, La Fave, LM, Ndiaye-Lobry, D, Shin, JY, Bhatt, PK, Patel, JP, Zhao, X, Park, CY, Bernstein, BE, Aifantis, I, Levine, RL. Deletion of Asxl1 Results in Myelodysplasia and Severe Developmental Defects in Vivo (Abstract 308). *Blood* 120(21). American Society of Hematology 2012 Meeting.

Presentations:

2012   American Society of Hematology, Biology of MDS Oral Session, Atlanta, GA.
2013   Clinical Translation of Epigenetics in Cancer Therapy, Asheville NC

2013   St. Jude's Children's Research Hospital, Dept. Pharmaceutical Sciences
Seminar Series
2013   American Association of Cancer Research, Current Concepts Session "The
          Genetic and Epigenetic Landscape of Leukemia Revealed"
2013   Society of Hematologic Oncology (SOHO) Meeting, Houston, Texas. "Epigenetic
          Drivers of Myelodysplasia"

Development of novel genetically engineered murine models:
Developed the following murine models of bone marrow failure, all of which are currently
published:
-*In vivo* shRNA-mediated depletion of Asxl1 combined with retroviral overexpression of
NRasG12D (Abdel-Wahab, O, *et al. Cancer Cell* 2012)
-Conditional knockout of Asxl1 in an *Mx1-cre Asxl1fl/fl* and *Vav-cre Asxl1fl/fl* model
(Abdel-Wahab, O, *et al. J Exp Med* 2013 (in press))
-Conditional knockout of Tet2 and Asxl1 together in a *Vav-cre Asxl1fl/flf Tet2fl/fl* model
(Abdel-Wahab, O, *et al. J Exp Med* 2013 (in press))

Informatics:
-Published gene expression microarray data of knockdown of ASXL1 using shRNA in a
variety of *ASXL1* wildtype human leukemia cell lines (Abdel-Wahab, O, *et al. Cancer
Cell* 2012). This data has been deposited in a public gene expression repository (*)
-Published genome-wide localization of Asxl1 by chromatin immunoprecipitation followed
by next-generation sequencing (ChIP-Seq) technology (Abdel-Wahab, O, *et al. J Exp
Med* 2013 (in press)). This sequencing data will soon be deposited in a public gene
expression repository.
-Published RNA-Sequencing data of the effects of *Asxl1* deletion in the hematopoietic
stem cells (lineage-negative Sca1+ c-KIT+ cells) and myeloid progenitor cells (lineage-
negative Sca1- c-KIT+) in one year-old *Mx1-cre Asxl1fl/fl* and littermate controls (Abdel-
Wahab, O, *et al. J Exp Med* 2013 (in press)). This sequencing data will soon be
deposited in a public gene expression repository.
-Published RNA-Sequencing data of the effects of *Asxl1* deletion, *Tet2* deletion, and
combined Asxl1/Tet2 double deletion in the hematopoietic stem cells (lineage-negative
Sca1+ c-KIT+ cells) of 6-week-old *Mx1-cre Asxl1fl/fl* and littermate controls (Abdel-
Wahab, O, *et al. J Exp Med* 2013 (in press)). This sequencing data will soon be
deposited in a public gene expression repository.

Funding applied for based on this work:
-Applied for and successfully received a Damon Runyon Clinical Investigator Award to
study altered histone modifers in myeloid malignancies based on all of the above work.

Conclusion

     Advancement in sequencing technologies has led to the rapid discovery of recurrent
genetic mutations in patients with MDS. Despite this, the functional importance of these
mutations in the pathogenesis of MDS as well as the potential importance to the therapy of
patients with MDS was previously not well characterized. Since award of this grant we have
identified a novel role for ASXL1 in PRC2 function, generated multiple novel genetically-
engineered mouse models including some of the first genetically accurate models of MDS. In
the ongoing work in this award, we hope to understand the therapeutic implications of mutations
in epigenetic modifiers. We will utilize hematopoietic cells from our genetically-engineered
mouse models to screen for compounds which specifically target cells bearing genetic defects

common in MDS patients. We have already demonstrated the proof-of-concept of this approach with the observation that Tet2-deficient murine hematopoietic stem cells are preferentially sensitive to HDAC inhibition compared with their wildtype counterparts. We also hope to perform genetic analyses of MDS patients with bone marrow fibrosis (as outlined in the initial award).

References

None

Appendices (please see next page)

ASXL1 Mutations Promote Myeloid Transformation through Loss of PRC2-Mediated Gene Repression

Omar Abdel-Wahab,[1,12] Mazhar Adli,[2,12] Lindsay M. LaFave,[1,3,12] Jie Gao,[5] Todd Hricik,[1] Alan H. Shih,[1] Suveg Pandey,[1] Jay P. Patel,[1] Young Rock Chung,[1] Richard Koche,[2] Fabiana Perna,[4] Xinyang Zhao,[6] Jordan E. Taylor,[7] Christopher Y. Park,[1] Martin Carroll,[8] Ari Melnick,[9] Stephen D. Nimer,[11] Jacob D. Jaffe,[7] Iannis Aifantis,[4] Bradley E. Bernstein,[2,*] and Ross L. Levine[1,10,*]

[1]Human Oncology and Pathogenesis Program and Leukemia Service, Memorial Sloan-Kettering Cancer Center, 1275 York Avenue, Box 20, New York, NY 10065, USA
[2]Howard Hughes Medical Institute, Broad Institute of Harvard and MIT, Department of Pathology, Massachusetts General Hospital, and Harvard Medical School, MGH-Simches Research Building, CPZN 8400,185 Cambridge Street, Boston, MA 02114, USA
[3]Gerstner Sloan Kettering School of Biomedical Sciences
[4]Molecular Pharmacology and Chemistry Program
Memorial Sloan-Kettering Cancer Center, New York, NY 10065, USA
[5]Howard Hughes Medical Institute and Department of Pathology, New York University School of Medicine, New York, NY 10016, USA
[6]Department of Biochemistry and Molecular Genetics, University of Alabama, Birmingham, AL 35233, USA
[7]Broad Institute of Harvard and MIT, Cambridge, MA 02142, USA
[8]Division of Hematology and Oncology, University of Pennsylvania, Philadelphia, PA 19104, USA
[9]Division of Hematology/Oncology
[10]Biochemistry and Molecular Biology Program
Weill Cornell Medical College, New York, NY 10065, USA
[11]Sylvester Comprehensive Cancer Center, University of Miami, Miami, FL 33136, USA
[12]These authors contributed equally to this work
*Correspondence: bernstein.bradley@mgh.harvard.edu (B.E.B.), leviner@mskcc.org (R.L.L.)
http://dx.doi.org/10.1016/j.ccr.2012.06.032

SUMMARY

Recurrent somatic *ASXL1* mutations occur in patients with myelodysplastic syndrome, myeloproliferative neoplasms, and acute myeloid leukemia, and are associated with adverse outcome. Despite the genetic and clinical data implicating *ASXL1* mutations in myeloid malignancies, the mechanisms of transformation by *ASXL1* mutations are not understood. Here, we identify that *ASXL1* mutations result in loss of polycomb repressive complex 2 (PRC2)-mediated histone H3 lysine 27 (H3K27) tri-methylation. Through integration of microarray data with genome-wide histone modification ChIP-Seq data, we identify targets of ASXL1 repression, including the posterior *HOXA* cluster that is known to contribute to myeloid transformation. We demonstrate that ASXL1 associates with the PRC2, and that loss of ASXL1 in vivo collaborates with *NRASG12D* to promote myeloid leukemogenesis.

INTRODUCTION

Recent genome-wide and candidate-gene discovery efforts have identified a series of novel somatic genetic alterations in patients with myeloid malignancies with relevance to pathogenesis, prognostication, and/or therapy. Notably, these include mutations in genes with known or putative roles in the epigenetic regulation of gene transcription. One such example is the mutations in the gene *Addition of sex combs-like 1* (*ASXL1*), which is mutated in ≈15%–25% of patients with myelodysplastic

Significance

Mutations in genes involved in modification of chromatin have recently been identified in patients with leukemias and other malignancies. Here, we demonstrate a specific role for ASXL1, a putative epigenetic modifier frequently mutated in myeloid malignancies, in polycomb repressive complex 2 (PRC2)-mediated transcriptional repression in hematopoietic cells. *ASXL1* loss-of-function mutations in myeloid malignancies result in loss of PRC2-mediated gene repression of known leukemogenic target genes. Our data provide insight into how *ASXL1* mutations contribute to myeloid transformation through dysregulation of Polycomb-mediated gene silencing. This approach also demonstrates how epigenomic and functional studies can be used to elucidate the function of mutations in epigenetic modifiers in malignant transformation.

syndrome and ≈10%–15% of patients with myeloproliferative neoplasms and acute myeloid leukemia (Abdel-Wahab et al., 2011; Bejar et al., 2011; Gelsi-Boyer et al., 2009). Clinical studies have consistently indicated that mutations in *ASXL1* are associated with adverse survival in myelodysplastic syndrome and acute myeloid leukemia (Bejar et al., 2011; Metzeler et al., 2011; Pratcorona et al., 2012; Thol et al., 2011).

ASXL1 is the human homolog of *Drosophila Additional sex combs* (*Asx*). *Asx* deletion results in a homeotic phenotype characteristic of both Polycomb (PcG) and Trithorax group (TxG) gene deletions (Gaebler et al., 1999), which led to the hypothesis that Asx has dual functions in silencing and activation of homeotic gene expression. In addition, functional studies in *Drosophila* suggested that *Asx* encodes a chromatin-associated protein with similarities to PcG proteins (Sinclair et al., 1998). More recently, it was demonstrated that *Drosophila* Asx forms a complex with the chromatin deubiquitinase Calypso to form the Polycomb-repressive deubiquitinase (PR-DUB) complex, which removes monoubiquitin from histone H2A at lysine 119. The mammalian homolog of Calypso, BAP1, directly associates with ASXL1, and the mammalian BAP1-ASXL1 complex was shown to possess deubiquitinase activity in vitro (Scheuermann et al., 2010).

The mechanisms by which *ASXL1* mutations contribute to myeloid transformation have not been delineated. A series of in vitro studies in non-hematopoietic cells have suggested a variety of activities for ASXL1, including physical cooperativity with HP1a and LSD1 to repress retinoic acid-receptor activity and interaction with peroxisome proliferator-activated receptor gamma (PPARg) to suppress lipogenesis (Cho et al., 2006; Lee et al., 2010; Park et al., 2011). In addition, a recent study using a gene-trap model reported that constitutive disruption of *Asxl1* results in significant perinatal lethality; however, the authors did not note alterations in stem/progenitor numbers in surviving Asxl1 gene trap mice (Fisher et al., 2010a, 2010b). Importantly, the majority of mutations in *ASXL1* occur as nonsense mutations and insertions/deletions proximal or within the last exon prior to the highly conserved plant homeo domain. It is currently unknown whether mutations in *ASXL1* might confer a gain-of-function due to expression of a truncated protein, or whether somatic loss of ASXL1 in hematopoietic cells leads to specific changes in epigenetic state, gene expression, or hematopoietic functional output. The goals of this study were to determine the effects of *ASXL1* mutations on ASXL1 expression as well as the transcriptional and biological effects of perturbations in ASXL1 which might contribute toward myeloid transformation.

RESULTS

ASXL1 Mutations Result in Loss of ASXL1 Expression

ASXL1 mutations in patients with myeloproliferative neoplasms, myelodysplastic syndrome, and acute myeloid leukemia most commonly occur as somatic nonsense mutations and insertion/deletion mutations in a clustered region adjacent to the highly conserved PHD domain (Abdel-Wahab et al., 2011; Gelsi-Boyer et al., 2009). To assess whether these mutations result in loss of ASXL1 protein expression or in expression of a truncated isoform, we performed western blots using N- and C-terminal anti-ASXL1 antibodies in a panel of human myeloid

leukemia cell lines and primary acute myeloid leukemia samples, which are wild-type or mutant for *ASXL1*. We found that myeloid leukemia cells with homozygous frameshift/nonsense mutations in *ASXL1* (NOMO1 and KBM5) have no detectable ASXL1 protein expression (Figure 1A). Similarly, leukemia cells with heterozygous *ASXL1* mutations have reduced or absent ASXL1 protein expression. Western blot analysis of ASXL1 using an N-terminal anti-ASXL1 antibody in primary acute myeloid leukemia samples wild-type and mutant for *ASXL1* revealed reduced/absent full-length ASXL1 expression in samples with *ASXL1* mutations compared to *ASXL1* wild-type samples (Figure S1A available online). Importantly, we did not identify truncated ASXL1 protein products in mutant samples using N- or C-terminal directed antibodies in primary acute myeloid leukemia samples or leukemia cell lines. Moreover, expression of wild-type ASXL1 cDNA or cDNA constructs bearing leukemia-associated mutant forms of ASXL1 revealed reduced stability of mutant forms of ASXL1 relative to wild-type ASXL1, with more rapid degradation of mutant ASXL1 isoforms following cycloheximide exposure (Figure S1B). These data are consistent with ASXL1 functioning as a tumor suppressor with loss of ASXL1 protein expression in leukemia cells with mutant *ASXL1* alleles.

ASXL1 Knockdown in Hematopoietic Cells Results in Upregulated *HOXA* Gene Expression

Given that *ASXL1* mutations result in loss of ASXL1 expression, we investigated the effects of ASXL1 knockdown in primary hematopoietic cells. We used a pool of small interfering RNAs (siRNA) to perform knockdown of ASXL1 in primary human CD34+ cells isolated from umbilical cord blood. ASXL1 knockdown was performed in triplicate and confirmed by qRT-PCR analysis (Figure 1B), followed by gene-expression microarray analysis. Gene-set enrichment analysis (GSEA) of this microarray data revealed a significant enrichment of genes found in a previously described gene expression signature of leukemic cells from bone marrow of *MLL-AF9* knock-in mice (Kumar et al., 2009), as well as highly significant enrichment of a gene signature found in primary human cord blood CD34+ cells expressing *NUP98-HOXA9* (Figure S1C and Table S1) (Takeda et al., 2006). Specifically, we found that ASXL1 knockdown in human primary CD34+ cells resulted in increased expression of 145 genes out of the 279 genes, which are overexpressed in the *MLL-AF9* gene expression signature (p < 0.05, FDR < 0.05). These gene expression signatures are characterized by increased expression of posterior *HOXA* cluster genes, including *HOXA5-9.*

In order to ascertain whether loss of ASXL1 was associated with similar transcriptional effects in leukemia cells, we performed short hairpin RNA (shRNA)-mediated stable knockdown of *ASXL1* in the *ASXL1*-wild-type human leukemia cell lines UKE1 (Figures 1C and 1D) and SET2 (Figure 1D) followed by microarray and qRT-PCR analysis. Gene expression analysis in UKE-1 cells expressing ASXL1 shRNA compared to control cells revealed significant enrichment of the same *HOXA* gene expression signatures as were seen with ASXL1 knockdown in CD34+ cells (Figure 1C and Table S2). Upregulation of 5′ *HOXA* genes was confirmed by qRT-PCR in UKE1 (Figure 1D) cells and by western blot analysis (Figure 1D) in SET2 cells expressing ASXL1 shRNA compared to control. Quantitative mRNA profiling (Nanostring nCounter) of the entire *HOXA* cluster revealed
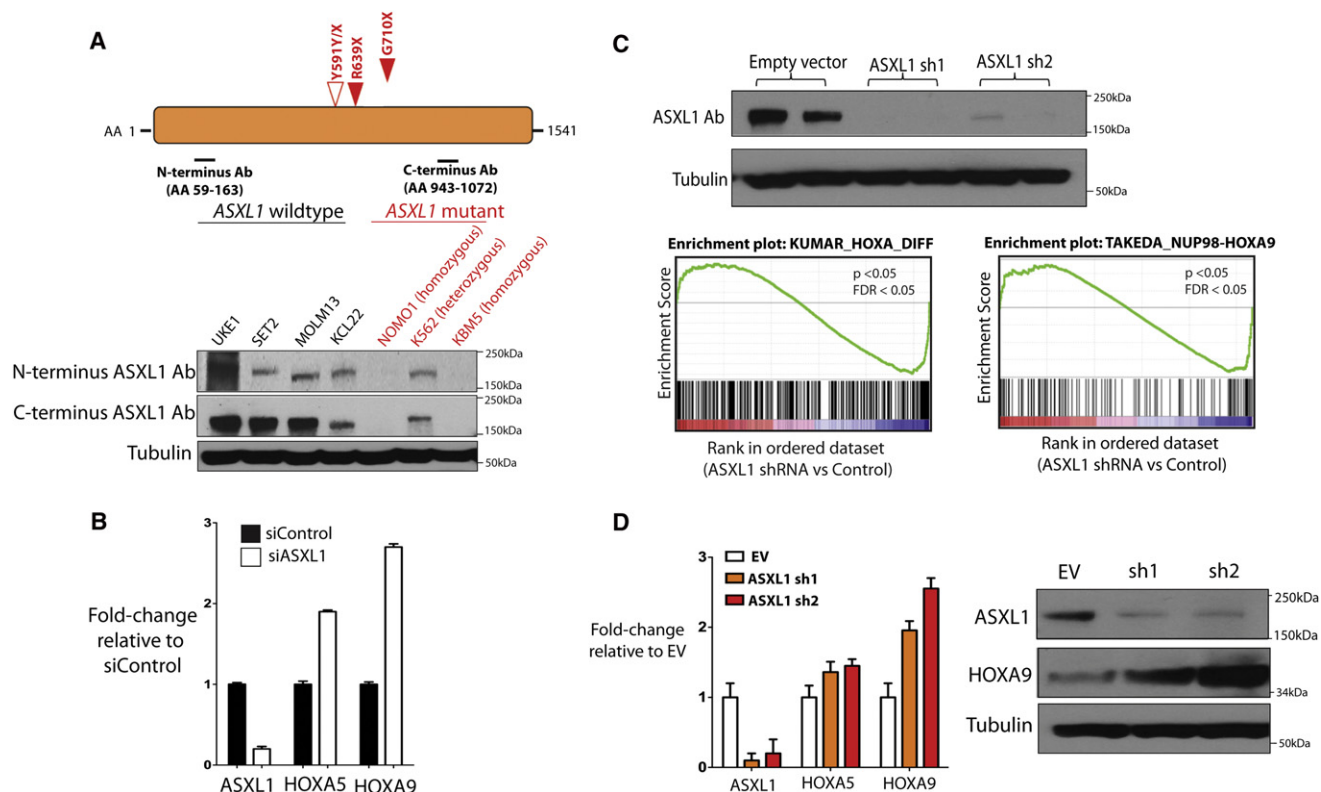
Figure 1. Leukemogenic *ASXL1* Mutations Are Loss-of-Function Mutations and ASXL1 Loss Is Associated with Upregulation of *HOXA* Gene Expression

(A) Characterization of ASXL1 expression in leukemia cells with nonsense mutations in *ASXL1* reveals loss of ASXL1 expression at the protein level in cells with homozygous *ASXL1* mutations as shown by western blotting using N- and C-terminal anti-ASXL1 antibodies.

(B) Displayed are the *ASXL1*-mutant cell line lines NOMO1 (homozygous *ASXL1* R639X), K562 (heterozygous *ASXL1* Y591Y/X), and KBM5 (homozygous *ASXL1* G710X) and a panel of *ASXL1*-wild-type cell lines. *ASXL1* siRNA in human primary CD34+ cells form cord blood results in upregulation of *HOXA5* and *HOXA9* with ASXL1 knockdown (KD) as revealed by quantitative real-time PCR (qRT-PCR) analysis.

(C and D) Stable KD of ASXL1 in *ASXL1*-wild-type transformed human myeloid leukemia UKE1 cells (as shown by western blot) followed by GSEA reveals significant enrichment of gene sets characterized by upregulation of 5′ *HOXA* genes (C) as was confirmed by qRT-PCR (D). Statistical significance is indicated in (D) by the p value and false-discovery rate (FDR). Similar upregulation of *HOXA9* is seen by the western blot following stable ASXL1 KD in the *ASXL1*-wild-type human leukemia SET2 cells.

Error bars represent standard deviation of expression relative to control. See also Figure S1 and Tables S1 and S2.

upregulation of multiple *HOXA* members, including *HOXA5, 7, 9,* and *10*, in SET2 cells with ASXL1 knockdown compared to control cells (Figure S1D). These results indicate consistent upregulation of *HOXA* gene expression following ASXL1 loss in multiple hematopoietic contexts.

ASXL1 Forms a Complex with BAP1 in Leukemia Cells, but BAP1 Loss Does Not Upregulate *HoxA* Gene Expression in Hematopoietic Cells

Mammalian ASXL1 forms a protein complex in vitro with the chromatin deubiquitinase BAP1, which removes monoubiquitin from histone H2A at lysine 119 (H2AK119) (Scheuermann et al., 2010). In *Drosophila* loss of either Asx or Calypso resulted in similar effects on genome-wide H2AK119 ubiquitin levels and on target gene expression. Recent studies have revealed recurrent germline and somatic loss-of-function *BAP1* mutations in mesothelioma and uveal melanoma (Bott et al., 2011; Harbour et al., 2010; Testa et al., 2011). However, we have not identified *BAP1* mutations in patients with myeloproliferative neoplasms or

acute myeloid leukemia (O.A.-W., J.P.P., and R.L.L., unpublished data). Co-immunopreciptation studies revealed an association between ASXL1 and BAP1 in human myeloid leukemia cells wild-type for *ASXL1* but not in those cells mutant for *ASXL1* due to reduced/absent ASXL1 expression (Figure 2A). Immunoprecipitation of FLAG-tagged wild-type ASXL1 and FLAG-tagged leukemia-associated mutant forms of ASXL1 revealed reduced interaction between mutant forms of ASXL1 and endogenous BAP1 (Figure S2A). Despite these findings, BAP1 knockdown did not result in upregulation of *HOXA5* and *HOXA9* in UKE1 cells, although a similar extent of ASXL1 knockdown in the same cells reproducibly increased *HOXA5* and *HOXA9* expression (Figure 2B). We obtained similar results with knockdown of Asxl1 or Bap1 in the Ba/F3 murine hematopoietic cell line (Figure 2C). In Ba/F3 cells, knockdown of *Asxl1* resulted in upregulated *Hoxa9* gene expression commensurate with the level of Asxl1 downregulation, whereas knockdown of Bap1 does not impact *Hoxa* expression (Figure 2C). ASXL1 knockdown in SET-2 cells failed to reveal an effect of ASXL1
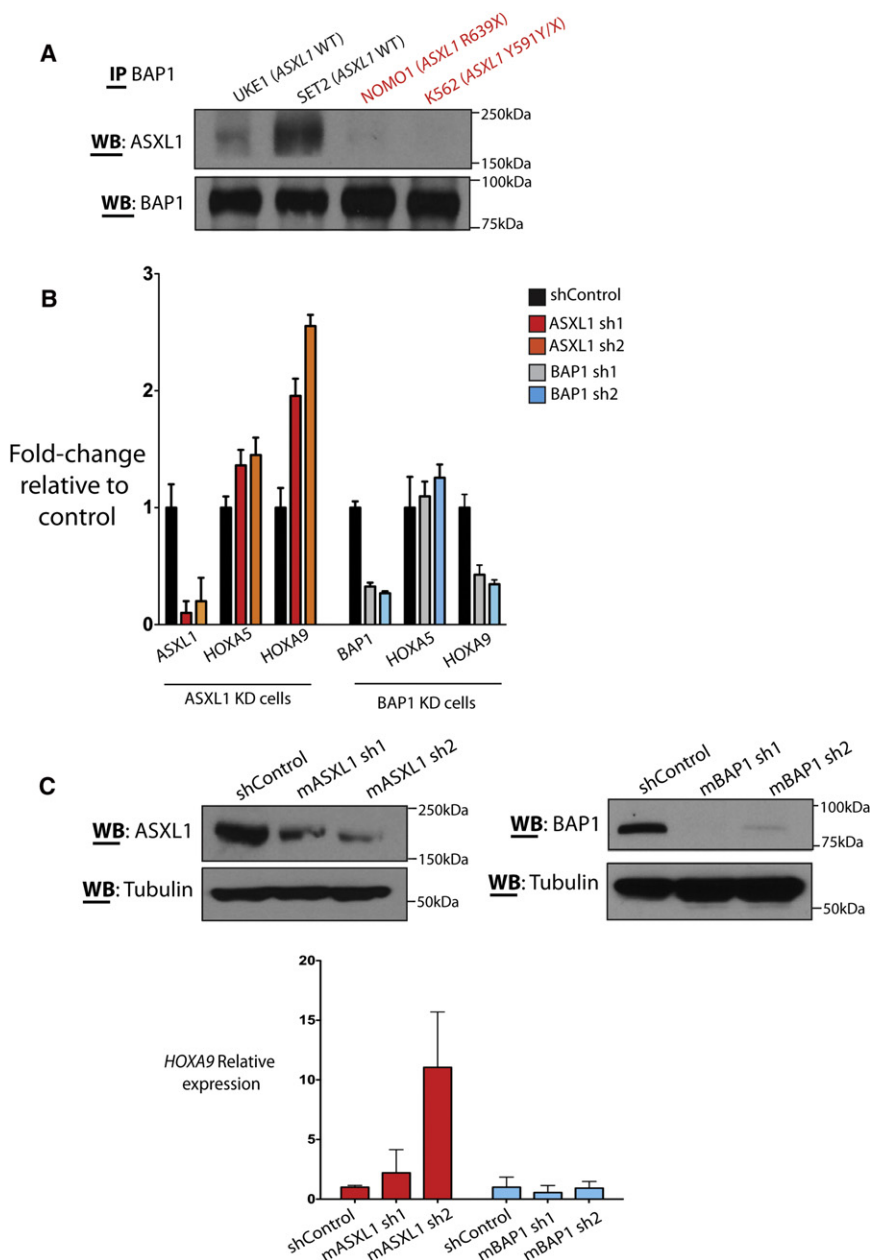
Figure 2. ASXL1 and BAP1 Physically Interact in Human Hematopoietic Cells but BAP1 Loss Does Not Result in Increased *HoxA* Gene Expression

(A) Immunoprecipitation of BAP1 in a panel of *ASXL1*-wild-type and mutant human myeloid leukemia cells reveals co-association of ASXL1 and BAP1.

(B) Cells with heterozygous or homozygous mutations in *ASXL1* with reduced or absent ASXL1 expression have minimal interaction with BAP1 in vitro. BAP1 knockdown in the *ASXL1/BAP1* wild-type human leukemia cell line UKE1 fails to alter *HOXA* gene expression. In contrast, stable knockdown of ASXL1 in the same cell type results in a significant upregulation of *HOXA9*.

(C) Similar results are seen with knockdown of Asxl1 or Bap1 in murine precursor-B lymphoid Ba/F3 cells.

Error bars represent standard deviation of expression relative to control. See also Figure S2.

matin immunoprecipitation followed by next generation sequencing (ChIP-seq) for histone modifications known to be associated with PcG [histone H3 lysine 27 trimethylation (H3K27me3)] or TxG activity [histone H3 lysine 4 trimethylation (H3K4me3)] in UKE1 cells expressing empty vector or two independent validated shRNAs for ASXL1. ChIP-Seq data analysis revealed a significant reduction in genome-wide H3K27me3 transcriptional start site occupancy with ASXL1 knockdown compared to empty vector (p = 2.2×10^{-16}; Figure 3A). Approximately 20% of genes (n = 4,686) were initially marked by H3K27me3 in their promoter regions (defined as 1.5 kb downstream and 0.5 kb upstream of the transcriptional start site). Among these genes, ~27% had a 2-fold reduction in H3K27me3 (n = 1,309) and ~66% had a 1.5-fold reduction in H3K27me3 (n = 3,092), respectively, upon ASXL1 knockdown. No significant effect was seen on H3K4me3 transcriptional start site occupancy with ASXL1 depletion (Figure 3A). We next evaluated whether loss of ASXL1 might be associated with loss of H3K27me3 globally by performing western blot analysis on purified histones from UKE1 cells transduced with empty vector or shRNAs for ASXL1 knockdown. This analysis revealed a significant decrease in global H3K27me3 with ASXL1 loss (Figure 3B), despite preserved expression of the core polycomb repressive complex 2 (PRC2) members EZH2, SUZ12, and EED. Similar effects on total H3K27me3 levels were seen following Asxl1 knockdown in Ba/F3 cells (Figure S3A). These results demonstrate that ASXL1 depletion leads to a marked reduction in genome-wide H3K27me3 in hematopoietic cells.
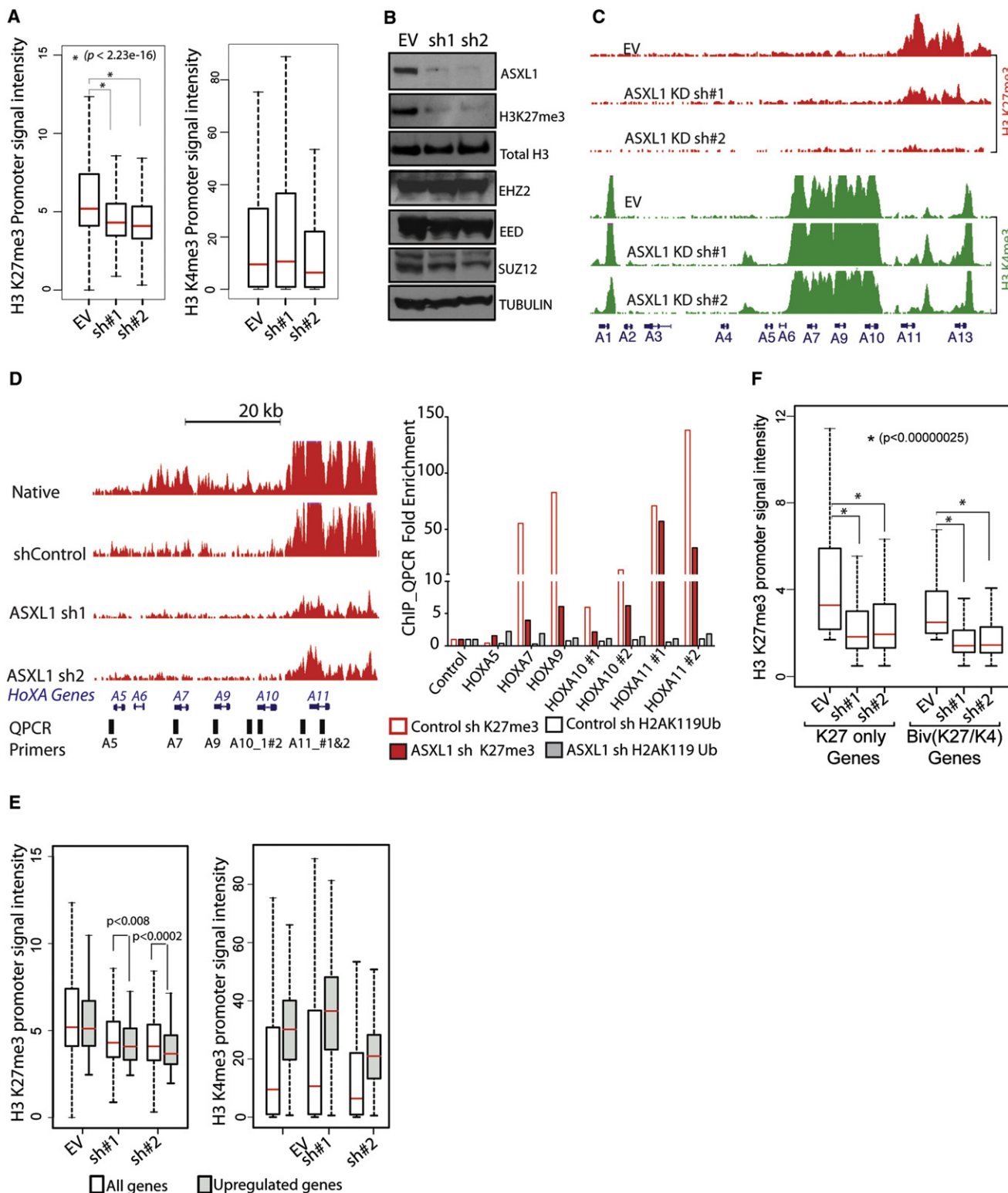
loss on H2AK119Ub levels as assessed by western blot of purified histones from shRNA control and ASXL1 knockdown cells (Figure S2B). By contrast, SET2 cells treated with MG132 (25 μM) had a marked decrease in H2AK119Ub, as has been previously described (Dantuma et al., 2006). These data suggest that ASXL1 loss contributes to myeloid transformation through a BAP1-independent mechanism.

Loss of ASXL1 Is Associated with Global Loss of H3K27me3

The results described above led us to hypothesize that ASXL1 loss leads to BAP1-independent effects on chromatin state and on target gene expression. To assess the genome-wide effects of ASXL1 loss on chromatin state, we performed chro-

Figure 3. ASXL1 Loss Is Associated with Loss of H3K27me3 and with Increased Expression of Genes Poised for Transcription

(A) ASXL1 loss is associated with a significant genome-wide decrease in H3K27me3 as illustrated by box plot showing the 25th, 50th, and 75th percentiles for H3K27me3 and H3K4me3 enrichment at transcription start sites in UKE1 cells treated with an empty vector or shRNAs directed against ASXL1. The whiskers indicate the most extreme data point less than 1.5 interquartile range from box and the red bar represents the median.

(B) Loss of ASXL1 is associated with a global loss of H3K27me3 without affecting PRC2 component expression as shown by western blot of purified histones from cells with UKE1 knockdown and western blot for core PRC2 component in whole cell lysates from ASXL1 knockdown UKE1 cells.

Detailed analysis of ChIP-seq data revealed that genomic regions marked by large H3K27me3 domains in control cells displayed more profound loss of H3K27me3 upon loss of ASXL1. Genome-wide analysis of the ChIP-Seq data from control and ASXL1 shRNA treated cells revealed that the sites that lose H3K27me3 in the ASXL1 knockdown cells were on average ∼6.6 kb in length, while the sites that maintained H3K27me3 were on average ∼3.1 kb in length (p < 10^{-16}) (Figure S3B). This is visually illustrated by the reduction in H3K27me3 at the posterior *HOXA* cluster (Figure 3C) and at the *HOXB and HOXC* loci (Figure S3C). The association of ASXL1 loss with loss of H3K27me3 abundance at the *HOXA* locus was confirmed by ChIP for H3K27me3 in control and ASXL1 knockdown cells followed by qPCR (ChIP-qPCR) across the *HOXA* locus (Figure 3D). ChIP-qPCR in control and knockdown cells revealed a modest increase in H2AK119Ub with ASXL1 loss at the *HOXA* locus (Figure 3D), in contrast to the more significant reduction in H3K27me3. In contrast to the large decrease in H3K27me3 levels at the *HOXA* locus with ASXL1 knockdown, a subset of loci had much less significant reduction in H3K27me3, in particular at loci whose promoters were marked by sharp peaks of H3K27me3 (Figure S3D). Intersection of gene expression and ChIP-Seq data revealed that genes overexpressed in ASXL1 knockdown cells were simultaneously marked with both activating (H3K4me3) and repressive (H3K27me3) domains in control cells (Figures 3E and 3F). This finding suggests that the transcriptional repression mediated by ASXL1 in myeloid cells is most apparent at loci poised for transcription with bivalent chromatin domains. Indeed, the effects of ASXL1 loss on H3K27me3 occupancy were most apparent at genes whose promoters were marked by the dual presence of H3K27me3 and H3K4me3 (Figure 3F). We cannot exclude the possibility that H3K4me3 and H3K27me3 exist in different populations within the homogeneous cell lines being studied, but the chromatin and gene expression data are consistent with an effect of ASXL1 loss on loci with bivalent chromatin domains (Bernstein et al., 2006; Mikkelsen et al., 2007).

Enforced Expression of ASXL1 in Leukemic Cells Results in Suppression of *HOXA* Gene Expression, a Global Increase in H3K27me3, and Growth Suppression

We next investigated whether reintroduction of wild-type ASXL1 protein could restore H3K27me3 levels in *ASXL1* mutant leukemia cells. We stably expressed wild-type ASXL1 in NOMO1 and KBM5 cells, homozygous *ASXL1* mutant human

leukemia cell lines, which do not express ASXL1 protein (Figure 4A and Figure S4A). ASXL1 expression resulted in a global increase in H3K27me3 as assessed by histone western blot analysis (Figure 4A). Liquid chromotography/mass spectrometry of purified histones in NOMO1 cells expressing ASXL1 confirmed a ∼2.5-fold increase in trimethylated H3K27 peptide and significant increases in dimethylated H3K27 in NOMO1 cells expressing ASXL1 compared to empty vector control (Figure 4B). ASXL1 add-back resulted in growth suppression (Figure 4C) and in decreased *HOXA* gene expression in NOMO1 cells (Figure 4D). ASXL1 add-back similarly resulted in decreased expression of *HOXA* target genes in KBM5 cells (Figures S4A and S4B). ChIP-qPCR revealed a strong enrichment in ASXL1 binding at the *HOXA* locus in NOMO1 cells expressing ASXL1, demonstrating that the *HOXA* locus is a direct target of ASXL1 in hematopoietic cells (Figure 4E).

ASXL1 Loss Leads to Exclusion of H3K27me3 and EZH2 from the HoxA Cluster Consistent with a Direct Effect of ASXL1 on PRC2 Recruitment

We next investigated whether the effects of ASXL1 loss on H3K27me3 was due to inhibition of PRC2 recruitment to specific target loci. ChIP-qPCR for H3K27me3 in SET2 cells with ASXL1 knockdown or control revealed a loss of H3K27me3 enrichment at the posterior *HoxA* locus with ASXL1 knockdown (Figures 5A and 5B). We observed a modest, variable increase in H3K4me3 enrichment at the *HOXA* locus with *ASXL1* depletion in SET2 cells (Figure 5C). We similarly assessed H3K27me3 enrichment in primary bone marrow leukemic cells from acute myeloid leukemia patients, wild-type and mutant for *ASXL1,* which likewise revealed decreased H3K27me3 enrichment across the *HOXA* cluster in primary acute myeloid leukemia samples with *ASXL1* mutations compared to *ASXL1*-wild-type acute myeloid leukemia samples (Figure 5D).

Given the consistent effects of ASXL1 depletion on H3K27me3 abundance at the *HOXA* locus, we then evaluated the occupancy of EZH2, a core PRC2 member, at the *HoxA* locus. ChIP-Seq for H3K27me3 in native SET2 and UKE1 cells identified that H3K27me3 is present with a dome-like enrichment pattern at the 5′ end of the posterior *HOXA* cluster (Figure 5A); ChIP-qPCR revealed that EZH2 is prominently enriched in this same region in parental SET2 cells (Figure 5E). Importantly, ASXL1 depletion resulted in loss of EZH2 enrichment at the *HOXA* locus (Figure 5E), suggesting that ASXL1 is required for EZH2 occupancy and for PRC2-mediated repression of the posterior *HOXA* locus.

(C) Loss of H3K27me3 is evident at the *HOXA* locus as shown by ChIP-Seq promoter track signals across the *HOXA* locus in UKE1 cells treated with an EV or shRNA knockdown of ASXL1.

(D) H3K27me3 ChIP-Seq promoter track signals from *HOXA5* to *HOXA13* in UKE1 cells treated with shRNA control or one of 2 anti-*ASXL1* shRNAs with location of primers used in ChIP-quantitative PCR (ChIP-qPCR) validation. ChIP for H3K27me3 and H2AK119Ub followed by ChIP-qPCR in cells treated with control or ASXL1 knockdown confirms a significant decrease in H3K27me3 at the *HOXA* locus with ASXL1 knockdown but minimal effects of ASXL1 knockdown on H2AK119Ub levels at the same primer locations.

(E) Integrating gene-expression data with H3K27me3/H3K4me3 ChIP-Seq identifies a significant correlation between alterations in chromatin state and increases in gene expression following ASXL1 loss at loci normally marked by the simultaneous presence of H3K27me3 and H3K4me3 in control cells.

(F) Loss of H3K27me3 is seen at promoters normally marked by the presence of H3K27me3 alone or at promoters co-occupied by H3K27me3 and H3K4me3 in the control state.
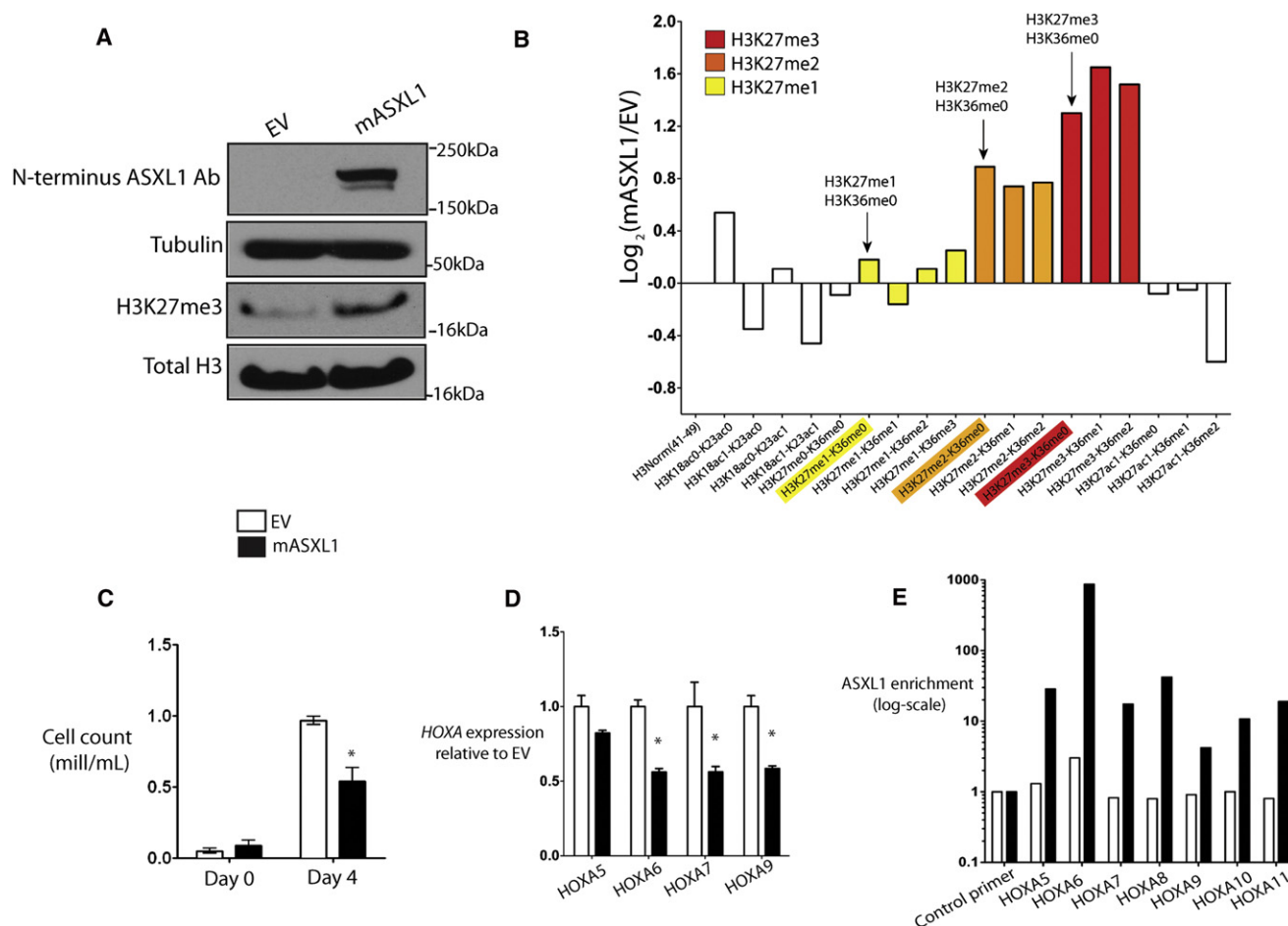
See also Figure S3.

Figure 4. Expression of ASXL1 in ASXL1-Null Leukemic Cells Results in Global Increase in H3K27me2/3, Growth Suppression, and Suppression of *HoxA* Gene Expression

(A and B) ASXL1 expression in ASXL1 null NOMO1 cells is associated with a global increase in H3K27me3 as detected by western blot of purified histones (A) as well as by quantitative liquid-chromatography/mass spectrometry of H3 peptides from amino acids 18–40 (B) (arrows indicate quantification of H3K27me1/2/3).
(C) ASXL1 overexpression results in growth suppression in 7-day growth assay performed in triplicate.
(D) Overexpression of ASXL1 was associated with a decrement in posterior *HoxA* gene expression in NOMO1 cells as shown by qRT-PCR for *HOXA5, 6, 7, and 9*.
(E) This downregulation in *HOXA* gene expression was concomitant with a strong enrichment of ASXL1 at the loci of these genes as shown by chromatin immunoprecipitation of ASXL1 followed by quantitative PCR with BCRRP1 as a control locus.
Error bars represent standard deviation of target gene expression relative to control. See also Figure S4.

ASXL1 Physically Interacts with Members of the PRC2 in Human Myeloid Leukemic Cells

Given that ASXL1 localizes to PRC2 target loci and ASXL1 depletion leads to loss of PRC2 occupancy and H3K27me2, we investigated whether ASXL1 might physically interact with the PRC2 complex in hematopoietic cells. Co-immunoprecipitation studies using an anti-FLAG antibody in HEK293T cells expressing empty vector, hASXL1-FLAG alone, or hASXL1-FLAG plus hEZH2 cDNA revealed a clear co-immunoprecipitation of FLAG-ASXL1 with endogenous EZH2 and with ectopically expressed EZH2 (Figure 6A). Similarly, co-immuniprecipitation of FLAG-ASXL1 revealed physical association between ASXL1 and endogenous SUZ12 in 293T cells (Figure 6A). Immunoprecipitations were performed in the presence of benzonase to ensure that the protein-protein interactions observed were DNA-independent (Figure 6B) (Muntean et al., 2010). We then assessed whether endogenous ASXL1 formed a complex with PRC2 members in hematopoietic cells. We performed IP for EZH2 or ASXL1 followed by western blotting for partner proteins in SET2 and UKE1 cells, which are wild-type for *ASXL1*, *SUZ12*, *EZH2*, and *EED*. These co-immunoprecipitation assays all revealed a physical association between ASXL1 and EZH2 in SET2 (Figure 6B) and UKE1 cells (Figure S5). By contrast, immunoprecipitation of endogenous ASXL1 did not reveal evidence of protein-protein interactions between ASXL1 and BMI1 (Figure S5). Likewise, immunoprecipitation of BMI1 enriched for PRC1 member RING1A, but failed to enrich for ASXL1, suggesting a lack of interaction between ASXL1 and the PRC1 repressive complex (Figure 6C).

ASXL1 Loss Collaborates with NRasG12D In Vivo

We and others previously reported that *ASXL1* mutations are most common in chronic myelomonocytic leukemia and frequently co-occur with *N/K-Ras* mutations in chronic
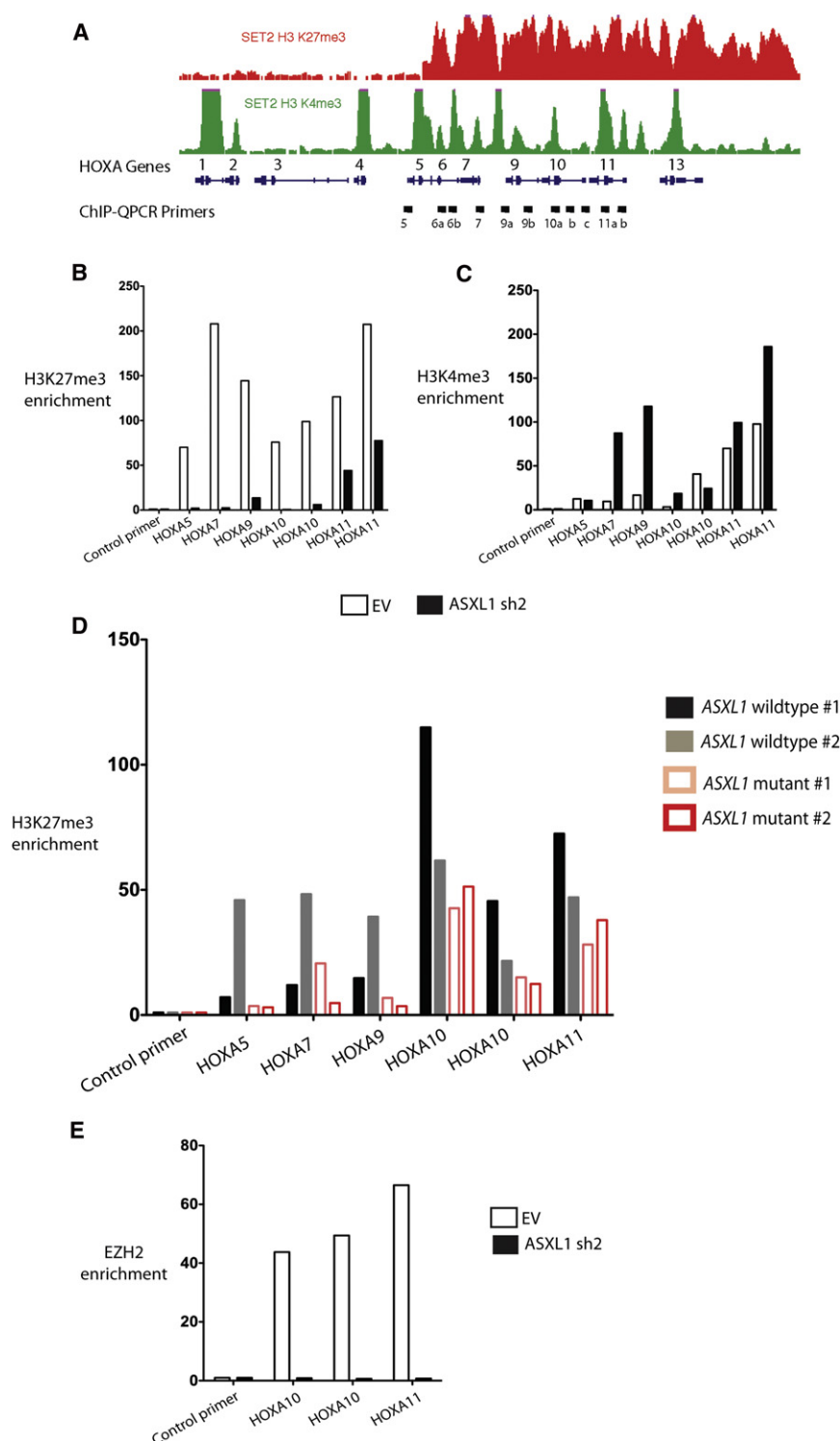
Figure 5. ASXL1 Loss Is Associated with Loss of PRC2 Recruitment at the *HOXA* Locus

(A) Chromatin-immunoprecipitation (ChIP) for H3K27me3 and H3K4me3 followed by next-generation sequencing reveals the abundance and localization of H3K27me3 and H3K4me3 at the *HoxA* locus in SET2 cells.

(B and C) ChIP for H3K27me3 (B) and H3K4me3 (C) followed by quantitative PCR (qPCR) across the 5' *HOXA* locus in SET2 cells treated with an empty vector or stable knockdown of ASXL1 reveals a consistent downregulation of H3K27me3 across the 5' *HOXA* locus following ASXL1 loss and a modest increase in H3K4me3 at the promoters of 5' *HOXA* genes with ASXL1 loss [primer locations are shown in (A)].

(D) Similar ChIP for H3K27me3 followed by qPCR across the *HOXA* locus in primary leukemic blasts from two patients with *ASXL1* mutations versus two without *ASXL1* mutations reveals H3K27me3 loss across the *HOXA* locus in *ASXL1* mutant cells.

(E) ChIP for EZH2 followed by qPCR at the 5' end of *HOXA* locus in SET2 cells reveals loss of EZH2 enrichment with ASXL1 loss in SET2 cells. CHIP-qPCR was performed in biologic duplicates and ChIP-qPCR data is displayed as enrichment relative to input. qPCR at the gene body of *RRP1*, a region devoid of H3K4me3 or H3K27me3, is utilized as a control locus.

The error bars represent standard deviation.

cells into lethally irradiated recipient mice. We validated our ability to effectively knock down ASXL1 in vivo by performing qRT-PCR in hematopoietic cells from recipient mice (Figure 7A and Figure S6A). Consistent with our in vitro data implicating the HoxA cluster as an ASXL1 target locus, we noted a marked increase in *HoxA9* and *HoxA10* expression in bone marrow nucleated cells from mice expressing *NRasG12D* in combination with Asxl1 shRNA compared to mice expressing *NRasG12D* alone (Figure 7B).

Expression of oncogenic *NRasG12D* and an empty shRNA vector control led to a progressive myeloproliferative disorder as previously described (MacKenzie et al., 1999). In contrast, expression of *NRasG12D* in combination with validated mASXL1 knockdown vectors re-

myelomonocytic leukemia (Abdel-Wahab et al., 2011; Patel et al., 2010). We therefore investigated the effects of combined *NRasG12D* expression and Asxl1 loss in vivo. To do this, we expressed *NRasG12D* in combination with an empty vector expressing GFP alone or one of two different Asxl1 shRNA constructs in whole bone marrow cells and transplanted these

sulted in accelerated myeloproliferation and impaired survival compared with mice transplanted with *NRasG12D*/EV (median survival 0.8 month for ASXL1 shRNA versus 3 months for control shRNA vector: p < 0.005; Figure 7C) We also noted impaired survival with an independent *mASXL1* shRNA construct (p < 0.01; Figure S6B) Mice transplanted with *NRasG12D*/Asxl1
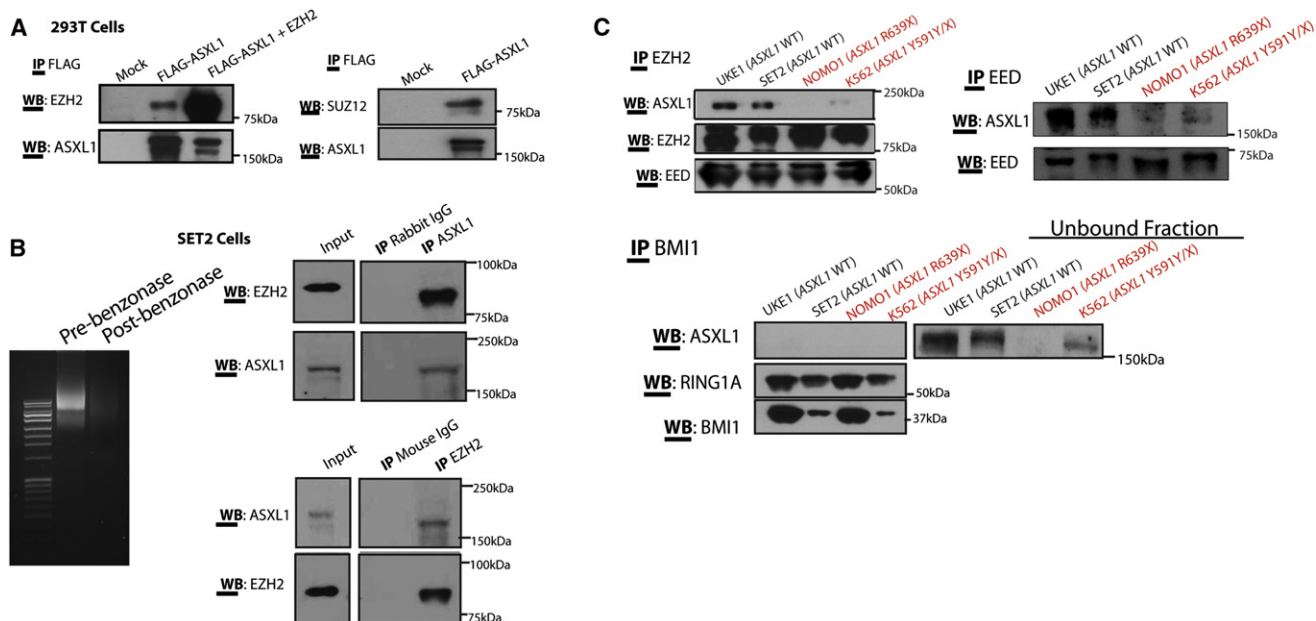
Figure 6. ASXL1 Interacts with the PRC2 in Hematopoietic Cells

(A) Physical interaction between ASXL1 and EZH2 is demonstrated by transient transfection of HEK293T cells with FLAG-hASXL1 cDNA with or without hEZH2 cDNA followed by immunoprecipitation (IP) of FLAG epitope and western blotting for EZH2 and ASXL1.

(B) HEK293T cells were transiently transfected with FLAG-hASXL1 cDNA followed by IP of FLAG epitope and western blotting for SUZ12 and ASXL1. Endogenous interaction of ASXL1 with PRC2 members was also demonstrated by IP of endogenous EZH2 and ASXL1 followed by western blotting of the other proteins in whole cell lysates from SET2 cells.

(C) Lysates from the experiment shown in (B) were treated with benzonase to ensure nucleic acid free conditions in the lysates prior to IP as shown by ethidium bromide staining of an agarose gel before and after benzonase treatment. IP of endogenous EZH2 and embryonic ectoderm development (EED) in a panel of ASXL1-wild-type and mutant human leukemia cells reveals a specific interaction between ASXL1 and PRC2 members in *ASXL1*-wildype human myeloid leukemia cells. In contrast, IP of the PRC1 member BMI1 failed to pull down ASXL1.

See also Figure S5.

shRNA had increased splenomegaly and hepatomegaly compared with *NRasG12D*/EV transplanted mice (Figures 7D and 7E; Figure S6C). Histological analysis revealed a significant increase in myeloid infiltration of the spleen and livers of mice transplanted with *NRasG12D*/Asxl1 shRNA (Figure S6D).

Mice transplanted with *NRasG12D*/*Asxl1* shRNA, but not *NRasG12D*/EV, experienced progressive, severe anemia (Figure 7F). It has previously been identified that expression of oncogenic *K/N-Ras* in multiple models of human/murine hematopoietic systems results in alterations in the erythroid compartment (Braun et al., 2006; Darley et al., 1997; Zhang et al., 2003). We noted an expansion of CD71^{high}/Ter119^{high} erythroblasts in the bone marrow of mice transplanted with *NRasG12D*/Asxl1 shRNA compared with *NRasG12D*/EV mice (Figure S6E). We also noted increased granulocytic expansion in mice engrafted with *NRasG12D*/Asxl1 shRNA positive cells, as shown by the presence of increased neutrophils in the peripheral blood (Figure S6D) and the expansion of Gr1/Mac1 double-positive cells in the bone marrow by flow cytometry (Figure S6F).

Previous studies have shown that hematopoietic cells from mice expressing oncogenic *Ras* alleles or other mutations that activate kinase signaling pathways do not exhibit increased self-renewal in colony replating assays (Braun et al., 2004; MacKenzie et al., 1999). This is in contrast to the immortalization of hematopoietic cells in vitro seen with expression of *MLL-AF9*

(Somervaille and Cleary, 2006) or deletion of *Tet2* (Moran-Crusio et al., 2011). Bone marrow cells from mice with combined over-expression of NRasG12D plus Asxl1 knockdown had increased serial replating (to five passages) compared to bone marrow cells from mice engrafted with *NRasG12D*/EV cells (Figure 7G). These studies demonstrate that Asxl1 loss cooperates with oncogenic *NRasG12D* in vivo.

DISCUSSION

The data presented here identify that ASXL1 loss in hematopoietic cells results in reduced H3K27me3 occupancy through inhibition of PRC2 recruitment to specific oncogenic target loci. Recent studies have demonstrated that genetic alterations in the PRC2 complex occur in a spectrum of human malignancies (Bracken and Helin, 2009; Margueron and Reinberg, 2011; Sauvageau and Sauvageau, 2010). Activating mutations and overexpression of *EZH2* occur most commonly in epithelial malignancies and in lymphoid malignancies (Morin et al., 2010; Varambally et al., 2002). However, there are increasing genetic data implicating mutations that impair PRC2 function in the pathogenesis of myeloid malignancies. These include the loss-of-function mutations in *EZH2* (Abdel-Wahab et al., 2011; Ernst et al., 2010; Nikoloski et al., 2010) and less common somatic loss-of-function mutations in *SUZ12*, *EED*, and *JARID2* (Score
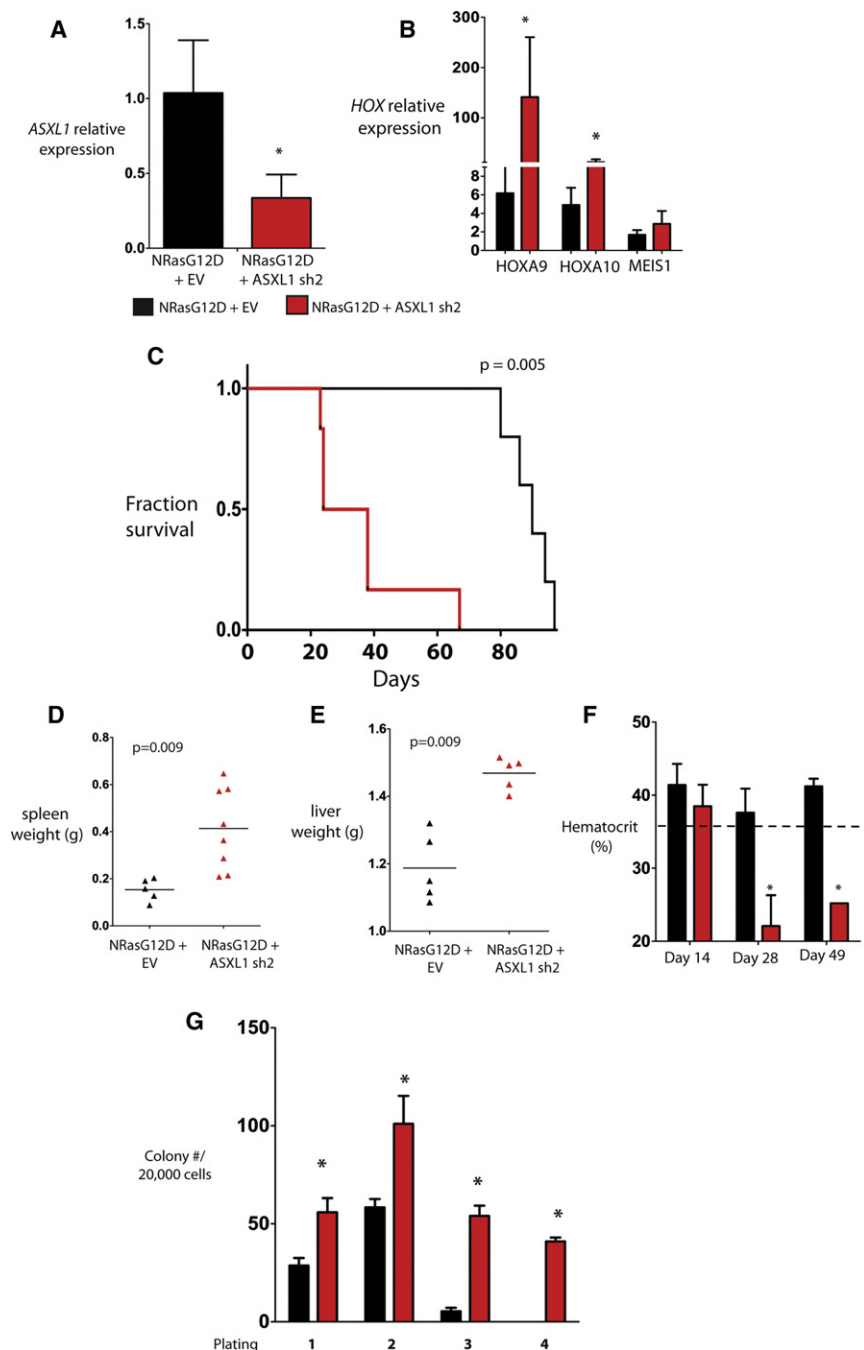
Figure 7. Asxl1 Silencing Cooperates with NRasG12D In Vivo

(A) Retroviral bone marrow transplantation of NRasG12D with or without an shRNA for Asxl1 resulted in decreased *Asxl1* mRNA expression as shown by qRT-PCR results in nucleated peripheral blood cells from transplanted mice at 14 days following transplant.

(B) qRT-PCR revealed an increased expression of *HOXA9* and *HOXA10* but not *MEIS1* in the bone marrow of mice sacrificed 19 days following transplantation.

(C) Transplantation of bone marrow cells bearing overexpression of NRasG12D in combination with downregulation of Asxl1 led to a significant hastening of death compared to mice transplanted with NRasG12D/EV.

(D–F) Mice transplanted with NRasG12D/ASXL1 shRNA experienced increased splenomegaly (D) and hepatomegaly (E), and progressive anemia (F) compared with mice transplanted with NRasG12D + an empty vector (EV).

(G) Bone marrow cells from mice with combined NRasG12D overexpression/Asxl1 knockdown revealed increased serial replating compared with cells from NRasG12D/EV mice. Error bars represent standard deviation relative to control. Asterisk indicates $p < 0.05$ (two-tailed, Mann Whitney U test).

See also Figure S6.

myeloid malignancies. In many cases, patients present with concomitant heterozygous mutations in multiple PRC2 members or in *EZH2* and *ASXL1*; these data suggest that haploinsufficiency for multiple genes that regulate PRC2 function can cooperate in hematopoietic transformation through additive alterations in PRC2 function.

Many studies have investigated how mammalian PcG proteins are recruited to chromatin in order to repress gene transcription and specify cell fate in different tissue contexts. Recent in silico analysis suggested that ASXL proteins found in animals contain a number of domains that likely serve in the recruitment of chromatin modulators and transcriptional effectors to DNA (Aravind and Iyer, 2012). Data from ChIP and co-immunoprecipitation experiments presented here suggest a specific role for ASXL1 in epigenetic regulation of gene expression by facilitating PRC2-mediated transcriptional repression of known leukemic oncogenes. Thus, ASXL1 may serve as a scaffold for recruitment of the PRC2 complex to specific loci in hematopoietic cells, as has been demonstrated for JARID2 in embryonic stem cells (Landeira et al., 2010; Pasini et al., 2010; Peng et al., 2009; Shen et al., 2009).

Recent data suggested that ASXL1 might interact with BAP1 to form a H2AK119 deubiquitanase (Scheuermann et al., 2010).

et al., 2012) in patients with myeloproliferative neoplasms, myelodysplastic syndrome, and chronic myelomonocytic leukemia. The data from genetically-engineered mice also support this concept with Ezh2 overexpression models, revealing evidence of promotion of malignant transformation (Herrera-Merchan et al., 2012), and recent studies demonstrate a role for Ezh2 loss in leukemogenesis (Simon et al., 2012). Thus, it appears that alterations in normal PRC2 activity and/or H3K27me3 abundance in either direction may promote malignant transformation. Our data implicate *ASXL1* mutations as an additional genetic alteration that leads to impaired PRC2 function in patients with

However, our data suggest that ASXL1 loss leads to BAP1-independent alterations in chromatin state and gene expression in hematopoietic cells. These data are consonant with recent genetic studies, which have shown that germline loss of BAP1 increases susceptibility to uveal melanoma and mesothelioma (Testa et al., 2011; Wiesner et al., 2011). In contrast, germline loss of ASXL1 is seen in the developmental disorder Bohring-Opitz Syndrome (Hoischen et al., 2011), but has not, to date, been observed as a germline solid tumor susceptibility locus. Whether alterations in H2AK119 deubiquitanase function due to alterations in BAP1 and/or ASXL1 can contribute to leukemogenesis or to the pathogenesis of other malignancies remains to be determined.

Integration of gene expression and chromatin state data following ASXL1 loss identified specific loci with a known role in leukemogenesis that are altered in the setting of *ASXL1* mutations. These include the posterior *HOXA* cluster, including *HOXA9,* which has a known role in hematopoietic transformation. We demonstrate that ASXL1 normally serves to tightly regulate *HOXA* gene expression in hematopoietic cells, and that loss of ASXL1 leads to disordered *HOXA* gene expression in vitro and in vivo. Overexpression of 5′ *HOXA* genes is a well-described oncogenic event in hematopoietic malignancies (Lawrence et al., 1996), and previous studies have shown that *HOXA9* overexpression leads to transformation in vitro and in vivo when co-expressed with *MEIS1* (Kroon et al., 1998). Interestingly, *ASXL1* loss was not associated with an increase in *MEIS1* expression, suggesting that transformation by *ASXL1* mutations requires the co-occurrence of oncogenic disease alleles which dysregulate additional target loci. These data and our in vivo studies suggest that *ASXL1* loss, in combination with co-occurring oncogenes, can lead to hematopoietic transformation and increased self-renewal. Further studies in mice expressing ASXL1 shRNA or with conditional deletion of *Asxl1* alone and in concert with leukemogeneic disease alleles will provide additional insight into the role of ASXL1 loss in hematopoietic stem/progenitor function and in leukemogenesis.

Given that somatic mutations in chromatin modifying enzymes (Dalgliesh et al., 2010), DNA methyltransferases (Ley et al., 2010), and other genes implicated in epigenetic regulation occur commonly in human cancers, it will be important to use epigenomic platforms to elucidate how these disease alleles contribute to oncogenesis in different contexts. The data here demonstrate how integrated epigenetic and functional studies can be used to elucidate the function of somatic mutations in epigenetic modifiers. In addition, it is likely that many known oncogenes and tumor suppressors contribute, at least in part, to transformation through direct or indirect alterations in the epigenetic state (Dawson et al., 2009). Subsequent epigenomic studies of human malignancies will likely uncover novel routes to malignant transformation in different malignancies, and therapeutic strategies that reverse epigenetic alterations may be of specific benefit in patients with mutations in epigenetic modifiers.

EXPERIMENTAL PROCEDURES

Cell Culture
HEK293T cells were cultured in Dulbecco's modified Eagle's medium (DMEM) supplemented with 10% fetal bovine serum (FBS) and nonessential amino acids. Human leukemia cell lines were cultured in RPMI-1640 medium supplemented with 10% FBS+1 mM hydrocortisone+10% horse serum (UKE1 cells), RPMI-1640 supplemented with 10% FBS (K562, MOLM13, KCL22, KU812 cells), RPMI-1640 supplemented with 20% FBS (SET2, NOMO1, Monomac-6 cells), or IMDM + 20% FBS (KBM5 cells). For proliferation studies, 1×10^3 cells were seeded in 1 ml volume of media in triplicate and cell number was counted manually daily for 7 days by Trypan blue exclusion.

Plasmid Constructs, Mutagenesis Protocol, Short Hairpin RNA, and Small Interfering RNA
See Supplemental Information.

Primary Acute Myeloid Leukemia Patient Samples and *ASXL1, BAP1, EZH2, SUZ12,* and *EED* Genomic DNA Sequencing Analysis
Approval was obtained from the institutional review boards at Memorial Sloan-Kettering Cancer Center and at the Hospital of the University of Pennsylvania for these studies, and informed consent was provided according to the Declaration of Helsinki. Please see Supplemental Information for details on DNA sequence analysis.

Western Blot and Immunoprecipitation Analysis
Western blots were carried out using the following antibodies: ASXL1 (Clone N-13; Santa Cruz (sc-85283); N-terminus directed), ASXL1 (Clone 2049C2a; Santa Cruz (sc-81053); C terminus directed), BAP1 [clone 3C11; Santa Cruz (sc-13576)], BMI1 (Abcam ab14389), EED (Abcam ab4469), EZH2 (Active Motif 39933 or Millipore 07-689), FLAG (M2 FLAG; Sigma A2220), Histone H3 lysine 27 trimethyl (Abcam ab6002), Histone H2A Antibody II (Cell Signaling Technologies 2578), Ubiquityl-Histone H2AK119 (Clone D27C4; Cell Signaling Technologies 8240), RING1A (Abcam ab32807), SUZ12 (Abcam ab12073), and total histone H3 (Abcam ab1791), and tubulin (Sigma, T9026). Antibodies different from the above used for immunoprecipitation include: ASXL1 [clone H105X; Santa Cruz (sc-98302)], FLAG (Novus Biological Products; NBP1-06712), and EZH2 (Active Motif 39901). Immunoprecipitation and pull-down reactions were performed in an immunoprecipitation buffer (150 mM NaCl, 20 mM Tris (pH 7.4–7.5), 5 mM EDTA, 1% Triton, 100 mM sodium orthovanadate, protease arrest (Genotec), 1 mM PMSF, and phenylarsene oxide). To ensure nuclease-free immunoprecipitation conditions, immunoprecipitations were also performed using the following methodology (Muntean et al., 2010): cells were lysed in BC-300 buffer (20 mM Tris-HCl (pH 7.4), 10% glycerol, 300 mM KCl, 0.1% NP-40) and the cleared lysate was separated from the insoluble pellet and treated with MgCl2 to 2.5 mM and benzonase (Emanuel Merck, Darmstadt) at a concentration of 1,250 U/ml. The lysate was then incubated for 1–1.5 hr at 4°. The reaction was then stopped with addition of 5 mM EDTA. DNA digestion is confirmed on an ethidium bromide agarose gel. We then set up our immunoprecipitation by incubating our lysate overnight at 4°.

Histone Extraction and Histone LC/MS Analysis
See Supplemental Information.

Gene Expression Analysis
Total RNA was extracted from cells using QIAGEN's RNeasy Plus Mini kit (Valencia, CA, USA). cDNA synthesis, labeling, hybridization, and quality control were carried out as previously described (Figueroa et al., 2008). Ten micrograms of RNA was then used for generation of labeled cRNA according to the manufacturer's instructions (Affymetrix, Santa Clara, CA, USA). Hybridization of the labeled cRNA fragments and washing, staining, and scanning of the arrays were carried out as per instructions of the manufacturer. Labeled cRNA from CD34+ cells treated with either ASXL1 siRNA or controls were analyzed using the Affymetrix HG-U133-Plus2.0 platform and from UKE1 cells using the Illumina Href8 array. All expression profile experiments were carried out using biological duplicates. "Present" calls in ≥80% of samples were captured and quantile normalized across all samples on a per-chip basis. Raw expression values generated by Genome Studio (Illumina) were filtered to exclude probesets having expression values below negative background in ≥80% of samples. Probesets remaining after background filtering were log-2 transformed and quantile normalized on a per-chip basis. qRT-PCR was performed on cDNA using SYBR green quantification in an ABI 7500

sequence detection system. The sequences of all qRT-PCR primers are listed in the Supplemental Information.

Chromatin Immunoprecipitation and Antibodies

ChIP experiments for H3K4me3, H3K27me3, and H3K36me3 were carried out as described previously (Bernstein et al., 2006; Mikkelsen et al., 2007). Cells were cross-linked in 1% formaldehyde, lysed, and sonicated with a Branson 250 Sonifier to obtain chromatin fragments in a size range between 200 and 700 bp. Solubilized chromatin was diluted in ChIP dilution buffer (1:10) and incubated with antibody overnight at 4°C. Protein A sepharose beads (Sigma) were used to capture the antibody-chromatin complex and washed with low salt, LiCl, as well as TE (pH 8.0) wash buffers. Enriched chromatin fragments were eluted at 65°C for 10 min, subjected to cross-link reversal at 65°C for 5 hr, and treated with Proteinase K (1 mg/ml), before being extracted by phenol-chloroform-isoamyl alcohol, and ethanol precipitated. ChIP DNA was then quantified by QuantiT Picogreen dsDNA Assay kit (Invitrogen). ChIP experiments for ASXL1 were carried out on nuclear preps. Cross-linked cells were incubated in swelling buffer (0.1 M Tris pH 7.6, 10 mM KOAc, 15 mM MgOAc, 1% NP40), on ice for 20 minutes, passed through a 16G needle 20 times and centrifuged to collect nuclei. Isolated nuclei were then lysed, sonicated, and immunoprecipitated as described above. Antibodies used for ChIP include anti-H3K4me3 (Abcam ab8580), anti-H3K27me3 (Upstate 07-449), anti-H3K36me3 (Abcam ab9050), and anti-ASXL1 [clone H105X; Santa Cruz (sc-98302)], and Ubiquityl-Histone H2AK119 (Clone D27C4; Cell Signaling Technologies 8240).

Sequencing Library Preparation, Illumina/Solexa Sequencing, and Read Alignment and Generation of Density Maps

See Supplemental Information.

HOXA Nanostring nCounter Gene Expression CodeSet

Direct digital mRNA analysis of *HOXA* cluster gene expression was performed using a Custom CodeSet including each *HOXA gene* (NanoString Technologies). Synthesis of the oligonucleotides was done by NanoString Technologies, and hybridization and analysis were done using the Prep Station and Digital Analyzer purchased from the company.

Animal Use, Retroviral Bone Marrow Transplantation, Flow Cytometry, and Colony Assays

Animal care was in strict compliance with institutional guidelines established by the Memorial Sloan-Kettering Cancer Center, the National Academy of Sciences Guide for the Care and Use of Laboratory Animals, and the Association for Assessment and Accreditation of Laboratory Animal Care International. All animal procedures were approved by the Institutional Animal Care and Use Committee (IACUC) at Memorial Sloan-Kettering Cancer Center. See Supplemental Information for more details on animal experiments.

Statistical Analysis

Statistical significance was determined by the Mann-Whitney U test and Fisher's exact test using Prism GraphPad software. Significance of survival differences was calculated using Log-rank (Mantel-Cox) test. $p < 0.05$ was considered statistically significant. Normalized expression data from CD34+ cord blood was used as a Gene Set Enrichment Analysis query of the C2 database (MSig DB) where 1,000 permutations of the genes was used to generate a null distribution. A pre-ranked gene list, containing genes upregulated at least $\log_2$ 0.5-fold, in which the highest ranked genes corresponds to the genes, with the largest fold-difference between Asxl1 hairpin-treated UKE1 cells and those treated with empty vector, was used to query the C2 MSig DB as described above.

ACCESSION NUMBERS

All microarray data used in this manuscript are deposited in Gene Expression Omnibus (http://www.ncbi.nlm.nih.gov/geo/) under GEO accession number GSE38692. The ChIP-Seq data are deposited under GEO accession number GSE38861.

SUPPLEMENTAL INFORMATION

Supplemental Information includes six figures, two tables, and Supplemental Experimental Procedures and can be found with this article online at http://dx.doi.org/10.1016/j.ccr.2012.06.032.

REFERENCES

Abdel-Wahab, O., Pardanani, A., Patel, J., Wadleigh, M., Lasho, T., Heguy, A., Beran, M., Gilliland, D.G., Levine, R.L., and Tefferi, A. (2011). Concomitant analysis of EZH2 and ASXL1 mutations in myelofibrosis, chronic myelomonocytic leukemia and blast-phase myeloproliferative neoplasms. Leukemia 25, 1200–1202.

Aravind, L., and Iyer, L.M. (2012). The HARE-HTH and associated domains: Novel modules in the coordination of epigenetic DNA and protein modifications. Cell Cycle 11, 119–131.

Bejar, R., Stevenson, K., Abdel-Wahab, O., Galili, N., Nilsson, B., Garcia-Manero, G., Kantarjian, H., Raza, A., Levine, R.L., Neuberg, D., and Ebert, B.L. (2011). Clinical effect of point mutations in myelodysplastic syndromes. N. Engl. J. Med. 364, 2496–2506.

Bernstein, B.E., Mikkelsen, T.S., Xie, X., Kamal, M., Huebert, D.J., Cuff, J., Fry, B., Meissner, A., Wernig, M., Plath, K., et al. (2006). A bivalent chromatin structure marks key developmental genes in embryonic stem cells. Cell 125, 315–326.

Bott, M., Brevet, M., Taylor, B.S., Shimizu, S., Ito, T., Wang, L., Creaney, J., Lake, R.A., Zakowski, M.F., Reva, B., et al. (2011). The nuclear deubiquitinase BAP1 is commonly inactivated by somatic mutations and 3p21.1 losses in malignant pleural mesothelioma. Nat. Genet. 43, 668–672.

Bracken, A.P., and Helin, K. (2009). Polycomb group proteins: navigators of lineage pathways led astray in cancer. Nat. Rev. Cancer 9, 773–784.

Braun, B.S., Tuveson, D.A., Kong, N., Le, D.T., Kogan, S.C., Rozmus, J., Le Beau, M.M., Jacks, T.E., and Shannon, K.M. (2004). Somatic activation of oncogenic Kras in hematopoietic cells initiates a rapidly fatal myeloproliferative disorder. Proc. Natl. Acad. Sci. USA 101, 597–602.

Braun, B.S., Archard, J.A., Van Ziffle, J.A., Tuveson, D.A., Jacks, T.E., and Shannon, K. (2006). Somatic activation of a conditional KrasG12D allele causes ineffective erythropoiesis in vivo. Blood 108, 2041–2044.

Cho, Y.S., Kim, E.J., Park, U.H., Sin, H.S., and Um, S.J. (2006). Additional sex comb-like 1 (ASXL1), in cooperation with SRC-1, acts as a ligand-dependent coactivator for retinoic acid receptor. J. Biol. Chem. 281, 17588–17598.

Dalgliesh, G.L., Furge, K., Greenman, C., Chen, L., Bignell, G., Butler, A., Davies, H., Edkins, S., Hardy, C., Latimer, C., et al. (2010). Systematic sequencing of renal carcinoma reveals inactivation of histone modifying genes. Nature 463, 360–363.

Dantuma, N.P., Groothuis, T.A., Salomons, F.A., and Neefjes, J. (2006). A dynamic ubiquitin equilibrium couples proteasomal activity to chromatin re-modeling. J. Cell Biol. *173*, 19–26.

Darley, R.L., Hoy, T.G., Baines, P., Padua, R.A., and Burnett, A.K. (1997). Mutant N-RAS induces erythroid lineage dysplasia in human CD34+ cells. J. Exp. Med. *185*, 1337–1347.

Dawson, M.A., Bannister, A.J., Göttgens, B., Foster, S.D., Bartke, T., Green, A.R., and Kouzarides, T. (2009). JAK2 phosphorylates histone H3Y41 and excludes HP1alpha from chromatin. Nature *461*, 819–822.

Ernst, T., Chase, A.J., Score, J., Hidalgo-Curtis, C.E., Bryant, C., Jones, A.V., Waghorn, K., Zoi, K., Ross, F.M., Reiter, A., et al. (2010). Inactivating mutations of the histone methyltransferase gene EZH2 in myeloid disorders. Nat. Genet. *42*, 722–726.

Figueroa, M.E., Reimers, M., Thompson, R.F., Ye, K., Li, Y., Selzer, R.R., Fridriksson, J., Paietta, E., Wiernik, P., Green, R.D., et al. (2008). An integrative genomic and epigenomic approach for the study of transcriptional regulation. PLoS One *3*, e1882.

Fisher, C.L., Lee, I., Bloyer, S., Bozza, S., Chevalier, J., Dahl, A., Bodner, C., Helgason, C.D., Hess, J.L., Humphries, R.K., and Brock, H.W. (2010a). Additional sex combs-like 1 belongs to the enhancer of trithorax and polycomb group and genetically interacts with Cbx2 in mice. Dev. Biol. *337*, 9–15.

Fisher, C.L., Pineault, N., Brookes, C., Helgason, C.D., Ohta, H., Bodner, C., Hess, J.L., Humphries, R.K., and Brock, H.W. (2010b). Loss-of-function Additional sex combs-like1 mutations disrupt hematopoiesis but do not cause severe myelodysplasia or leukemia. Blood *115*, 38–46.

Gaebler, C., Stanzl-Tschegg, S., Heinze, G., Holper, B., Milne, T., Berger, G., and Vécsei, V. (1999). Fatigue strength of locking screws and prototypes used in small-diameter tibial nails: a biomechanical study. J. Trauma *47*, 379–384.

Gelsi-Boyer, V., Trouplin, V., Adélaïde, J., Bonansea, J., Cervera, N., Carbuccia, N., Lagarde, A., Prebet, T., Nezri, M., Sainty, D., et al. (2009). Mutations of polycomb-associated gene ASXL1 in myelodysplastic syndromes and chronic myelomonocytic leukaemia. Br. J. Haematol. *145*, 788–800.

Harbour, J.W., Onken, M.D., Roberson, E.D., Duan, S., Cao, L., Worley, L.A., Council, M.L., Matatall, K.A., Helms, C., and Bowcock, A.M. (2010). Frequent mutation of BAP1 in metastasizing uveal melanomas. Science *330*, 1410–1413.

Herrera-Merchan, A., Arranz, L., Ligos, J.M., de Molina, A., Dominguez, O., and Gonzalez, S. (2012). Ectopic expression of the histone methyltransferase Ezh2 in haematopoietic stem cells causes myeloproliferative disease. Nat Commun *3*, 623.

Hoischen, A., van Bon, B.W., Rodríguez-Santiago, B., Gilissen, C., Vissers, L.E., de Vries, P., Janssen, I., van Lier, B., Hastings, R., Smithson, S.F., et al. (2011). De novo nonsense mutations in ASXL1 cause Bohring-Opitz syndrome. Nat. Genet. *43*, 729–731.

Kroon, E., Krosl, J., Thorsteinsdottir, U., Baban, S., Buchberg, A.M., and Sauvageau, G. (1998). Hoxa9 transforms primary bone marrow cells through specific collaboration with Meis1a but not Pbx1b. EMBO J. *17*, 3714–3725.

Kumar, A.R., Li, Q., Hudson, W.A., Chen, W., Sam, T., Yao, Q., Lund, E.A., Wu, B., Kowal, B.J., and Kersey, J.H. (2009). A role for MEIS1 in MLL-fusion gene leukemia. Blood *113*, 1756–1758.

Landeira, D., Sauer, S., Poot, R., Dvorkina, M., Mazzarella, L., Jørgensen, H.F., Pereira, C.F., Leleu, M., Piccolo, F.M., Spivakov, M., et al. (2010). Jarid2 is a PRC2 component in embryonic stem cells required for multi-lineage differentiation and recruitment of PRC1 and RNA Polymerase II to developmental regulators. Nat. Cell Biol. *12*, 618–624.

Lawrence, H.J., Sauvageau, G., Humphries, R.K., and Largman, C. (1996). The role of HOX homeobox genes in normal and leukemic hematopoiesis. Stem Cells *14*, 281–291.

Lee, S.W., Cho, Y.S., Na, J.M., Park, U.H., Kang, M., Kim, E.J., and Um, S.J. (2010). ASXL1 represses retinoic acid receptor-mediated transcription through associating with HP1 and LSD1. J. Biol. Chem. *285*, 18–29.

Ley, T.J., Ding, L., Walter, M.J., McLellan, M.D., Lamprecht, T., Larson, D.E., Kandoth, C., Payton, J.E., Baty, J., Welch, J., et al. (2010). DNMT3A mutations in acute myeloid leukemia. N. Engl. J. Med. *363*, 2424–2433.

MacKenzie, K.L., Dolnikov, A., Millington, M., Shounan, Y., and Symonds, G. (1999). Mutant N-ras induces myeloproliferative disorders and apoptosis in bone marrow repopulated mice. Blood *93*, 2043–2056.

Margueron, R., and Reinberg, D. (2011). The Polycomb complex PRC2 and its mark in life. Nature *469*, 343–349.

Metzeler, K.H., Becker, H., Maharry, K., Radmacher, M.D., Kohlschmidt, J., Mrózek, K., Nicolet, D., Whitman, S.P., Wu, Y.Z., Schwind, S., et al. (2011). ASXL1 mutations identify a high-risk subgroup of older patients with primary cytogenetically normal AML within the ELN Favorable genetic category. Blood *118*, 6920–6929.

Mikkelsen, T.S., Ku, M., Jaffe, D.B., Issac, B., Lieberman, E., Giannoukos, G., Alvarez, P., Brockman, W., Kim, T.K., Koche, R.P., et al. (2007). Genome-wide maps of chromatin state in pluripotent and lineage-committed cells. Nature *448*, 553–560.

Moran-Crusio, K., Reavie, L., Shih, A., Abdel-Wahab, O., Ndiaye-Lobry, D., Lobry, C., Figueroa, M.E., Vasanthakumar, A., Patel, J., Zhao, X., et al. (2011). Tet2 loss leads to increased hematopoietic stem cell self-renewal and myeloid transformation. Cancer Cell *20*, 11–24.

Morin, R.D., Johnson, N.A., Severson, T.M., Mungall, A.J., An, J., Goya, R., Paul, J.E., Boyle, M., Woolcock, B.W., Kuchenbauer, F., et al. (2010). Somatic mutations altering EZH2 (Tyr641) in follicular and diffuse large B-cell lymphomas of germinal-center origin. Nat. Genet. *42*, 181–185.

Muntean, A.G., Tan, J., Sitwala, K., Huang, Y., Bronstein, J., Connelly, J.A., Basrur, V., Elenitoba-Johnson, K.S., and Hess, J.L. (2010). The PAF complex synergizes with MLL fusion proteins at HOX loci to promote leukemogenesis. Cancer Cell *17*, 609–621.

Nikoloski, G., Langemeijer, S.M., Kuiper, R.P., Knops, R., Massop, M., Tönnissen, E.R., van der Heijden, A., Scheele, T.N., Vandenberghe, P., de Witte, T., et al. (2010). Somatic mutations of the histone methyltransferase gene EZH2 in myelodysplastic syndromes. Nat. Genet. *42*, 665–667.

Park, U.H., Yoon, S.K., Park, T., Kim, E.J., and Um, S.J. (2011). Additional sex comb-like (ASXL) proteins 1 and 2 play opposite roles in adipogenesis via reciprocal regulation of peroxisome proliferator-activated receptor gamma. J. Biol. Chem. *286*, 1354–1363.

Pasini, D., Cloos, P.A., Walfridsson, J., Olsson, L., Bukowski, J.P., Johansen, J.V., Bak, M., Tommerup, N., Rappsilber, J., and Helin, K. (2010). JARID2 regulates binding of the Polycomb repressive complex 2 to target genes in ES cells. Nature *464*, 306–310.

Peng, J.C., Valouev, A., Swigut, T., Zhang, J., Zhao, Y., Sidow, A., and Wysocka, J. (2009). Jarid2/Jumonji coordinates control of PRC2 enzymatic activity and target gene occupancy in pluripotent cells. Cell *139*, 1290–1302.

Pratcorona, M., Abbas, S., Sanders, M., Koenders, J., Kavelaars, F., Erpelinck-Verschueren, C., Zeilemaker, A., Lowenberg, B., and Valk, P. (2012). Acquired mutations in ASXL1 in acute myeloid leukemia: prevalence and prognostic value. Haematologica *97*, 388–392.

Sauvageau, M., and Sauvageau, G. (2010). Polycomb group proteins: multi-faceted regulators of somatic stem cells and cancer. Cell Stem Cell *7*, 299–313.

Scheuermann, J.C., de Ayala Alonso, A.G., Oktaba, K., Ly-Hartig, N., McGinty, R.K., Fraterman, S., Wilm, M., Muir, T.W., and Müller, J. (2010). Histone H2A deubiquitinase activity of the Polycomb repressive complex PR-DUB. Nature *465*, 243–247.

Score, J., Hidalgo-Curtis, C., Jones, A.V., Winkelmann, N., Skinner, A., Ward, D., Zoi, K., Ernst, T., Stegelmann, F., Dohner, K., et al. (2012). Inactivation of polycomb repressive complex 2 components in myeloproliferative and myelodysplastic/myeloproliferative neoplasms. Blood *119*, 1208–1213.

Shen, X., Kim, W., Fujiwara, Y., Simon, M.D., Liu, Y., Mysliwiec, M.R., Yuan, G.C., Lee, Y., and Orkin, S.H. (2009). Jumonji modulates polycomb activity and self-renewal versus differentiation of stem cells. Cell *139*, 1303–1314.

Simon, C., Chagraoui, J., Krosl, J., Gendron, P., Wilhelm, B., Lemieux, S., Boucher, G., Chagnon, P., Drouin, S., Lambert, R., et al. (2012). A key role

for EZH2 and associated genes in mouse and human adult T-cell acute leukemia. Genes Dev. *26*, 651–656.

Sinclair, D.A., Milne, T.A., Hodgson, J.W., Shellard, J., Salinas, C.A., Kyba, M., Randazzo, F., and Brock, H.W. (1998). The Additional sex combs gene of Drosophila encodes a chromatin protein that binds to shared and unique Polycomb group sites on polytene chromosomes. Development *125*, 1207–1216.

Somervaille, T.C., and Cleary, M.L. (2006). Identification and characterization of leukemia stem cells in murine MLL-AF9 acute myeloid leukemia. Cancer Cell *10*, 257–268.

Takeda, A., Goolsby, C., and Yaseen, N.R. (2006). NUP98-HOXA9 induces long-term proliferation and blocks differentiation of primary human CD34+ hematopoietic cells. Cancer Res. *66*, 6628–6637.

Testa, J.R., Cheung, M., Pei, J., Below, J.E., Tan, Y., Sementino, E., Cox, N.J., Dogan, A.U., Pass, H.I., Trusa, S., et al. (2011). Germline BAP1 mutations predispose to malignant mesothelioma. Nat. Genet. *43*, 1022–1025.

Thol, F., Friesen, I., Damm, F., Yun, H., Weissinger, E.M., Krauter, J., Wagner, K., Chaturvedi, A., Sharma, A., Wichmann, M., et al. (2011). Prognostic significance of ASXL1 mutations in patients with myelodysplastic syndromes. J. Clin. Oncol. *29*, 2499–2506.

Varambally, S., Dhanasekaran, S.M., Zhou, M., Barrette, T.R., Kumar-Sinha, C., Sanda, M.G., Ghosh, D., Pienta, K.J., Sewalt, R.G., Otte, A.P., et al. (2002). The polycomb group protein EZH2 is involved in progression of prostate cancer. Nature *419*, 624–629.

Wiesner, T., Obenauf, A.C., Murali, R., Fried, I., Griewank, K.G., Ulz, P., Windpassinger, C., Wackernagel, W., Loy, S., Wolf, I., et al. (2011). Germline mutations in BAP1 predispose to melanocytic tumors. Nat. Genet. *43*, 1018–1021.

Zhang, J., Socolovsky, M., Gross, A.W., and Lodish, H.F. (2003). Role of Ras signaling in erythroid differentiation of mouse fetal liver cells: functional analysis by a flow cytometry-based novel culture system. Blood *102*, 3938–3946.

Deletion of Asxl1 Results in Myelodysplasia and Severe Developmental Defects in Vivo

Omar Abdel-Wahab[1,2,15], Jie Gao[3,15], Mazhar Adli[4,15], Anwesha Dey[7], Thomas Trimarchi[3], Young Rock Chung[1], Cem Kuscu[4], Todd Hricik[1], Delphine Ndiaye-Lobry[3], Lindsay M. LaFave[2,8], Richard Koche[5,6], Alan H. Shih[1,2], Olga A. Guryanova[1], Eunhee Kim[1], Sheng Li[11], Suveg Pandey[1], Joseph Y. Shin[1], Leon Telis[1], Jinfeng Liu[9], Parva K. Bhatt[1], Sebastien Monette[12], Xinyang Zhao[13], Christopher E. Mason[11], Christopher Y. Park[1,14], Bradley E. Bernstein[5,6], Iannis Aifantis[3,16], and Ross L. Levine[1,2,8,10,16].

[1] Human Oncology and Pathogenesis Program, Memorial Sloan-Kettering Cancer Center, New York, NY 10065; [2] Leukemia Service, Memorial Sloan-Kettering Cancer Center, New York, NY 10065; [3] Howard Hughes Medical Institute and Department of Pathology, New York University School of Medicine, New York, NY 10016, USA; [4] Dept. of Biochemistry and Molecular Genetics, University of Virginia, Charlottesville, VA 22903; [5] Broad Institute of Harvard and MIT, Cambridge, MA 02142, USA; [6] Howard Hughes Medical Institute, Department of Pathology, Massachusetts General Hospital, and Harvard Medical School,185 Cambridge Street, Boston, MA 02114, USA; [7] Department of Molecular Biology, Genentech, South San Francisco, California 94080, USA; [8] Gerstner Sloan Kettering School of Biomedical Sciences, Memorial Sloan-Kettering Cancer Center, New York, NY 10065; [9] Department of Bioinformatics and Computational Biology, Genentech, South San Francisco, California 94080, USA; [10] Graduate School of Biomedical Sciences, Weill Medical College of Cornell University, New York, NY 10065; [11] Department of Physiology and Biophysics, Weill Cornell Medical College, 1305 York Ave., New York, NY 10065, USA; [12] Tri-Institutional Laboratory of Comparative Pathology, Memorial Sloan-Kettering Cancer Center, Weill Cornell Medical College, Rockefeller University, New York, NY 10065; [13] Department of Biochemistry & Molecular Genetics, University of Alabama, Birmingham, AL 35294; [14] Department of Pathology, Memorial Sloan-Kettering Cancer Center, New York, NY 10065

[15] These authors contributed equally to this work.

[16] **Correspondance:**
Ross L. Levine, M.D.
Human Oncology and Pathogenesis Program
Leukemia Service, Department of Medicine
Memorial Sloan Kettering Cancer Center
1275 York Avenue, Box 20
New York, NY 10065
leviner@mskcc.org
Phone: 646-888-2767
or to: Iannis Aifantis, Ph.D.
Howard Hughes Medical Institute
Department of Pathology
NYU School of Medicine
522 First Avenue, SRB 1303
New York, NY, 10016, USA
Email: iannis.aifantis@nyumc.org

Condensed title: Conditional deletion of Asxl1 results in MDS

Character count: 45,168

Abstract:

Somatic *Addition of Sex Combs Like 1* (*ASXL1*) mutations occur in 10-30% of patients with myeloid malignancies, most commonly in myelodysplastic syndromes (MDS), and are associated with adverse outcome. Germline *ASXL1* mutations occur in patients with Bohring-Opitz Syndrome. Here we show that constitutive loss of *Asxl1* results in developmental abnormalities including anopthalmia, microcephaly, cleft palates, and mandibular malformations. By contrast, hematopoietic-specific deletion of *Asxl1* resulted in progressive, multilineage cytopenias and dysplasia in the context of increased numbers of hematopoietic stem/progenitor cells (HSPCs), characteristic features of human MDS. Serial transplantation of *Asxl1*-null hematopoietic cells resulted in a lethal myeloid disorder at a shorter latency than primary *Asxl1* knockout mice. *Asxl1* deletion reduced hematopoietic stem-cell self-renewal, which was restored by concomitant deletion of *Tet2*, a gene commonly co-mutated with *ASXL1* in MDS patients. Moreover, compound *Asxl1/Tet2* deletion resulted in an MDS phenotype with hastened death compared to single-gene knockout mice. *Asxl1* loss resulted in a global reduction of H3K27 trimethylation and dysregulated expression of known regulators of hematopoiesis. RNA-seq/ChIP-seq analyses of Asxl1 in hematopoietic cells identified a subset of differentially expressed genes as direct targets of Asxl1. These findings underscore the importance of Asxl1 in Polycomb-group function, development, and hematopoiesis.

Introduction

Candidate gene and genome-wide discovery studies have identified a set of novel disease alleles in patients with myelodysplastic syndromes (MDS), acute myeloid leukemia (AML), and myeloproliferative neoplasms (MPN). These include somatic mutations in genes with a known, or putative role in the epigenetic regulation of gene expression (Shih et al., 2012). *Addition of Sex Combs Like 1 (ASXL1)* is a Polycomb-associated protein which has been shown to be an essential co-factor for the nuclear deubiquitinase BAP1 (Dey et al., 2012) as well as a critical mediator of the function of the Polycomb repressive complex 2 (PRC2) (Abdel-Wahab et al., 2012). Recurrent somatic loss-of-function mutations and deletions in *ASXL1* are observed in MDS, MPN, and AML patients (Gelsi-Boyer et al., 2009). *ASXL1* mutations are most common in MDS patients (Bejar et al., 2011; Bejar et al., 2012; Sanada and Ogawa, 2012; Thol et al., 2011) including in 15-20% of MDS patients and in 40-60% in patients with MDS/MPN overlap syndromes (Boultwood et al., 2010; Gelsi-Boyer et al., 2009; Jankowska et al., 2011). *ASXL1* mutations are associated with adverse overall survival in MDS, chronic myelomonocytic leukemia (CMML), AML, and MPN (Bejar et al., 2011; Bejar et al., 2012; Itzykson et al., 2013; Metzeler et al., 2011; Patel et al., 2012; Vannucchi et al., 2013), highlighting the relevance of *ASXL1* mutations to myeloid transformation and clinical outcome.

More recently, *de novo* constitutive *ASXL1* mutations were identified in children with the developmental disorder Bohring-Optiz Syndrome (Hoischen et al., 2011; Magini et al., 2012). Although these genetic data strongly implicate *ASXL1* mutations in myeloid malignancies and in developmental defects, our understanding of the role of Asxl1 in steady-state hematopoiesis, hematopoietic stem/progenitor function, and myeloid malignances has been limited by a lack of murine model for conditional- and tissue-specific deletion of Asxl1. Fisher *et al.* investigated the role of Asxl1 in hematopoiesis through the creation and analysis of a model of constitutive *Asxl1* deletion with targeted insertion of a neo cassette into the *Asxl1* locus (Fisher et al., 2010a; Fisher et al., 2010b). Disruption of *Asxl1* expression in this manner resulted in partial perinatal lethality. Analysis of the remaining aged (beyond 15 weeks of age) *Asxl1* mutant mice revealed impairment of B and T cell lymphopoiesis and myeloid differentiation. However, constitutive *Asxl1* loss did not alter long-term reconstitution in competitive repopulation studies using *Asxl1-null* fetal liver cells (Fisher et al., 2010a; Fisher et al., 2010b). These results suggested that *Asxl1* has an important role in normal hematopoiesis, however the effects of somatic loss of *Asxl1* in

hematopoietic cells was not evaluated. Here we investigate the effects of *Asxl1* loss in a time- and tissue-dependent manner through the generation of a murine model for conditional deletion of *Asxl1*. We also characterized the effect of *Asxl1* loss on transcriptional output and gene regulation using epigenomic and transcriptomic analysis of hematopoietic stem and progenitor cells from wildtype and *Asxl1* deficient mice.

Results

Development of a Conditional *Asxl1* Knockout Allele

In order to delineate the role of *Asxl1* in development and in hematopoiesis, we generated a conditional allele targeting *Asxl1 in vivo* (**Fig. 1A** and **Fig. 1B**). We utilized ES cell targeting to insert two LoxP sites flanking exons 5-10 of *Asxl1,* as well as an Frt-flanked neomycin selection cassette in the upstream intron (**Fig. 1A** and **Fig. 1B**). The generated mice (*Asxl1$^{fl/fl}$*) were initially crossed to a germline Flp-deleter murine line to eliminate the neomycin cassette, and then subsequently crossed to germline *EIIa-cre* mice, IFNα-inducible *Mx1-cre*, and hematopoietic-specific *Vav-cre* (all as described below). Asxl1 protein expression was not detectable in hematopoietic tissue from *Vav-cre* and *Mx1-cre* mice (**Fig. 2B**) consistent with generation of a knockout allele.

Germline *Asx1* loss results in Embryonic Lethality and Craniofacial Abnormalities

We characterized the effects of constitutive deletion of *Asxl1* by crossing mice bearing floxed *Asxl1* alleles with germline *EIIa*-cre mice. The Asxl1 floxed allele was completely recombined in *EIIa-cre Asxl1$^{fl/fl}$* mice (data not shown). We observed 100% embryonic lethality in mice with germline complete deletion of *Asxl1* (*Asxl1$^{\Delta/\Delta}$*) while mice with heterozygous germline deletion of Asxl1 (*Asxl1$^{+/\Delta}$*) were born at expected Mendelian ratios (**Fig. 1C**). *Asxl1$^{\Delta/\Delta}$* mice were no longer viable by E19.5 and were characterized by micro-/anopthalmia (seen in 12/12 of homozygous *Asxl1*-null embryos examined) (**Fig. 1D** and **1E**), frequent cleft palates (seen in 5/12 of homozygous *Asxl1*-null embryos examined) (**Fig. 1E**), and multiple skeletal abnormalities (mandibular hypoplasia, loss of hyoid bone formation, and posterior homeotic transformations) (seen in 4/12 of homozygous *Asxl1*-null embryos examined) (**Fig. 1F**). *Asxl1$^{+/\Delta}$* were viable but exhibited craniofacial dysmorphism in 35% (14/40) of adult *Asxl1$^{+/\Delta}$* mice examined (**Fig. 1G**). Immunophenotypic analysis of hematopoietic stem/progenitor and erythroid

4

precursor cells in fetal liver from control, $Asxl1^{+/\triangle}$, and $Asxl1^{\triangle/\triangle}$ mice at E14.5 did not reveal differences amongst the genotypes (**Fig. 1H-I**).

Hematopoietic Specific Deletion of *Asxl1* results in MDS

Asxl1 is expressed throughout the adult hematopoietic compartment (**Fig. 2A**). In order to elucidate the effects of *Asxl1* loss on post-natal hematopoiesis, $Asxl1^{fl/fl}$ mice were crossed to *Vav-cre* and IFNα-inducible *Mx1-cre* transgenic mice for conditional deletion of *Asxl1* in the hematopoietic compartment (termed as *Asxl1* KO hereafter). In both cases, Asxl1 protein expression was not detectable in hematopoietic tissue (**Fig. 2B**). Mice with hematopoietic-specific deletion of *Asxl1* (*Vav-cre Asxl1*$^{fl/fl}$) developed progressive bone marrow (BM) and splenic hypocellularity relative to littermate controls (Cre-negative $Asxl1^{fl/fl}$) beginning at 6 weeks of age and likewise evident at 24 weeks of age (n=6-10 mice per genotype at each timepoint examined) (**Fig. 2C**). *Asxl1* KO mice, but not littermate controls, developed progressive leukopenia (**Fig. 2D**) and anemia (**Fig. 2E**) that was most apparent at 6-12 months of age. While the hemoglobin (Hb) in *Asxl1* KO mice was within normal limits (median of 13.4g/dL, range 12.9-14.8g/dL) in mice <6 months of age, between 6-12 months the Hb was a median of 8g/dL (range 1.94-13.9g/dL) in KO mice relative to a median of 11.4g/dL in age-matched littermate control mice (range, 7.17-14.2g/dL) (n=6-12 mice with each genotype at each timepoint examined) (**Fig. 2E**). Similarly, the white blood cell count (WBC) was within normal limits in *Asxl1*-null mice at less than 6 months of age (median, 7.64 cells x 10^9/uL; range 4.66-9.6), the WBC count fell to a median of 2.51 cells x 10^9/uL (range 0.88-5.18) in *Asxl1* KO mice between the ages of 6-12 months compared with age-matched littermate *Asxl1* wildtype mice (median WBC count 4.51 cells x 10^9/uL; range 2.62-13.8) (**Fig. 2D**). The leukopenia was due predominantly to decrements in B220+ mature B-cells, CD11b+ Gr1+ neutrophils, and CD11b+ Gr1-negative monocytes as indicated by flow cytometric and morphologic analysis of peripheral blood (**Fig. 2F-G**). The age-dependent anemia observed in *Asxl1* KO mice was accompanied by an increase (median 1.4- to 2-fold) in CD71-positive/Ter119-negative erythroid precursor cells in both the bone marrow and spleen consistent with impaired erythroid differentiation (**Fig. 3A**).

Pathologic analysis of *Asxl1* KO hematopoietic tissues at 6 months of age revealed morphologic dysplasia of circulating myeloid cells (**Fig. 3D**), frequent circulating nucleated red cells (**Fig. 3D**), hypocellular marrow (**Fig. 3B**), and dysplasia of erythroid precursors (**Fig. 3C**). Previous characterization of

hematopoetic stem and progenitor cells from patients with MDS (Martínez-Jaramillo and Flores-Figueroa…, 2002; Sawada et al., 1995; Sawada et al., 1993) and murine models of MDS (such as the *NUP98-HOXD13* transgenic mouse model (Choi et al., 2008)) have identified an impairment of sorted hematopoietic progenitors to form colonies *ex vivo* in methylcellulose containing myeloid and erythroid cytokines. Consistent with these prior observations and the impairment in mature myeloid and erythroid differentiation seen in *Asxl1*-deficient mice, *in vitro* analysis of sorted myeloid progenitor cells from 6-week-old *Asxl1* KO and control mice revealed a clear decrease in colony output of sorted common myeloid progenitor (CMP), granulocyte/macrophage progenitor (GMP), and megakaryocyte/erythroid progenitors (MEP) in KO versus control mice (**Fig. 3E-F**).

Consistent with the age-dependent development of impaired myeloid and erythroid output in *Asxl1* KO mice compared with age-matched littermate controls, *Asxl1* KO (*Mx1-cre Asxl1^{fl/fl}*) mice were found to have infiltration of liver with hematopoietic cells consistent with extramedullary hematopoiesis (EMH) with *Asxl1* deletion (**Fig. 3G**). In order to ascertain if this hematopoietic infiltrate represented inflammatory infiltration of hematopoietic cells versus EMH, we plated 200,000 cells harvested from the liver of *Asxl1* KO mice and littermate controls in methylcellulose semi-solid media containing myeloid-erythroid cytokines (rmIL-3, rmSCF, rh-EPO, and rh-IL6). Colonies plated with cells derived from *Asxl1* KO mice alone yielded abundant colonies (**Fig. 3H-I**) demonstrating EMH.

Cell Autonomous Effects of *Asxl1* loss

Transplantation of whole BM from Asxl1 KO (*Vav-cre Asxl1^{fl/fl}*) mice into lethally irradiated recipients resulted in a penetrant, lethal hematopoietic disorder (**Fig. 4A**) indicating that the phenotype induced by *Asxl1* loss was cell-autonomous. For example, transplantation of whole BM from 70-week-old primary *Asxl1* KO mice into lethally irradiated recipients resulted in death of recipient mice at a median of 50-weeks after transplant (range, 41-74 weeks) whereas no mice transplanted with *Asxl1* wildtype BM died during this period of observation. Further, serial transplantation into tertiary recipients resulted in shorter latency disease with mice dying 24-42 weeks after transplant (median of 28 weeks). Transplantation of purified lineage-negative Sca-1+ c-KIT+ (LSK) cells from the BM of secondary recipients led to a lethal myeloid disease in all tertiary transplant recipients with more rapid onset (10.3 median weeks, range 5.1-10.6

weeks) than transplantation of unfractionated BM cells from the same secondary recipients (**Fig. 4A**). Disease in transplanted mice was characterized by progressive anemia and cachexia (**Fig. 4B-C**), BM hypocellularity (**Fig. 4D**), and an increase in the relative frequency of hematopoietic stem and progenitor cells (HSPCs) in both the BM and the spleen (**Fig. 4E-F**). This was accompanied by splenomegaly due to EMH and effacement of splenic architecture (**Fig. 4G-I**). Anemia in the KO-transplanted recipient mice was evident even with gross inspection of bones (**Fig. 4J**). As in primary *Asxl1* KO mice this anemia occurred despite an increase in erythroid precursors in both the BM and spleen (**Fig. 4K-L**), consistent with a block in erythroid differentiation with *Asxl1* loss. This block in erythroid differentiation was characterized by a significant increase in CD71+/Ter119 double-positive erythroid precursors in the spleen (**Fig. 4L**).

Impaired Self-Renewal of Asxl1 Deficient Cells is Rescued by Concomitant Tet2 loss

We next assessed the effects of *Asxl1* loss on hematopoietic stem cell (HSC) frequency and function. We observed an increase in the absolute number of immunophenotypically-defined HSPCs in Asxl1 KO (*Vav-cre Asxl1$^{fl/fl}$*) mice at 6-weeks of age, including LT-HSC (CD150+CD48-Lin-Sca-1+c-Kit+) cells **(Fig. 5A** and **5B**) (quantified as the total number of live cells per femur). Although the number of immunophenotypic stem/progenitor cells was increased, we observed a decrease in serial plating *in vitro* in *Asxl1* KO cells (**Fig. 6A**) suggesting a potential defect in self-renewal. To assess the effects of *Asxl1* deletion *in vivo,* 500,000 whole BM nucleated cells from 6-week-old CD45.2 *Vav-cre Asxl1$^{fl/fl}$* mice or *Asxl1fl/fl* littermate controls were transplanted in competition with an equal number of 6-week-old CD45.1 competitor BM cells into lethally irradiated CD45.1 recipient mice (**Fig. 5C**). Chimerism was assessed based on evaluation of the ratio of CD45.1 to CD45.2 peripheral blood mononuclear cells beginning 2 weeks following transplantation and then monitored on a monthly basis until 16 weeks thereafter. Consistent with the *in vitro* data, we observed a clear reduction in self-renewal *in vivo. Asxl1* KO HSPCs had a significant disadvantage in competitive transplantation that was further accentuated with serial transplantation (**Fig. 5C** and **5D**).

After the final assessment of chimerism in the primary competitive transplantation experiments, primary recipient mice were sacrificed and a serial competitive transplantation experiment was carried out by transplanting 1 million whole bone marrow cells from primary recipient mice into lethally irradiated

CD45.1 secondary recipient mice (**Fig. 5D**). Serial competitive transplantation revealed an even further competitive disadvantage in *Asxl1*-deficient HSPCs (**Fig. 5D**).

Given that MDS is characterized by impaired myeloid differentiation, multilineage cytopenias, and clonal dominance over time, we hypothesized that mutations that occur in concert with *ASXL1* deletion/mutation in MDS might compensate for the impaired self-renewal observed with Asxl1 loss. Previous studies have shown that mutations in *TET2* are most commonly observed with mutations in *ASXL1* in MDS (Bejar et al., 2011; Bejar et al., 2012). We and others previously demonstrated increased hematopoietic self-renewal in Tet2-deficient mice (Ko et al., 2011; Li et al., 2011; Moran-Crusio et al., 2011; Quivoron et al., 2011). We analyzed the *in vitro* and *in vivo* phenotype of *Vav-cre Asxl1$^{fl/fl}$ Tet2$^{fl/fl}$* hematopoietic cells compared with control, *Vav-cre Asxl1$^{fl/fl}$*, and *Vav-cre Tet2$^{fl/fl}$* mice (**Fig. 6A**). Colony assays of whole BM cells from the same mice revealed reduced serial replating activity of *Asxl1* KO cells but restored serial-replating capacity of cells with compound *Asxl1/Tet2* loss (**Fig. 6A**). More importantly, competitive transplantation studies revealed a competitive advantage for *Vav-cre Asxl1$^{fl/fl}$ Tet2$^{fl/fl}$* whole BM compared to matched CD45.1 competitor BM (**Figs. 6B-D**). These data demonstrate concurrent Tet2 loss restores the self-renewal defect induced by *Asxl1* loss.

Concomitant deletion of *Asxl1* and *Tet2 in vivo* results in MDS

Given the restoration of self-renewal noted in mice with concomitant deletion of *Tet2* and *Asxl1* in the context of a competitive transplantation experiment*,* we investigated the phenotype of mice with compound deletion of *Tet2* and *Asxl1* compared with mice with deletion of each gene alone. A cohort of primary Cre-negative *Asxl1* wildtype *Tet2* wildtype, *Mx1-cre Asxl1$^{fl/fl}$* (*Asxl1 KO*), *Mx1-cre Tet2$^{fl/fl}$* (*Tet2 KO*), and *Mx1-cre Asxl1$^{fl/fl}$ Tet2 $^{fl/fl}$* (double knockout (DKO)) mice were treated with pIpC at 4 weeks of life and followed up to 50 weeks following birth (46 weeks following pIpC administration). At the end of this observation period, 40% of DKO mice (4/10) and 17.7% of Tet2 KO died (1/6) whereas no *Asxl1* KO (0/12) or control mice (0/5) died (**Fig. 7A**).

For further analyses, in order to obtain a sufficiently large number of mice for each genotype, BM from 6-week-old CD45.2 *Mx1-cre Asxl1* wildtype *Tet2* wildtype, *Mx1-cre Asxl1$^{fl/fl}$* (*Asxl1 KO*), *Mx1-cre Tet2$^{fl/fl}$* (*Tet2 KO*), and *Mx1-cre Asxl1$^{fl/fl}$ Tet2 $^{fl/fl}$* (double knockout (DKO)) mice were transplanted into lethally irradiated CD45.1 recipient mice (10 recipient mice per genotype). All recipient

mice (including those transplanted with *Mx1-cre Asxl1* wildtype *Tet2* wildtype bone marrow) were then treated with pIpC 2 weeks following transplantation to delete *Tet2* and/or *Asxl1*. At 72 weeks post-transplant *Asxl1*-null and/or *Asxl1/Tet2* compound-null mice had significantly lower WBC counts and hematocrit compared with wildtype or *Tet2* single KO control mice (**Fig. 7B-C**). As seen in mice with primary deletion of *Asxl1, Asxl1* KO mice here had reduced BM cellularity compared with control or *Tet2* KO mice (**Fig. 7D**). However, despite the similar blood counts between *Asxl1* KO and DKO mice, the DKO had greater BM cellularity than mice with deletion of just *Asxl1* or even *Tet2* (**Fig. 7D**). Examination of the HSPC compartment across mice with the 4 genotypes at 72 weeks indicated a greater total number as well as relative frequency of LSK and myeloid progenitor cells in the BM of DKO mice compared with other groups (**Fig. 7E-F**). Morphologically, BM of *Asxl1* KO mice was characterized by the presence of dysplastic erythroid precursor cells as seen in primary Asxl1 KO mice earlier (**Fig. 7G**). The BM of DKO mice likewise was characterized by a similar presence of dysplastic erythroid precursors as well as dysplastic myeloid cells (**Fig. 7G**) but lacked the hypocellularity seen in the BM of mice with Asxl1 deletion alone (**Fig. 7D**). Histologic analysis of liver tissue revealed increased hematopoietic cell infiltration in DKO mice compared with the other groups (**Fig. 7H**). The presence of morphologic dysplasia in precursor cells, decrease in peripheral circulating mature cells, and concurrent increased total BM cells and HSPC's were suggestive of the presence of MDS in the *Asxl1/Tet2* compound-deficient mice.

Transcriptional Effects of Asxl1 Loss

In order to understand the basis for the impaired myeloid differentiation and self-renewal observed with *Asxl1* loss we performed expression analysis of sorted LSK and MP cells from cytopenic 1 year old *Asxl1* KO mice and age-matched littermate controls (**Fig. 8A-B; Supplemental Tables 1-2**). Analysis of RNA-seq data identified a set of differentially expressed genes in Asxl1 KO LSK cells (797 genes) and MP cells (1095 genes). Integrative analysis identified a set of 75 genes that were differentially expressed in Asxl1 KO LSK and MP cells, including 41 up-regulated and 34 down-regulated genes in Asxl1 KO mice relative to controls (**Fig. 8B**).

Consistent with previous *in vitro* data (Abdel-Wahab et al., 2012), we observed increased expression of posterior *HoxA* genes in Asxl1 KO LSK cells, including *HoxA7* and *HoxA9* as well as the *Hox*-associated transcription factors *Hes5* and *Gdf11* (**Fig. 8C**). *Meis1* was not up-regulated with Asxl1 loss

consistent with prior reports in *in vitro* systems (Abdel-Wahab et al., 2012) (**Fig. 8C**). We also noted a progressive, age-dependent increase $p16^{INK4a}$ expression in LT-HSC and multipotent progenitor cells (MPP; lineage-negative Sca-1+ c-KIT+ CD48+ CD150-negative) of Asxl1 KO mice compared with age-matched controls (**Fig. 8D**). The $p16^{INK4a}$ locus is a known PRC2 target (Bracken et al., 2007; Hidalgo et al., 2012; Jacobs et al., 1999; Tanaka et al., 2012) and *in vitro* loss of Asxl1 has been linked to defective Polycomb repression and reduced H3K27 methylation (Abdel-Wahab et al., 2012). Given the increase in $p16^{INK4a}$ expression in KO MPP cells from *Asxl1* KO mice, we examined the *in vivo* cell proliferation of MPP cells from 72-week-old *Asxl1* KO (*Vav-cre Asxl1$^{fl/fl}$*) versus control mice (Cre-negative *Asxl1$^{fl/fl}$*) via an *in vivo* 5-bromo-2-deoxyuridine (BRDU) incorporation assay. The MPP cells of *Asxl1* KO mice showed a significant decrease in S-phase compared with littermate control cells (**Fig. 8E**). Flow-cytometric quantitative assessment of apoptosis in LSK cells of the same mice revealed a significant increase in Annexin-V+/DAPI-negative and Annexin-V+/DAPI-positive LSK cells (**Figure 8F**; n=5 mice per group) consistent with cell cycle exit and an increase in apoptosis *in vivo.*

In order to understand what transcriptional differences might exist between mice with compound deletion of Asxl1 and Tet2 relative to mice with deletion of *Asxl1*, *Tet2,* or neither gene, we performed RNA-Seq on LSK cells sorted from the BM of 6-week-old *Mx1-cre Asxl1* wildtype *Tet2* wildtype, *Mx1-cre Asxl1$^{fl/fl}$, Mx1-cre Tet2$^{fl/fl}$,* and *Mx1-cre Asxl1$^{fl/fl}$ Tet2$^{fl/fl}$* mice (**Fig. 8G; Supplemental Table 3**). Of the 1,744 genes significantly up-regulated in any knockout mice relative to controls, the majority of these genes were shared between Asxl1 KO and Tet2 KO LSKs but not DKO LSKs (32.6% of up-regulated genes (569/1,744 genes)) followed by genes shared between Asxl1 KO, Tet2 KO, and DKO mice (29.2% of up-regulated genes (510/1,744 genes)). Likewise, for the 1,363 significantly down-regulated genes, the majority of these were shared between Asxl1 KO and Tet2 KO LSKs but not DKO LSKs (37.6% of up-regulated genes (513/1,363 genes)) followed by genes shared between Asxl1 KO, Tet2 KO, and DKO mice (28.0% of up-regulated genes (382/1,363 genes)).

We next performed gene set enrichment analysis (GSEA) to identify gene sets enriched in HSPC's from Asxl1 KO mice or Asxl1/Tet2 DKO mice compared with other groups (Subramanian et al., 2005). We identified gene sets enriched in hematopoietic stem cells (Ramalho-Santos et al., 2002) and apoptosis (http://www.genome.jp/kegg/pathway/hsa/hsa04210.html) in mice with *Asxl1* deletion and with concomitant *Asxl1*/*Tet2* deletion (**Figure 8H**). We also identified

gene sets which were uniquely enriched in *Tet2/Asxl1* DKO mice and not seen in the other groups. This prominently included gene sets characteristic of apoptosis signatures, purified HSPCs (Ivanova et al., 2002), cell cycle regulators (http://www.genome.jp/kegg/pathway/hsa/hsa04110.html), and signatures from *MLL*-rearranged primary leukemias (Mullighan et al., 2007; Ross et al., 2003)(**Figure 8I**).

Genome-wide binding of Asxl1 and global effects of Asxl1 loss on the epigenome

Asxl1 has been shown to interact with epigenetic modifiers known to impact transcription (Dey et al., 2012) (Abdel-Wahab et al., 2012). This includes binding to the core members of the Polycomb Repressive Complex 2 (PRC2) where loss of *ASXL1* has previously been found to result in global downregulation of histone H3 lysine 27 (H3K27) methylation (Abdel-Wahab et al., 2012) *in vitro* and in *ex vivo ASXL1* mutant primary patient samples. Consistent with this, H3K27 trimethyl (H3K27me3) levels were significantly reduced after *Asxl1* deletion (**Fig. 9A**) despite sustained expression of the core Polycomb-repressive complex 2 (PRC2) components (**Fig. 9B**).

Although the effects of Asxl1 loss on transcription due to alterations in histone post-translational modifications has previously been described (Abdel-Wahab et al., 2012), direct transcriptional targets of Asxl1 through characterization of Asxl1 binding throughout the genome has never previously been assessed. We therefore performed chromatin-immunoprecipitation for Asxl1 followed by DNA sequencing (ChIP-Seq) in purified murine myeloid hematopoietic cells. Asxl1 was found to bind to many sites throughout the genome with the majority of significantly enriched Asxl1 peaks (78%) located at CpG-rich transcription start sites (**Fig. 9C-E** and **Supplemental Tables 4-5**). Motif enrichment analysis of the Asxl1-binding sites revealed that the top occurring motifs are most similar to known binding sites of Ets family of transcription factors (**Fig. 9F;** p=1e^{-59}, %target = 40.1%, % background = 21.4%). A significant subset of genes with dysregulated expression in Asxl1 KO LSK/MP cells were confirmed as direct targets of Asxl1 in our ChIP-Seq analysis (14 up-regulated genes and 9 down-regulated genes) (**Table 1**).

Discussion

Here we identify that conditional deletion of *Asxl1*, a gene commonly mutated in human MDS, in hematopoietic cells resulted in the development of

progressive anemia and leukopenia with concomitant multilineage myeloid dysplasia *in vivo*. *Asxl1* deletion was associated with an increase in the frequency and total number of HSPCs, increased apoptosis, and altered cell cycle distribution of HSPC's *in vivo*. Asxl1 loss also led to a reduction in myeloid colony output. MDS is characterized by variable cytopenias due to ineffective production of mature granulocyte, erythroid, and/or megakaryocyte populations and a risk of transformation to AML. Functional characterization of primary samples from patients with MDS has identified an expansion of the primitive hematopoietic stem cell compartment (comprised of long-term and short-term HSC's) (Pang et al., 2013; Will et al., 2012), the presence of specific genetic alterations throughout the diseased clone originating in the most immature HSC's (Nilsson et al., 2000; Nilsson et al., 2007; Pang et al., 2013; Tehranchi et al., 2010; Will et al., 2012), dysplastic clonogenic activity of HSCs with reduced *in vitro* colony formation from MDS-derived HSC's (Martínez-Jaramillo and Flores-Figueroa…, 2002; Sawada et al., 1995; Sawada et al., 1993; Will et al., 2012), and an increase in the frequency and absolute number of HSPC's in the setting of decreased mature circulating cells with a concomitant increase in apoptosis of HSPCs in MDS patients (Pang et al., 2013; Sawada et al., 1995; Sawada et al., 1993). Taken together, the phenotype of *Asxl1* loss recapitulates these central features of human MDS.

One aspect of the *Asxl1* conditional knockout mouse model which differs from human MDS is the BM hypocellularity observed in *Asxl1* KO mice, in contrast to the increased BM cellularity in most MDS patients. Nevertheless, the impaired production of mature myeloid and erythroid cells in the context of an increased relative and total numbers of HSPCs in *Asxl1* conditional knockout mice does recapitulate key features of human MDS. Moreover, concomitant loss of *Asxl1* and *Tet2* which are commonly mutated in concert in human MDS, resulted in increased BM cellularity and disease severity with pathologic evidence of multi-lineage dysplasia.

In contrast to MPN and AML, there are few previously described models of MDS, and to date no models of MDS based on mutations in recurrently mutated MDS disease alleles. The most widely utilized model of MDS is based on transgenic expression of a *NUP98-HOXD13* fusion allele (Lin et al., 2005). Although this model has many of the characteristic features of human MDS, the *NUP98-HOXD13* fusion was identified in a young patient with therapy-related AML (Raza-Egilmez et al., 1998) and has not been identified in MDS patients to date. By contrast, *ASXL1* mutations occur in 15-20% of patients with MDS.

Prior studies of the effects of *Asxl1* loss on development and hematopoiesis were performed using a constitutive *Asxl1* KO mouse model (Fisher et al., 2010a; Fisher et al., 2010b). Our conditional model allows for evaluation of the effects of post-natal deletion of *Asxl1* and obviates the problems associated with a high-frequency of perinatal lethality in mice with constitutive *Asxl1* deletion. Notably, Fischer *et al.* identified a 72% reduction in the expected number of *Asxl1* homozygous KO mice by post-natal day 21; when mice were backcrossed >8 generations to a consistent genetic background, KO mice were 100% embryonic lethal, preventing analysis of adult constitutive *Asxl1* KO mice. Similar to the germline model, we observed an age-dependent decrease in mature B lymphocytes, splenomegaly due to extramedullary hematopoiesis, and decreased formation of myeloid and erythroid colonies from *Asxl1* KO cells (Fisher et al., 2010a; Fisher et al., 2010b). In addition, Fisher *et al.* observed dysregulated expression of *HoxA* genes and homeotic transformation of homozygous *Asxl1*-mutant embryos (Fisher et al., 2010a; Fisher et al., 2010b), consistent with the current *Asxl1* germline and conditional KO models described in this report.

Despite these similarities, a number of differences exist, however, between the two models. First, no reproducible differences in peripheral blood counts, bone marrow cellularity or bone marrow cell morphology were seen in *Asxl1* constitutive KO mice. In contrast, mice with conditional, homozygous, post-natal deletion of *Asxl1* developed leukopenia, anemia, myelo-erythroid dysplasia and bone marrow hypocellularity starting at 6 months of life. This could be due to differences in the strain of the mice analyzed, the timing of *Asxl1* loss, or cell non-autonomous effects observed in the constitutive knockout model.

Of note, the more profound hematologic abnormalities seen with serial competitive and non-competitive transplantation of *Asxl1* conditional KO hematopoietic cells here have no counterpart in the reports of the prior constitutive KO model as serial transplantation was not performed in the prior studies. The marked impairment in serial transplantability observed with *Asxl1* loss is consistent with the progressive defects in hematopoietic stem cell function observed in mice with other alterations in other Polycomb-group function (Ohta et al., 2002).

Although non-competitive transplantation studies demonstrated that the MDS phenotype was cell autonomous, Asxl1-deficiency was associated with a defect in hematopoietic stem cell self renewal in competitive transplantation assays and in *in vitro* colony formation. These data suggested that concurrent

genetic or epigenetic alterations in *ASXL1*-mutant MDS cells must promote self-renewal to allow for clonal dominance of MDS cells. Indeed, concurrent *Tet2* loss restored the self-renewal defect induced by *Asxl1* loss. Moreover, mice with concomitant loss of *Asxl1* and *Tet2* developed a larger increase in HSPCs, increased BM cellularity, and decreased numbers of circulating mature cells compared with single gene knockout mice. This phenotype is consistent with more severe MDS and suggests a functional interdependency between these two disease alleles in MDS. Subsequent studies may identify additional disease alleles which can rescue the self-renewal defect seen in *ASXL1*-deficient stem cells, and may lead to the identification of additional mutational interdependencies in MDS and in other malignant contexts.

We previously demonstrated loss of *ASXL1 in vitro* results in global downregulation in H3K27me3 (Abdel-Wahab et al., 2012), the repressive histone modification placed by the PRC2. Here we demonstrate *Asxl1* deletion in the hematopoietic compartment results in reduced H3K27me3 *in vivo*. We used ChIP-Seq for Asxl1 itself to show that Asxl1 is enriched at gene-promoter regions throughout the genome suggesting a potential role for Asxl1 in direct regulation of gene transcription. In addition, motif enrichment analysis of Asxl1-binding sites revealed enrichment in known binding sites of the Ets family of transcription factors. The significant overlap between genome-wide binding of *Asxl1* and Ets family members is a critically supportive of the importance of Asxl1 in hematopoiesis as Ets family of transcription factors are very well understood to play a key role in the growth, survival, differentiation, and activation of hematopoietic cells (Choi et al., 2008; Koschmieder et al., 2005; Mizuki et al., 2003; Steidl et al., 2006; Vangala et al., 2003). Deletion, mutation, and translocation of ETS family members are well-described in myeloid malignancies (Gilliland, 2001), including *ETV6* mutations/translocations in MDS and CMML (Haferlach et al., 2012) and loss-of-function mutations of *PU.1* in AML (Mueller et al., 2002). Moreover, common oncogenic events seen in patients with myeloid malignancies have been demonstrated to transform myeloid cells through suppression of expression of key Ets members. For example, *FLT3-ITD* mutations and the AML1-ETO (t(8;21)) fusion oncoprotein have been demonstrated to suppress PU.1 expression and function (Mizuki et al., 2003; Vangala et al., 2003). In addition, down-regulation of PU.1 expression results in impaired myeloid differentiation (Rosenbauer et al., 2004; Steidl et al., 2006). Further work to understand the involvement of individual Ets family members and/or a shared transcriptional program between Asxl1 loss and Ets family

member loss (Steidl et al., 2006) in the pathogenesis of *ASXL1*-mutant myeloid malignancy will be critical.

Taken together, our studies reveal that deletion of *Asxl1* results in craniofacial and skeletal developmental abnormalities and mice with hematopoietic-specific *Asxl1* loss developed hallmark features of MDS, including progressive ineffective hematopoiesis, impaired myeloid differentiation, multi-lineage dysplasia, and increased apoptosis and altered cell cycle regulation of HSPCs. Given the paucity of murine models of human MDS based on known, recurrent MDS disease alleles, we believe the development of a genetically accurate model of MDS will inform subsequent studies aimed to elucidate the molecular basis for MDS and to develop novel therapies for MDS patients.

Acknowledgments

Author Contributions

O.A.-W., J.G., I.A. and R.L.L. designed the study. O.A.-W., J.G., M.M.A., Y.R.C., J.Y.S., P.K.B., O.A.G., E.K., L.T. and S.P. performed the experiments. D.N.-L., L.M.L.., A.H.S., and S.P. helped with animal generation, genotyping, and maintenance. S.M. and C.Y.P. performed phenotypic and histologic analysis of tissues. J.E.T., and J.D.J performed histone mass spectrometric analysis. M.A.A., A.D., T.T., R.K., C.K., V.D., and B.E.B. performed chromatin immunoprecipitation and sequencing analysis. O.A.-W., J.G., M.M.A., T.T., T.H., C.K., R.K., S.L. and C.E.M. analyzed the data. O.A.-W., J.G., I.A., and R.L.L. prepared the manuscript with input from the other authors.

Competing Financial Interests

The authors declare no competing financial interests.

Figure 1: Generation of a conditional *Asxl1* allele and characterization of mice with constitutive *Asxl1* loss. (A) Schematic depiction of the targeted *Asxl1* allele. Exons 5-10 are targeted and flanked by *LoxP* sites upon Frt-mediated deletion of the Neo cassette. (B) Verification of correct homologous recombination of Asxl1 targeted allele using Southern blots on targeted ES cells. (C) Enumeration of offspring derived from mating *EIIa-cre Asxl1$^{+/\Delta}$* parents reveal that homozygous constitutive deletion of *Asxl1* (*Asxl1$^{\Delta/\Delta}$*) is associated with 100% prenatal lethality. Although *Asxl1$^{\Delta/\Delta}$* mice are observed at 14.5 and 18.5 days post-coitus (dpc), fetal mice with germline homozygous loss of *Asxl1* are characterized by lack of eyes as shown by gross pathology (D) and tissue sections at E14.5 and E18.5 (E; section 1 and 2). Germline *Asxl1* null mice are also characterized frequent cleft palates (E; section 2). (F) Skeletal preparations from germline *Asxl1* null mice surviving to day E20.5 reveal frequent skeletal abnormalities including hypoplastic mandibles (asterisk), lack of hyoid bone (arrowhead), and lower lumbar/sacral posterior homeotic transformations (arrow). (G) Gross phenotype of *EIIa-cre Asxl1$^{+/\Delta}$* and littermate control mice revealing bilateral micro-opthalmia in *EIIa-cre Asxl1$^{+/\Delta}$* mice. (H) Immunophenotyping of fetal liver at day 14.5 days post-coitus (dpc) reveals no major alterations in the relative frequency of lineage-negative Sca-1+ Kit+ (LSK), multipotent progenitors (MPP; LSK, CD48+, CD150- cells), and long-term hematopoietic stem cells (LT-HSC; LSK, CD48-, CD150+ cells) between mice with germline loss of 0, 1, or 2 copies of *Asxl1*. FACS analysis was performed with 3-5 independent fetal liver samples per genotype. (I) Likewise, FACS analysis of fetal liver at 14.5 dpc reveals no major alterations in the relative frequency of CD71+ single-positive, CD71/Ter119 double-positive, or Ter119 single-positive cells with constitutive loss of *Asxl1*. Antibody stainings are as indicated and cells were gated on live cells in the parent gate. Error bars represent ± SD.

Figure 2: Conditional deletion of *Asxl1* results in age-dependent leukopenia, and anemia. (A) qRT-PCR showing relative expression level of *Asxl1* in purified progenitor and mature mouse hematopoietic stem and progenitor subsets. (B) Verification of *Mx1-cre* (left) and *Vav-cre* (right) mediated deletion of *Asxl1* at the level of protein expression in Western blot of splenocytes. (C) Enumeration of nucleated cells in bilateral femurs and tibiae or whole spleens of control (*Asxl1$^{fl/fl}$*) and *Asxl1* hematopoietic-specific knockout (KO) mice (*Vav-cre Asxl1$^{fl/fl}$*) reveals

significant decrease in hematopoietic cells in both compartments at 6 weeks as well as 24 weeks of age (n=6-10 mice per genotype at each timepoint examined). (D, E). Enumeration of peripheral white blood cells (WBC) (D), and hemoglobin (Hb) (E) reveals time-dependent development of leukopenia and anemia with post-natal deletion of *Asxl1* (performed using *Mx1-cre Asxl1*^{fl/fl} mice or Cre-negative *Asxl1*^{fl/fl} controls). Counts in aged *Asxl1* KO mice are compared to age-matched controls as well as younger KO and control mice (n=6-12 mice per genotype at each timepoint examined). (F,G) Flow cytometric enumeration of B220+, CD11b+/Gr1+, CD3+, and CD11b+/Gr1- cells in the peripheral blood of >6 month-old *Mx1-cre Asxl1*^{fl/fl} (KO) and *Asxl1*^{fl/fl} (C) mice (n=5 mice per genotype were utilized for FACS analysis of peripheral blood). Right panel reveals peripheral blood FACS analysis. Antibody stainings are as indicated and cells were gated on live cells in the parent gate.

Figure 3: Deletion of *Asxl1* results in myeloid and erythroid dysplasia and impaired progenitor differentiation consistent with myelodysplasia. (A) Relative frequency of CD71-positive/Ter119-negative erythroid precursors in bone marrow (BM) and spleen of 6.5 month-old *Mx1-cre Asxl1*^{fl/fl} (KO) and Cre-negative *Asxl1*^{fl/fl} control mice revealing a modest but statistically significant increase erythroid precursors in both compartments (expressed as percentage of live cells) (n=3-5 mice per genotype in each tissue type examined by FACS analysis). (B) Histologic (H&E) analysis of *Mx1-cre Asxl1*^{fl/fl} and Cre-negative *Asxl1*^{fl/fl} control BM from 6-month old littermate mice illustrating marrow hypocellularity (scale bar represents 50 μm). (C) BM cytospins (Wright-Giemsa) from the same mice illustrating erythroid precursor dysplasia (arrows indicating erythroid precursors with prominent irregular nuclear contours) in KO mice and normal morphology in littermate controls (scale bar represents 10 μm). (D) Representative morphology of peripheral blood myeloid cells (top) and nucleated red blood cells (bottom) in KO mice (Wright-Giemsa stain) (scale bar represents 5 μm). (E) Number of colonies formed 7 days after plating of 1,000 common myeloid progenitor (CMP), granulocyte/macrophage progenitor (GMP), or megakaryocyte/erythroid progenitor (MEP) cells into methylcellulose from 6-week-old *Vav-cre Asxl1*^{fl/fl} and littermate control (Cre-negative *Asxl1*[1fl/fl] control) mice. Experiment was performed in biological duplicate. (F) Photograph of methylcellulose colony plate 7 days after plating of MEP cells from 6-week-old KO and control mice. (G) Histologic analysis by H&E stain liver from 72-week-old *Mx1-cre Asxl1*^{fl/fl} mice and littermates revealing extramedullary myeloid infiltrates

in liver of KO mice. (H) Number of colonies formed 7 days after plating of 200,000 nucleated cells harvested from the liver of 72-week-old *Mx1-cre Asxl1^{fl/fl}* or littermate control mice in methylcellulose containing rmIL-3, rm-SCF, rh-IL6, rh-EPO (liver cells from n=5 mice per genotype plated in methylcellulose). (I) Photomicrograph of colonies grown from cells taken from the liver and plated in methylcellulose is shown on right (scale bar represents 200 μm). Error bars represent ± SD. Asterisk represents *p*<0.05 (Mann-Whitney U test).

Figure 4: Serial non-competitive transplantation of *Asxl1*-null cells results in lethal myelodysplastic disorder. (A) Kaplan-Meier survival curve of recipient mice transplanted with 70-week-old *Vav-cre Asxl1^{fl/fl}* or Cre-negative *Asxl1^{fl/fl}* littermate control whole bone marrow following secondary and tertiary transplantation. Also shown is the survival of mice transplanted with purified lineage-negative, Sca-1+, c-Kit+ (LSK), cells in tertiary transplantation (tertiary transplant of *Asxl1^{fl/fl}* control LSK cells is not shown; no recipient mice from this group died by 40 weeks (n=5)). Cre-negative *Asxl1^{fl/fl}* littermate controls were similarly transplanted in parallel in each experiment. 4-6 recipient mice were transplanted in each experiment. (B) Hematocrit over time of secondary recipient mice transplanted with *Asxl1*-null or littermate control whole bone marrow in a non-competitive manner. Dashed bar represent lower-limit of normal hematocrit for C57/B6 mice (n=4-6 mice per genotype at each time point). (C) Body weight of secondarily transplanted mice at 50 weeks following transplantation (n=4 mice per genotype). (D) Bone marrow histopathology of secondary recipient mice transplanted with *Asxl1*-null or littermate control whole bone marrow at 50 weeks (scale-bar represents 50 μm). (E) Relative frequency of lineage-negative, Sca-1+, c-Kit+, (LSK), multipotent progenitor (MPP; LSK+, CD150-, CD48+), and long-term hematopoietic stem cells (LT-HSC; LSK+ CD150+ CD48-) in bone marrow and spleen at 50 weeks following non-competitive secondary transplantation. Frequencies are expressed as frequency of live cells (n=4 mice per genotype examined for FACS experiments). (F) Relative frequency of myeloid progenitors (lineage-negative c-Kit+ Sca-1-), common myeloid progenitor (CMP; lineage-negative, c-Kit+, Sca-1-, FcγR-, CD34+), granulocyte-macrophage progenitor (GMP; lineage-negativec-Kit+Sca-1-, FcγR+CD34+), and megakaryocyte-erythroid progenitor (MEP; lineage-negativec-Kit+Sca-1-FcγR-CD34-) cells at 50 weeks following non-competitive secondary transplantation. Frequencies are expressed as frequency of live cells. (G) Photographs of spleens from secondary

recipient mice transplanted with *Vav-cre Asxl1*^{fl/fl} or Cre-negative *Asxl1* [fl/fl] littermate control whole bone marrow 50 weeks following lethal irradiation. (H) Weight of the same spleens as shown in (G) (n=4 mice per genotype). (I) Histopathology of spleens from secondary recipient mice transplanted with *Asxl1-*null or wild-type littermate control whole bone marrow 50 weeks following non-competitive secondary transplantation revealing loss of normal splenic architecture (scale bar represents 50 μm). (J) Photographs of representative femur (top) and tibia (below) from secondary recipient mice transplanted with *Vav-cre Asxl1*^{fl/fl} or Cre-negative *Asxl1* [fl/fl] littermate control whole bone marrow 50 weeks following non-competitive secondary transplantation. (K) Relative quantification of CD71+/Ter119-negative and CD71/Ter119 double-positive cells from bone marrow and spleen of secondary recipient mice transplanted with *Vav-cre Asxl1*^{fl/fl} or Cre-negative *Asxl1* [fl/fl] littermate control whole bone marrow 50 weeks following non-competitive secondary transplantation. Frequencies are expressed as percentage of live cells (n=4 mice per genotype examined by FACS analysis). (L) Representative FACS plots of data shown in (K) from splenoctyes. Staining is as shown and live cells were gated in parent gate. Error bars represent ± SD. Asterisk represents *p*<0.05 (Mann-Whitney U test).

Figure 5: *Asxl1*^{−/−} mice have increased stem/progenitor cells but impaired self-renewal. (A) Flow cytometric enumeration of bone marow lineage-negative Sca-1+ c-Kit+ cells (LSK), long-term hematopoietic stem cells (LT-HSC; LSK CD150+ CD48-), and multipotent progenitor cells (MPP; LSK CD150- CD48+) in wild-type (*Asxl1*^{fl/fl}) and knockout (*Vav-cre Asxl1*^{fl/fl}) mice at 6 weeks of age reveals a significant increase in immunophenotypically-defined LSK and LT-HSC cells (n=4-6 mice per genotype as indicated). Data are expressed as total number of live cells per femur. (B) Representative FACS analysis of bone marrow stem cell populations of *Asxl1*^{-/-} (*Vav-cre Asxl1*^{fl/fl}) and wild-type (*Asxl1*^{fl/fl}) at 6 weeks. Antibody stains are as indicated and parent gate is live, lineage-negative cells. (C) Schematic depiction of the competitive transplantation assay. *Asxl1*^{fl/fl} and *Vav-cre Asxl1*^{fl/fl} are positive for CD45.2 while wild-type competitor cells are positive for CD45.1. Recipient mice are also CD45.1. Representative FACS plots of the percentage of CD45.1 versus CD45.2 total chimerism in the peripheral blood of recipient animals at 16 weeks following competitive transplantation is shown. (D) Percentage of CD45.1 versus CD45.2 total chimerism in the peripheral blood of recipient animals at 4 weeks and 16 weeks in primary competitive transplant and serial secondary competitive transplants

are shown (n=5 recipient mice for each genotype) (C: control and KO: *Asxl1* knockout). Experiment was performed in biological duplicate. Asterisk represents *p*<0.05 (Mann-Whitney U test).

Figure 6: Combined loss of *Asxl1* and *Tet2* rescues the impaired self-renewal of *Asxl1*-deficient hematopoietic stem cells (HSCs). (A) Enumeration of colonies and serial replating capacity of 20,000 whole BM cells from 6-week-old littermate mice with hematopoietic-specific deletion of *Asxl1* (*Vav-cre Asxl1$^{fl/fl}$*), *Tet2 (Vav-cre Tet2$^{fl/fl}$*), or both (*Vav-cre Asxl1$^{fl/fl}$ Tet2$^{fl/fl}$*) reveals increased replating capacity of *Asxl1*-null/*Tet2*-null cells compared with *Asxl1*-null cells alone. At the same time, *Asxl1/Tet2* double-knockout cells have impaired colony formation compared with *Tet2* single-knockout cells at extended replating. The same whole BM cells were also used for *in vivo* competitive transplantation. (B) Schematic depiction of the competitive transplantation experiment. Control, *Vav-cre Asxl1$^{fl/fl}$*, *Vav-cre Tet2$^{fl/fl}$*, and *Vav-cre Asxl1$^{fl/fl}$Tet2$^{fl/fl}$* cells are positive for CD45.2 while wild-type competitor cells are positive for CD45.1. On the right, monthly assessment of donor chimerism in the peripheral blood of recipient animals is shown up to 16 weeks post-transplant (n=5 recipient mice were used for each genotype and experiment was performed in biological duplicate). 16-week chimerism was significantly higher in *Tet2$^{-/-}$* transplanted mice compared with all other genotypes. *p*-value determined by Mann-Whitney U test. (C) Representative FACS analysis of peripheral blood of mice transplanted with each genotype at 16 weeks. Staining schemes are as indicated and parental gate was live cells. (D) Proportion of CD45.2+ peripheral blood cells of each lineage at 16 weeks in mice transplanted with each genotype (n=5 mice analyzed for each genotype) as determined by FACS analysis. Each competitive transplantation experiment was performed in biological duplicate with 5 recipient mice per genotype in each experiment. Error bars represent ± SD. Asterisk represents *p*<0.05 (Mann-Whitney U test).

Figure 7: Concomitant deletion of *Asxl1* and *Tet2* results in myelodysplasia in mice. (A) Kaplan-Meier survival curve of primary Cre-negative *Asxl1fl/fl* (n=5)*, Mx1-cre Asxl1$^{fl/fl}$* (n=12), *Mx1-cre Tet2 $^{fl/fl}$* (n=6), *Mx1-cre Asxl1 $^{fl/fl}$ Tet2 $^{fl/fl}$* (n=10 mice per genotype). Mice were treated with pIpC at 4 weeks following birth and then followed for 50 weeks. (B) Peripheral white blood cell (WBC) count and differential of recipient mice transplanted with bone marrow from 6-week-old *Mx1-cre Asxl1* wildtype *Tet2* wildtype (control; C), *Mx1-cre Asxl1$^{fl/fl}$* (Asxl1 KO),

Mx1-cre Tet2 fl/fl (Tet2 KO), and *Mx1-cre Asxl1 fl/fl Tet2 fl/fl (Asxl1/Tet2* DKO) mice 66 weeks after transplantation (68 weeks after polyinosinic-polycytidylic acid (pIpC) administration to recipient mice) (n=10 mice per genotype). Asxl1 KO and Asxl1/Tet2 DKO mice had significantly lower WBC counts compared with control and Tet2 KO mice. Differential was determined by flow cytometric analysis of peripheral blood. (C) Hematocrit and (D) total number of nucleated bone marrow (BM) cells of same mice as shown in (B). (E) Representative flow cytometric assessment of relative frequencies of myeloid progenitor and lineage-negative Sca-1+ c-KIT+ (LSK) cells in 72-week-old mice. Parent population was live, lineage-negative cells. (F) Total numbers of LSK and myeloid progenitor cells (lineage-negative Sca-1- c-Kit+) in mice from each genotype at 72-weeks of age. This was determined by flow-cytometric quantification of living LSK and MP cells from c-KIT enriched BM cells harvested from spine plus bilateral femurs, tibiae, and humeri of each mouse from each genotype at 72 weeks of age (n=3 mice per group). (G) Wright-giemsa stain of BM representative erythroid precursor from cytospins of 72-week-old control, Asxl1 KO, Tet2 KO, or Asx1/Tet2 DKO mice. Dysplasia of erythroid precursors is seen in Asxl1 KO and Asxl1/Tet2 DKO genotypes as evidenced by erythroid precursors with prominent multinuclearity and nuclear fragmentation (arrows; scale bar represents 5 μm). (H) Representation histologic sections of liver from 72-week-old control, Asxl1 KO, Tet2 KO, or Asx1/Tet2 DKO mice revealing hematopoietic cell infiltrates in the Asxl1 KO, Tet2 KO, or Asxl1/Tet2 DKO mice suggestive of extramedullary hematopoiesis in all genotypes except control (scale bar represents 50 μm). Hematopoietic cell infiltrate is most prominent in the Asx1/Tet2 DKO mice. For (A) and (B) n=10 mice per group, for all (C)-(H) n=3 mice per group. Error bars represent ± SD. Asterisk represents *p*<0.05 (Mann-Whitney U test).

Figure 8: Identification of genes significantly dysregulated with deletion of *Asxl1* alone and in concert with deletion of *Tet2* and their functional impact. (A) Volcano plot of differentially expressed transcripts from RNA-Seq data of 1-year old control versus littermate *Asxl1* knockout (KO; *Mx1-cre Asxl1 fl/fl*) lineage-negativeSca-1+c-Kit+ (LSK) cells and myeloid progenitor (lineage-negativeSca-1- c-Kit+) cells (experiment included cells from 2 individual mice per genotype). (B) Venn diagrams of genes significantly up-regulated and down-regulated with Asxl1 loss in lineage-negative Sca-1+ cKit+ (LSK) and myeloid progenitor (MP; lineage-negative, Sca-1-negative, cKit+) cells from 1 year-old *Mx1-cre Asxl1 fl/fl* mice and littermate Cre-negative controls as identified in (A). (C) Quantitative

real-time PCR (qRT-PCR) analysis of *HoxA* and *Hox*-associated transcription factor genes in LSK cells of 1-year old Cre-negative *Asxl1*^{fl/fl} control versus littermate *Vav-cre Asxl1*^{fl/fl}. (D) qRT-PCR analysis of *p16*[INK4a] in long-term hematopoietic stem cells (LT-HSC; lineage-negative, Sca-1+, c-Kit+, CD150+, CD48-) and multipotent progenitor cells (MPP; lineage-negative, Sca-1+, c-Kit+, CD150-, CD48+) from 6-weeks and 6-months old control (C) versus littermate *Vav-cre Asxl1*^{fl/fl} (KO) mice. (E) Cell cycle analysis of MPPs from 72-week-old *Vav-cre Asxl1*^{fl/fl} or littermate Cre-negative *Asxl1* [fl/fl] control mice with *in vivo* 5-bromo-2-deoxyuridine (BRDU) administration. Representative FACS plot analysis showing gating on MPP cells followed by BRDU versus DAPI stain is shown on left (parent gate is lineage-negative Sca-1+ c-KIT+ (LSK) cells). Relative quantification of the percentage of MPP cells in S-phase, G2/M-phase, and G0/1-phase is shown on right (n=5 mice per group) and reveals modest but statistically significant decrement in the proportion of MPP cells from KO mice in S-phase relative to controls. (F) Assessment of proportion of hematopoietic stem/progenitor cells undergoing apoptosis was performed by Annexin V/DAPI stain of LSK cells from 72-week-old *Vav-cre Asxl1*^{fl/fl} mice or Cre-negative *Asxl1*^{fl/fl} littermate controls. Representative FACS plot analysis showing gating on LSK cells followed by Annexin-V versus DAPI stain is shown on left (parent gate is lineage-negative cells). Relative quantification of the percentage of annexin V+/DAPI- and annexin V+/DAPI+ LSK cells is shown on right (n=5 mice per group) and reveals increase in annexin V+ cells in LSK cells from KO mice relative to controls. (G) Comparison of significant differentially expressed genes in LSK cells from 6-week-old *Mx1-cre Asxl*^{fl/fl}, *Mx1-cre Tet2*^{fl/fl}, or *Mx1-cre Asxl1*^{fl/fl} *Tet2*^{fl/fl} relative to controls (or *Mx1-cre Asxl1* wildtype *Tet2* wildtype). 99 genes are uniquely donwregulated in *Asxl1/Tet2* double-knockout mice relative to all other genotypes (left) whereas 49 genes are significantly up-regulated (right). (H) Gene set enrichment analysis (GSEA) of overlapping and statistically significant gene sets enriched in the LSK cells of mice with deletion of *Asxl1* alone or with combined *Asxl1* and *Tet2* deletion identifies enrichment of apoptosis and stem cell signatures as shown. (I) Gene sets uniquely enriched in mice with concomitant deletion of *Asxl1* and *Tet2* relative to all other genotypes as determined by GSEA. Asterisks denoted *p*<0.05. *p*-value determined by Mann-Whitney U test. Error bars represent ± SD.

Figure 9: Effect of *Asxl1* loss *in vivo* on histone H3 lysine 27 trimethylation (H3K27me3) and identification of Asxl1 regulated genes by chromatin

immunoprecipitation followed by sequencing (ChIP-Seq). (A) Loss of *Asxl1 in vivo* is associated with global loss of H3K27me3 as revealed by H3K27me3 Western blot in splenocytes of 6-week-old *Vav-cre Asxl1*^{fl/fl} mice. (B) Levels of core-Polycomb repressive complex 2 members Ezh2, Suz12, and Eed in splenocytes of same mice as shown in (A). (C) Characterization of Asxl1 binding sites identified by anti-Asxl1 ChIP-seq analysis in murine wild-type bone-marrow derived macrophages. (D) Heatmap representation of Asxl1 ChIP-Seq signal centered around transcription start sites (TSS) (+/- 2kb) of CpG (left) and non-CpG (right) promoters. (E) Average Asxl1 ChIP-Seq signal density of CpG-(blue) and non-CpG (red) promoters centered around TSS +/- 10kb. (F) Motif enrichment analysis of Asxl1 binding sites identified significant enrichment of Ets transcription factor binding sites (p=1e^{-59}, % target=40.1%, and % background=21.4%).

Table 1: Genes directly regulated by Asxl1 as determined by differential expression in hematopoietic stem and progenitor cells with *Asxl1* deletion and directly bound by Asxl1.

Gene	Myeloid Progenitors		LSK Cells		anti-Asxl1 ChIP-Seq		
	log2(fold_change)	*p* value	log2(fold_change)	*p* value	peak *p* value	fold Enrichment	peak FDR
Tmem87a	3.90831	9.60E-06	3.10699	3.68E-06	2.77971E-07	4.21	0.29
Pusl1	1.54208	2.21E-07	1.3018	0.00129402	3.04089E-08	5.24	0.15
Ddx23	1.44554	1.15E-10	1.08572	0.00178776	7.44732E-15	6.93	0.09
Pan3	1.00691	1.36E-05	0.794084	0.000821079	4.48745E-29	9.3	0
Srrm2	0.863611	6.02E-08	0.984717	1.61E-06	1.84927E-12	4.49	0.06
Dusp6	0.79909	0.000411111	0.632273	0.00245225	4.47713E-30	8.43	0
Cdca2	0.768423	6.77E-08	0.61555	0.000384148	3.78443E-08	3.6	0.16
Apobec3	0.536153	2.25E-10	0.359169	0.000828676	4.47713E-10	6.18	0.09
Cdc40	0.407387	0.00016795	0.585597	1.93E-05	4.7863E-10	5.91	0.09
Rpl30	0.392082	1.73E-10	0.310882	5.74E-05	1.57398E-22	6.99	0
Rad51	0.390944	0.00316768	0.511981	0.00347602	2.2751E-10	7.16	0.1
Nbr1	0.342763	4.65E-08	0.427205	0	4.03645E-19	5.69	0
Slc24a6	0.295986	0.000465747	0.819679	3.24E-10	7.51623E-11	8.09	0.1
Dhrs3	0.284957	0.00426814	0.372768	0.000215795	4.32514E-49	5.15	0
Cdk2	0.230661	0.000151398	0.207111	0.000393793	1.05682E-16	7.89	0.11
Ifngr1	0.179453	0.00458996	0.380563	0.000199363	3.01995E-20	11.89	0
Hsp90ab1	0.163265	0.00108147	0.238185	9.11E-05	1.40929E-45	12.71	0
Mtmr9	-0.435049	0.000453214	-0.466798	0.000362118	4.0738E-11	7.19	0.11
Ppp1cb	-0.478957	1.35E-08	-0.637022	2.14E-07	5.79429E-12	4.77	0.09
Mthfr	-0.507239	0.00164734	-0.467733	0.00121057	2.46604E-09	4.82	0.11
Ncf4	-0.522396	7.21E-09	-0.662578	4.38E-05	2.16272E-18	7.53	0.07
Slc25a19	-0.95942	7.68E-11	-0.748011	3.50E-06	2.24388E-07	6.64	0.28
Rpl29	-1.17739	0	-0.764969	0	2.46604E-09	5.96	0.11
Mettl23	-1.32733	8.43E-10	-1.10156	1.21E-05	1.09648E-07	3.68	0.2
Caskin2	-1.54016	3.42E-05	-2.45432	0.000153492	4.96592E-13	5.6	0.07
Thbs1	-1.75238	4.71E-07	-1.84188	1.63E-06	9.52796E-08	5.06	0.19

1) Differentially expressed genes in RNA sequencing of myeloid progenitors (lineage-negative, Sca-1-negative c-KIT-positive cells) from 1 year-old *Mx1-cre Asxl1*^{fl/fl} mice relative to Cre-negative *Asxl1*^{fl/fl} littermate controls.

2) Differentially expressed genes in RNA sequencing of LSK cells (lineage-negative, Sca-1-positive c-KIT-positive cells) from 1 year-old *Mx1-cre Asxl1*^{fl/fl} mice relative to Cre-negative *Asxl1*^{fl/fl} littermate controls.

3) Data derived from anti-Asxl1 chromatin immunoprecipitation followed by next-generation (ChIP-Seq) in wildtype C57/B6H bone marrow-derived macrophages.

Materials and Methods

Animals

All animals were housed at New York University School of Medicine or at Memorial Sloan-Kettering Cancer Center. All animal procedures were conducted in accordance with the Guidelines for the Care and Use of Laboratory Animals and were approved by the Institutional Animal Care and Use Committees (IACUCs) at New York University School of Medicine and Memorial Sloan-Kettering Cancer Center.

Generation of *Asxl1*-Deficient Mice

The *Asxl1* allele was deleted by targeting exons 5-10. Two *LoxP* sites flanking exon 5-10 and a *Frt*-flanked neomycin selection cassette were inserted in the upstream intron (**Fig. 1A**). Ten micrograms of the targeting vector was linearized by *Not*I and then transfected by electroporation of BAC-BA1 (C57BL/6 x 129/SvEv) hybrid embryonic stem cells. After selection with G418 antibiotic, surviving clones were expanded for PCR analysis to identify recombinant ES clones. Secondary confirmation of positive clones identified by PCR was performed by Southern blotting analysis. DNA was digested with *BamH*I and electrophoretically separated on a 0.8% agarose gel. After transfer to a nylon membrane, the digested DNA was hybridized with a probe targeted against the 3' or 5' external region. DNA from C57BL/6 (B6), 129/SvEv (129), and BA1 (C57Bl/6 x 129/SvEv) (Hybrid) mouse strains was used as wild-type controls. Positive ES clones were expanded and injected into blastocysts.

The generated mice (*Asxl1^{fl/fl}*) were initially crossed to a germline *Flp*-deletor (Jackson Laboratories), to eliminate the neomycin cassette, and subsequently to the IFNα-inducible *Mx1-cre* (Jackson Laboratories), the hematopoietic- specific *Vav-cre*, and the germline *EIIa-cre*(Kuhn et al., 1995; Lakso et al., 1996; Stadtfeld and Graf, 2005). Mice were backcrossed for six generations to C57BL/6 mice.

Asxl1^{fl/fl}, *Asxl1^{fl/+}*, and *Asxl1^{+/+}* littermate mice were genotyped by PCR with primers Asxl1-F3 (5'–CAGCCGTTTTACCACAGTTT-3') and Asxl1-R3 (5'-AGGGAAAGGGACAGAATGAC-3') using the following parameters: 95°C for 4 min, followed by 35 cycles of 95°C for 45 sec, 56°C for 45 sec, and 72°C for 1 min, and then 72°C for 5 min. Wild-type allele was detected as a band at 200 base pair (bp) while floxed allele was detected as a band of 380 bp. Excision

after Cre recombination was confirmed by PCR with primers to detect a floxed portion of the construct (Asxl1-RecF: 5'–ACGCCGGCTTAAGTGTACACG-3' and Asxl1-RecR: 5'– GACTAAGTTGCCGTGGGTGCT-3') using the same parameters as the above.

In Vivo Studies

Mx1-cre Asxl1^{fl/fl} conditional and Cre-negative *Asxl1*^{fl/fl} control mice received five intraperitoneal injections of poly(I:C) every other day at a dose of 20 mg/kg of body weight starting at 2 weeks post-birth. For the hematopoietic-specific *Vav-cre* line, Asxl1^{fl/fl}*Vav-cre+*, and Asxl1^{fl/fl}*Vav-cre-* mice were analyzed between 3 and 60 weeks of age. Bone marrow, spleen, and peripheral blood were analyzed by flow cytometry. Formalin-fixed paraffin-embedded tissue sections were stained with hematoxylin and eosin. Peripheral blood was smeared on a slide and stained using the Wright-Giemsa staining method. Tissue sections and blood smears were evaluated by a hematopathologist (C.Y.P.) Deletion of the *Asxl1* allele and transcript was measured by genomic PCR and Western blot analysis.

Bone Marrow Transplantation

Freshly dissected femurs and tibias were isolated from *Asxl1*^{fl/fl} CD45.2+ or *Vav-cre+Asxl1*^{fl/fl} CD45.2+ mice. Bone marrow was flushed with a 3 cc insulin syringe into PBS supplemented with 3% fetal bovine serum. The bone marrow was spun at 0.5 x *g* by centrifugation at 4^0C, and red blood cells were lysed in ammonium chloride-potassium bicarbonate lysis buffer for 5 min. After centrifugation, cells were resuspended in PBS plus 3% FBS, passed through a cell strainer, and counted. Finally, 0.5×10^6 total bone marrow cells of *Asxl1*^{fl/fl} CD45.2+ or *Vav-cre+ Asxl1*^{fl/fl} CD45.2+ mice were mixed with 0.5×10^6 wild-type CD45.1+-support bone marrow and transplanted via tail-vein injection into lethally irradiated (two times 450 cGy) CD45.1+ host mice. Chimerism was measured by FACS in peripheral blood at 4 weeks post-transplant (week 0, pre-polyI-polyC). Chimerism was followed via FACS in the peripheral blood every 4 weeks (week 0, 4, 6, 8, 12, and 16 after polyI-polyC injection). Additionally, for each bleeding, whole blood cell counts were measured on a blood analyzer, and peripheral blood smears were scored. Chimerism in the bone marrow, spleen, and thymus was evaluated at 16 weeks via animal sacrifice and subsequent FACS analysis. The above procedure was also repeated with *Asxl1*^{fl/fl} CD45.2+, *Vav-cre+ Asxl1*^{fl/fl} CD45.2+ mice, *Vav-cre+ Tet2*^{fl/fl} CD45.2+, and *Vav-cre+ Asxl1*^{fl/fl} *Tet2*^{fl/fl} CD45.2+ mice for competitive transplantation of mice with loss of Asxl1, Tet2, or both. For non-

competitive transplantation studies, 1 x 10^6 total bone marrow cells of *Asxl1*$^{fl/fl}$ CD45.2+, littermate *Vav-cre+ Asxl1*$^{fl/fl}$ CD45.2+ mice, or littermate *Mx1-cre+ Asxl1*$^{fl/fl}$ CD45.2+ mice were injected into lethally irradiated (two times 450 cGy) CD45.1+ host mice. Similarly, for LSK transplants, 1,000 FACS-sorted LSK cells from secondarily transplanted *Asxl1* KO or control mice were transplanted into lethally irradiated CD45.1 host mice. Recipient mice were then followed until moribund or 80-weeks following transplantation.

In Vitro Colony-Forming Assays

LSK, CMP, GMP, and MEP cells were sorted from the bone marrow of *Asxl1*$^{fl/fl}$ and littermate *Vav-cre+ Asxl1*$^{fl/fl}$ mice and seeded at a density of 500 cells/replicate for LSK cells and 1,000 cells/replicate for CMP, GMP, and MEP subsets into cytokine-supplemented methylcellulose medium (Methocult, M3434; STEMCELL Technologies). Colonies propagated in culture were scored at day 7. Representative colonies were isolated from the plate for cytospins. Remaining cells were resuspended, counted, and a portion was taken for replating (20,000 cells/replicate) for a total of 7 platings. Cytospins were performed by resuspending in warm PBS and spun onto the slides at 350 x *g* for 5 min. Slides were air-dried and stained using the Giemsa-Wright method.

Antibodies, FACS, and Western Blot Analysis

Antibody staining and FACS analysis was performed as previously described(Klinakis et al., 2011). Bone marrow or spleen mononuclear cells were stained with a lineage cocktail comprised of antibodies targeting CD4, CD8, B220, NK1.1, Gr-1, CD11b, Ter119, and IL-7Rα. Cells were also stained with antibodies against c-Kit, Sca-1, FcγRII/III, and CD34. Cell populations were analyzed using a FACS-LSRII (Becton Dickinson) and sorted with a FACSAria instrument (Becton Dickinson). All antibodies were purchased from BD-Pharmingen or eBioscience. We used the following antibodies: c-Kit (2B8), Sca-1 (D7), Mac-1/CD11b (M1/70), Gr-1 (RB6-8C5), NK1.1 (PK136), Ter-119, IL7-Rα(A7R34), CD34 (RAM34), FcγRII/III (2.4G2), CD4 (RM4-5), CD4 (H129.19), CD8 (53-6.7), CD45.1 (A20), CD45.2 (104), CD150 (9D1), CD48 (HM48-1).

The following antibodies were used for Western blot analysis: Asxl1 (Clone N-13; Santa Cruz (sc-85283), Ezh2 (Millipore 07-689), Suz12 (Abcam ab12073), EED (Abcam ab4469), H3K27me3 (Abcam ab6002), total H3 (Abcam ab179), and tubulin (Sigma, T9026).

Cell Cycle and Apoptosis Analyses. For cell cycle analysis, the BRDU-APC kit was used (BD Pharmingen 557892) according to the manufacturer's protocol. Mice were treated with 1mg BRDU intraperitoneally followed by harvest of BM cells 24 hours later. For evaluation of apoptosis, the Annexin V-FITC apoptosis detection kit was used (BD Pharmingen 556570) according to the manufacturer's recommendations. DAPI was used as counterstain in both BRDU and annexin V experiments.

Histological Analyses. Mice were sacrificed and autopsied, then dissected tissue samples or were fixed for 24h in 4% paraformaldehye, dehydrated and embedded in paraffin. Paraffin blocks were sectioned at 4µm and stained with haematoxylin and eosin. Images were acquired using a Zeiss Axio Observer A1 microscope (Zeiss).

Peripheral Blood Analysis. Blood was collected by retro-orbital bleeding using heparinized microhematocrit capillary tubes (Fisher). Automated peripheral blood counts were obtained using a HemaVet 950 (Drew Scientific) following standard manufacturer's instruction. Differential blood counts were realized on blood smears stained using Wright-Giemsa staining and visualized using a Zeiss Axio Observer A1 microscope (Zeiss).

RNA Sequencing (RNA-Seq) and Quantitative Real-Time PCR Analysis
Total RNA was isolated using the RNeasy Plus Mini Kit (Qiagen) and cDNA was synthesized using the SuperScript First-Strand Kit (Invitrogen). Quantitative PCR was performed using SYBR green iMaster and a LightCycler 480 (Roche). For RNA-Seq analysis, Fastq files were aligned to mm9 using TopHatV1.4 with default parameters. Differential expression tests were done using the Cuffdiff module of Cufflinks with RefSeq genes provided as an annotation (-N, -u and –M options engaged). We considered genes that had a q<0.05 to be significantly different between genotypes.

Chromatin Immunoprecipitation Sequencing (ChIP-Seq) and Analysis
Since low chromatin yields from hematopoietic stem/progenitor cell populations precluded ChIP-Seq studies, bone marrow derived macrophages (BMDM) from wildtype C57BL/6 mice were used as a surrogate to identify genome-wide Asxl1 binding sites. The antibody used for Asxl1 ChIP-Seq studies was from Santa Cruz (sc-85283). ChIP was performed as described previously (Dey et al., 2012).

ChIP and input DNAs were prepared for amplification by converting overhangs into phosphorylated blunt ends and adding an adenine to the 3' ends. Illumina adaptors were added and the library was size-selected (175-225 bp) on an agarose gel. The adaptor- ligated libraries were amplified for 18 cycles. The resulting DNA libraries were purified, quantified, and tested by qPCR at the same specific genomic regions as the original ChIP DNA to assess quality of the amplification reactions. DNA libraries then were sequenced on the Illumina Genome Analyzer II.

Sequenced reads were aligned to the reference genomes (mm9) using bowtie with maximum two mismatches, keeping only uniquely mapping reads. Peak calling was performed using MACS1.4 with the following options: -p 1e-7, --nomodel True, --shiftsize 100, --keep-dup 1. Peaks were assigned to genes using bedtools. We considered Asxl1-bound genes to be any mouse RefSeq entry containing a peak overlapping the gene or 2kb upstream of the TSS. ChIP-Seq read profile and heatmap densites were generated using genomic-tools. Mouse RefSeq and CpG island annotations were downloaded from the UCSC table browser (genome.ucsc.edu).

Skeletal preparations.

Skeletal preparations were performed as described previously(de Pontual et al., 2011).

References

Abdel-Wahab, O., M. Adli, L.M. Lafave, J. Gao, T. Hricik, A.H. Shih, S. Pandey, J.P. Patel, Y.R. Chung, R. Koche, F. Perna, X. Zhao, J.E. Taylor, C.Y. Park, M. Carroll, A. Melnick, S.D. Nimer, J.D. Jaffe, I. Aifantis, B.E. Bernstein, and R.L. Levine. 2012. ASXL1 Mutations Promote Myeloid Transformation through Loss of PRC2-Mediated Gene Repression. *Cancer Cell* 22:180-193.

Bejar, R., K. Stevenson, O. Abdel-Wahab, N. Galili, B. Nilsson, G. Garcia-Manero, H. Kantarjian, A. Raza, R.L. Levine, D. Neuberg, and B.L. Ebert. 2011. Clinical effect of point mutations in myelodysplastic syndromes. *The New England journal of medicine* 364:2496-2506.

Bejar, R., K.E. Stevenson, B.A. Caughey, O. Abdel-Wahab, D.P. Steensma, N. Galili, A. Raza, H. Kantarjian, R.L. Levine, D. Neuberg, G. Garcia-Manero, and B.L. Ebert. 2012. Validation of a prognostic model and the impact of mutations in patients with lower-risk myelodysplastic syndromes. *J Clin Oncol* 30:3376-3382.

Boultwood, J., J. Perry, A. Pellagatti, M. Fernandez-Mercado, C. Fernandez-Santamaria, M.J. Calasanz, M.J. Larrayoz, M. Garcia-Delgado, A. Giagounidis, L. Malcovati, M.G. Della Porta, M. Jadersten, S. Killick, E. Hellstrom-Lindberg, M. Cazzola, and J.S. Wainscoat. 2010. Frequent mutation of the polycomb-associated gene ASXL1 in the myelodysplastic syndromes and in acute myeloid leukemia. *Leukemia : official journal of the Leukemia Society of America, Leukemia Research Fund, U.K* 24:1062-1065.

Bracken, A.P., D. Kleine-Kohlbrecher, N. Dietrich, D. Pasini, G. Gargiulo, C. Beekman, K. Theilgaard-Monch, S. Minucci, B.T. Porse, J.C. Marine, K.H. Hansen, and K. Helin. 2007. The Polycomb group proteins bind throughout the INK4A-ARF locus and are disassociated in senescent cells. *Genes Dev* 21:525-530.

Choi, C., Y. Chung, C. Slape, and P. Aplan. 2008. Impaired differentiation and apoptosis of hematopoietic precursors in a mouse model of myelodysplastic syndrome. *Haematologica* 93:1394-1397.

de Pontual, L., E. Yao, P. Callier, L. Faivre, V. Drouin, S. Cariou, A. Van Haeringen, D. Genevieve, A. Goldenberg, M. Oufadem, S. Manouvrier, A. Munnich, J.A. Vidigal, M. Vekemans, S. Lyonnet, A. Henrion-Caude, A. Ventura, and J. Amiel. 2011. Germline deletion of the miR-17 approximately 92 cluster causes skeletal and growth defects in humans. *Nat Genet* 43:1026-1030.

Dey, A., D. Seshasayee, R. Noubade, D.M. French, J. Liu, M.S. Chaurushiya, D.S. Kirkpatrick, V.C. Pham, J.R. Lill, C.E. Bakalarski, J. Wu, L. Phu, P. Katavolos, L.M. LaFave, O. Abdel-Wahab, Z. Modrusan, S. Seshagiri, K. Dong, Z. Lin, M. Balazs, R. Suriben, K. Newton, S. Hymowitz, G. Garcia-Manero, F. Martin, R.L. Levine, and V.M. Dixit. 2012. Loss of the tumor suppressor BAP1 causes myeloid transformation. *Science* 337:1541-1546.

Fisher, C.L., I. Lee, S. Bloyer, S. Bozza, J. Chevalier, A. Dahl, C. Bodner, C.D. Helgason, J.L. Hess, R.K. Humphries, and H.W. Brock. 2010a. Additional sex combs-like 1 belongs to the enhancer of trithorax and polycomb group and genetically interacts with Cbx2 in mice. *Dev Biol* 337:9-15.

Fisher, C.L., N. Pineault, C. Brookes, C.D. Helgason, H. Ohta, C. Bodner, J.L. Hess, R.K. Humphries, and H.W. Brock. 2010b. Loss-of-function Additional sex combs like 1 mutations disrupt hematopoiesis but do not cause severe myelodysplasia or leukemia. *Blood* 115:38-46.

Gelsi-Boyer, V., V. Trouplin, J. Adelaide, J. Bonansea, N. Cervera, N. Carbuccia, A. Lagarde, T. Prebet, M. Nezri, D. Sainty, S. Olschwang, L. Xerri, M. Chaffanet, M.J. Mozziconacci, N. Vey, and D. Birnbaum. 2009. Mutations of polycomb-associated gene ASXL1 in myelodysplastic syndromes and chronic myelomonocytic leukaemia. *Br J Haematol* 145:788-800.

Gilliland, D.G. 2001. The diverse role of the ETS family of transcription factors in cancer. *Clin Cancer Res* 7:451-453.

Haferlach, C., U. Bacher, S. Schnittger, T. Alpermann, M. Zenger, W. Kern, and T. Haferlach. 2012. ETV6 rearrangements are recurrent in myeloid malignancies and are frequently associated with other genetic events. *Genes Chromosomes Cancer* 51:328-337.

Hidalgo, I., A. Herrera-Merchan, J.M. Ligos, L. Carramolino, J. Nunez, F. Martinez, O. Dominguez, M. Torres, and S. Gonzalez. 2012. Ezh1 Is Required for Hematopoietic Stem Cell Maintenance and Prevents Senescence-like Cell Cycle Arrest. *Cell Stem Cell* 11:649-662.

Hoischen, A., B.W. van Bon, B. Rodriguez-Santiago, C. Gilissen, L.E. Vissers, P. de Vries, I. Janssen, B. van Lier, R. Hastings, S.F. Smithson, R. Newbury-Ecob, S. Kjaergaard, J. Goodship, R. McGowan, D. Bartholdi, A. Rauch, M. Peippo, J.M. Cobben, D. Wieczorek, G. Gillessen-Kaesbach, J.A. Veltman, H.G. Brunner, and B.B. de Vries. 2011. De novo nonsense mutations in ASXL1 cause Bohring-Opitz syndrome. *Nature genetics* 43:729-731.

Itzykson, R., O. Kosmider, A. Renneville, V. Gelsi-Boyer, M. Meggendorfer, M. Morabito, C. Berthon, L. Ades, P. Fenaux, O. Beyne-Rauzy, N. Vey, T. Braun, T. Haferlach, F. Dreyfus, N.C. Cross, C. Preudhomme, O.A. Bernard, M. Fontenay, W. Vainchenker, S. Schnittger, D. Birnbaum, N. Droin, and E. Solary. 2013. Prognostic Score Including Gene Mutations in Chronic Myelomonocytic Leukemia. *J Clin Oncol*

Ivanova, N., J. Dimos, C. Schaniel, J. Hackney, K. Moore, and I. Lemischka. 2002. A stem cell molecular signature. *Science (New York, N.Y.)* 298:601-604.

Jacobs, J.J., K. Kieboom, S. Marino, R.A. DePinho, and M. van Lohuizen. 1999. The oncogene and Polycomb-group gene bmi-1 regulates cell proliferation and senescence through the ink4a locus. *Nature* 397:164-168.

Jankowska, A.M., H. Makishima, R.V. Tiu, H. Szpurka, Y. Huang, F. Traina, V. Visconte, Y. Sugimoto, C. Prince, C. O'Keefe, E.D. Hsi, A. List, M.A. Sekeres, A. Rao, M.A. McDevitt, and J.P. Maciejewski. 2011. Mutational spectrum analysis of chronic myelomonocytic leukemia includes genes associated with epigenetic regulation: UTX, EZH2, and DNMT3A. *Blood* 118:3932-3941.

Klinakis, A., C. Lobry, O. Abdel-Wahab, P. Oh, H. Haeno, S. Buonamici, I. van De Walle, S. Cathelin, T. Trimarchi, E. Araldi, C. Liu, S. Ibrahim, M. Beran, J. Zavadil, A. Efstratiadis, T. Taghon, F. Michor, R.L. Levine, and I. Aifantis. 2011. A novel tumour-suppressor function for the Notch pathway in myeloid leukaemia. *Nature* 473:230-233.

Ko, M., H.S. Bandukwala, J. An, E.D. Lamperti, E.C. Thompson, R. Hastie, A. Tsangaratou, K. Rajewsky, S.B. Koralov, and A. Rao. 2011. Ten-Eleven-Translocation 2 (TET2) negatively regulates homeostasis and differentiation of hematopoietic stem cells in mice. *Proc Natl Acad Sci U S A* 108:14566-14571.

Koschmieder, S., F. Rosenbauer, U. Steidl, B. Owens, and D. Tenen. 2005. Role of transcription factors C/EBPalpha and PU.1 in normal hematopoiesis and leukemia. *International journal of hematology* 81:368-377.

Kuhn, R., F. Schwenk, M. Aguet, and K. Rajewsky. 1995. Inducible gene targeting in mice. *Science* 269:1427-1429.

Lakso, M., J.G. Pichel, J.R. Gorman, B. Sauer, Y. Okamoto, E. Lee, F.W. Alt, and H. Westphal. 1996. Efficient in vivo manipulation of mouse genomic sequences at the zygote stage. *Proc Natl Acad Sci U S A* 93:5860-5865.

Li, Z., X. Cai, C.L. Cai, J. Wang, W. Zhang, B.E. Petersen, F.C. Yang, and M. Xu. 2011. Deletion of Tet2 in mice leads to dysregulated hematopoietic stem cells and subsequent development of myeloid malignancies. *Blood* 118:4509-4518.

Lin, Y.W., C. Slape, Z. Zhang, and P.D. Aplan. 2005. NUP98-HOXD13 transgenic mice develop a highly penetrant, severe myelodysplastic syndrome that progresses to acute leukemia. *Blood* 106:287-295.

Magini, P., M. Della Monica, M.L. Uzielli, P. Mongelli, G. Scarselli, E. Gambineri, G. Scarano, and M. Seri. 2012. Two novel patients with Bohring-Opitz syndrome caused by de novo ASXL1 mutations. *Am J Med Genet A* 158A:917-921.

Martínez-Jaramillo, G., and E. Flores-Figueroa…. 2002. Comparative analysis of the in vitro proliferation and expansion of hematopoietic progenitors from patients with aplastic anemia and myelodysplasia. *Leukemia research*

Metzeler, K.H., H. Becker, K. Maharry, M.D. Radmacher, J. Kohlschmidt, K. Mrozek, D. Nicolet, S.P. Whitman, Y.Z. Wu, S. Schwind, B.L. Powell, T.H. Carter, M. Wetzler, J.O. Moore, J.E. Kolitz, M.R. Baer, A.J. Carroll, R.A. Larson, M.A. Caligiuri, G. Marcucci, and C.D. Bloomfield. 2011. ASXL1 mutations identify a high-risk subgroup of older patients with primary cytogenetically normal AML within the ELN Favorable genetic category. *Blood* 118:6920-6929.

Mizuki, M., J. Schwable, C. Steur, C. Choudhary, S. Agrawal, B. Sargin, B. Steffen, I. Matsumura, Y. Kanakura, F. Böhmer, C. Müller-Tidow, W. Berdel, and H. Serve. 2003. Suppression of myeloid transcription factors and induction of STAT response genes by AML-specific Flt3 mutations. *Blood* 101:3164-3173.

Moran-Crusio, K., L. Reavie, A. Shih, O. Abdel-Wahab, D. Ndiaye-Lobry, C. Lobry, M.E. Figueroa, A. Vasanthakumar, J. Patel, X. Zhao, F. Perna, S. Pandey, J. Madzo, C. Song, Q. Dai, C. He, S. Ibrahim, M. Beran, J. Zavadil, S.D. Nimer, A. Melnick, L.A. Godley, I. Aifantis, and R.L. Levine. 2011. Tet2 loss leads to increased hematopoietic stem cell self-renewal and myeloid transformation. *Cancer Cell* 20:11-24.

Mueller, B., T. Pabst, M. Osato, N. Asou, L. Johansen, M. Minden, G. Behre, W. Hiddemann, Y. Ito, and D. Tenen. 2002. Heterozygous PU.1 mutations are associated with acute myeloid leukemia. *Blood* 100:998-1007.

Mullighan, C., A. Kennedy, X. Zhou, I. Radtke, L. Phillips, S. Shurtleff, and J. Downing. 2007. Pediatric acute myeloid leukemia with NPM1 mutations is characterized by a gene expression profile with dysregulated HOX gene expression distinct from MLL-rearranged leukemias. *Leukemia* 21:2000-2009.

Nilsson, L., I. Astrand-Grundström, I. Arvidsson, B. Jacobsson, E. Hellström-Lindberg, R. Hast, and S. Jacobsen. 2000. Isolation and characterization of hematopoietic progenitor/stem cells in 5q-deleted myelodysplastic syndromes: evidence for involvement at the hematopoietic stem cell level. *Blood* 96:2012-2021.

Nilsson, L., P. Edén, E. Olsson, R. Månsson, I. Astrand-Grundström, B. Strömbeck, K. Theilgaard-Mönch, K. Anderson, R. Hast, E. Hellström-Lindberg, J. Samuelsson, G. Bergh, C. Nerlov, B. Johansson, M. Sigvardsson, A. Borg, and S. Jacobsen. 2007. The molecular signature of MDS stem cells supports a stem-cell origin of 5q myelodysplastic syndromes. *Blood* 110:3005-3014.

Ohta, H., A. Sawada, J.Y. Kim, S. Tokimasa, S. Nishiguchi, R.K. Humphries, J. Hara, and Y. Takihara. 2002. Polycomb group gene rae28 is required for sustaining activity of hematopoietic stem cells. *J Exp Med* 195:759-770.

Pang, W., J. Pluvinage, E. Price, K. Sridhar, D. Arber, P. Greenberg, S. Schrier, C. Park, and I. Weissman. 2013. Hematopoietic stem cell and progenitor cell mechanisms in myelodysplastic syndromes. *Proceedings of the National Academy of Sciences of the United States of America* 110:3011-3016.

Patel, J.P., M. Gonen, M.E. Figueroa, H. Fernandez, Z. Sun, J. Racevskis, P. Van Vlierberghe, I. Dolgalev, S. Thomas, O. Aminova, K. Huberman, J. Cheng, A. Viale, N.D. Socci, A. Heguy, A. Cherry, G. Vance, R.R. Higgins, R.P. Ketterling, R.E. Gallagher, M. Litzow, M.R. van den Brink, H.M. Lazarus, J.M. Rowe, S. Luger, A. Ferrando, E. Paietta, M.S. Tallman, A. Melnick, O. Abdel-Wahab, and R.L. Levine. 2012. Prognostic relevance of integrated genetic profiling in acute myeloid leukemia. *N Engl J Med* 366:1079-1089.

Quivoron, C., L. Couronne, V. Della Valle, C.K. Lopez, I. Plo, O. Wagner-Ballon, M. Do Cruzeiro, F. Delhommeau, B. Arnulf, M.H. Stern, L. Godley, P. Opolon, H. Tilly, E. Solary, Y. Duffourd, P. Dessen, H. Merle-Beral, F. Nguyen-Khac, M. Fontenay, W. Vainchenker, C. Bastard, T. Mercher, and O.A. Bernard. 2011. TET2 inactivation results in pleiotropic hematopoietic abnormalities in mouse and is a recurrent event during human lymphomagenesis. *Cancer Cell* 20:25-38.

Ramalho-Santos, M., S. Yoon, Y. Matsuzaki, R. Mulligan, and D. Melton. 2002. "Stemness": transcriptional profiling of embryonic and adult stem cells. *Science (New York, N.Y.)* 298:597-600.

Raza-Egilmez, S.Z., S.N. Jani-Sait, M. Grossi, M.J. Higgins, T.B. Shows, and P.D. Aplan. 1998. NUP98-HOXD13 gene fusion in therapy-related acute myelogenous leukemia. *Cancer research* 58:4269-4273.

Rosenbauer, F., K. Wagner, J. Kutok, H. Iwasaki, M. Le Beau, Y. Okuno, K. Akashi, S. Fiering, and D. Tenen. 2004. Acute myeloid leukemia induced by graded reduction of a lineage-specific transcription factor, PU.1. *Nature genetics* 36:624-630.

Ross, M., X. Zhou, G. Song, S. Shurtleff, K. Girtman, W. Williams, H.-C. Liu, R. Mahfouz, S. Raimondi, N. Lenny, A. Patel, and J. Downing. 2003. Classification of pediatric acute lymphoblastic leukemia by gene expression profiling. *Blood* 102:2951-2959.

Sanada, M., and S. Ogawa. 2012. Genome-wide analysis of myelodysplastic syndromes. *Curr Pharm Des* 18:3163-3169.

Sawada, K., N. Sato, A. Notoya, T. Tarumi, S. Hirayama, H. Takano, K. Koizumi, T. Yasukouchi, M. Yamaguchi, and T. Koike. 1995. Proliferation and differentiation of myelodysplastic CD34+ cells: phenotypic subpopulations of marrow CD34+ cells. *Blood* 85:194-202.

Sawada, K., N. Sato, T. Tarumi, N. Sakai, K. Koizumi, S. Sakurama, M. Ieko, T. Yasukouchi, Y. Koyanagawa, and M. Yamaguchi. 1993. Proliferation and differentiation of myelodysplastic CD34+ cells in serum-free medium: response to individual colony-stimulating factors. *British journal of haematology* 83:349-358.

Shih, A.H., O. Abdel-Wahab, J.P. Patel, and R.L. Levine. 2012. The role of mutations in epigenetic regulators in myeloid malignancies. *Nature reviews. Cancer* 12:599-612.

Stadtfeld, M., and T. Graf. 2005. Assessing the role of hematopoietic plasticity for endothelial and hepatocyte development by non-invasive lineage tracing. *Development* 132:203-213.

Steidl, U., F. Rosenbauer, R. Verhaak, X. Gu, A. Ebralidze, H. Otu, S. Klippel, C. Steidl, I. Bruns, D. Costa, K. Wagner, M. Aivado, G. Kobbe, P. Valk, E. Passegué, T. Libermann, R. Delwel, and D. Tenen. 2006. Essential role of Jun family transcription factors in PU.1 knockdown-induced leukemic stem cells. *Nature genetics* 38:1269-1277.

Subramanian, A., P. Tamayo, V. Mootha, S. Mukherjee, B. Ebert, M. Gillette, A. Paulovich, S. Pomeroy, T. Golub, E. Lander, and J. Mesirov. 2005. Gene set enrichment analysis: a knowledge-based approach for interpreting genome-wide expression profiles. *Proceedings of the National Academy of Sciences of the United States of America* 102:15545-15550.

Tanaka, S., S. Miyagi, G. Sashida, T. Chiba, J. Yuan, M. Mochizuki-Kashio, Y. Suzuki, S. Sugano, C. Nakaseko, K. Yokote, H. Koseki, and A. Iwama. 2012. Ezh2 augments leukemogenicity by reinforcing differentiation blockage in acute myeloid leukemia. *Blood* 120:1107-1117.

Tehranchi, R., P. Woll, K. Anderson, N. Buza-Vidas, T. Mizukami, A. Mead, I. Astrand-Grundström, B. Strömbeck, A. Horvat, H. Ferry, R. Dhanda, R. Hast, T. Rydén, P. Vyas, G. Göhring, B. Schlegelberger, B. Johansson, E. Hellström-Lindberg, A. List, L. Nilsson, and S. Jacobsen. 2010. Persistent malignant stem cells in del(5q) myelodysplasia in remission. *The New England journal of medicine* 363:1025-1037.

Thol, F., I. Friesen, F. Damm, H. Yun, E.M. Weissinger, J. Krauter, K. Wagner, A. Chaturvedi, A. Sharma, M. Wichmann, G. Gohring, C. Schumann, G. Bug, O. Ottmann, W.K. Hofmann, B. Schlegelberger, M. Heuser, and A. Ganser. 2011. Prognostic significance of ASXL1 mutations in patients with myelodysplastic syndromes. *J Clin Oncol* 29:2499-2506.

Vangala, R., M. Heiss-Neumann, J. Rangatia, S. Singh, C. Schoch, D. Tenen, W. Hiddemann, and G. Behre. 2003. The myeloid master regulator transcription

factor PU.1 is inactivated by AML1-ETO in t(8;21) myeloid leukemia. *Blood* 101:270-277.

Vannucchi, A.M., T.L. Lasho, P. Guglielmelli, F. Biamonte, A. Pardanani, A. Pereira, C. Finke, J. Score, N. Gangat, C. Mannarelli, R.P. Ketterling, G. Rotunno, R.A. Knudson, M.C. Susini, R.R. Laborde, A. Spolverini, A. Pancrazzi, L. Pieri, R. Manfredini, E. Tagliafico, R. Zini, A. Jones, K. Zoi, A. Reiter, A. Duncombe, D. Pietra, E. Rumi, F. Cervantes, G. Barosi, M. Cazzola, N.C. Cross, and A. Tefferi. 2013. Mutations and prognosis in primary myelofibrosis. *Leukemia*

Will, B., L. Zhou, T. Vogler, S. Ben-Neriah, C. Schinke, R. Tamari, Y. Yu, T. Bhagat, S. Bhattacharyya, L. Barreyro, C. Heuck, Y. Mo, S. Parekh, C. McMahon, A. Pellagatti, J. Boultwood, C. Montagna, L. Silverman, J. Maciejewski, J. Greally, B. Ye, A. List, C. Steidl, U. Steidl, and A. Verma. 2012. Stem and progenitor cells in myelodysplastic syndromes show aberrant stage-specific expansion and harbor genetic and epigenetic alterations. *Blood* 120:2076-2086.
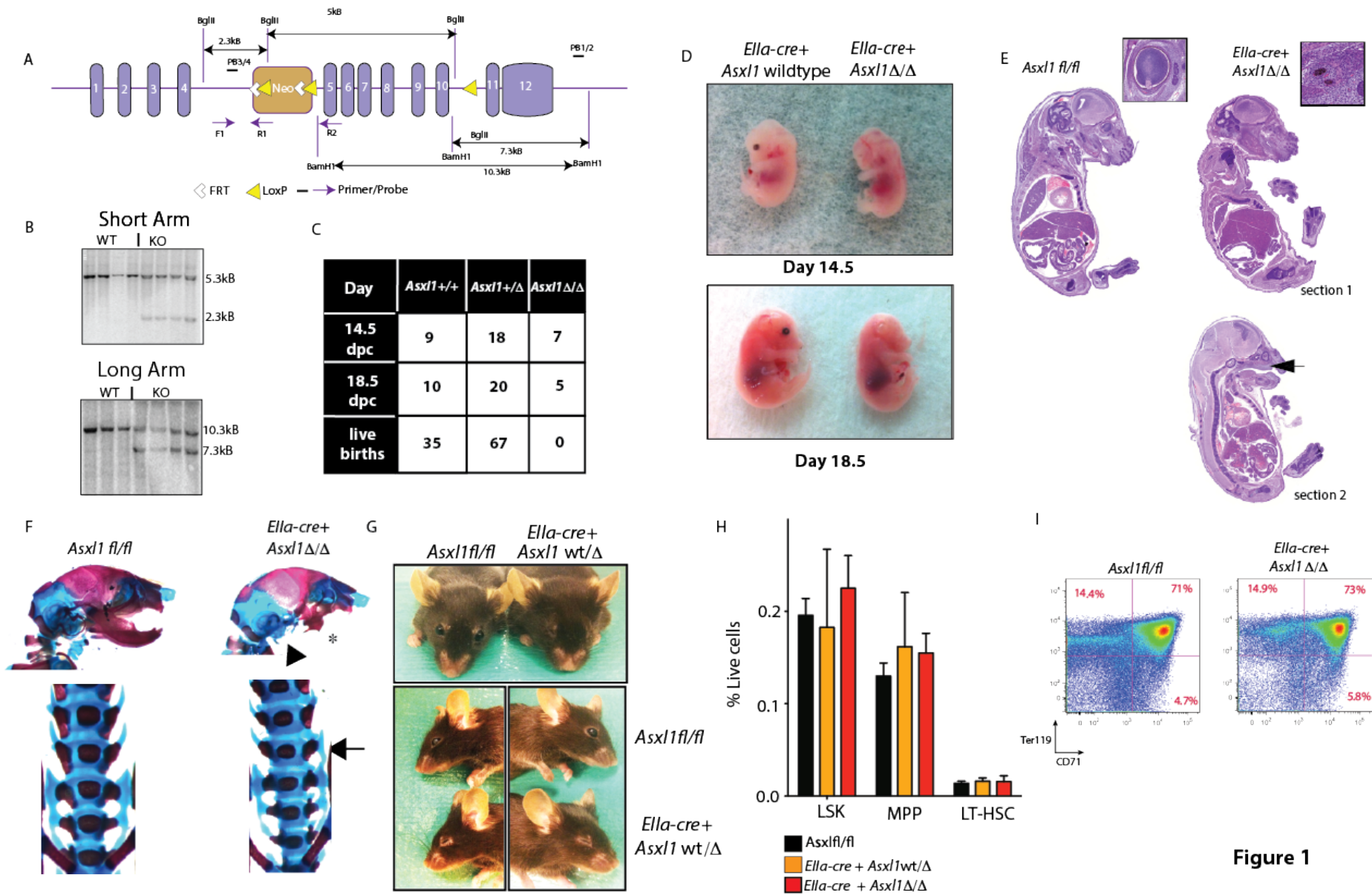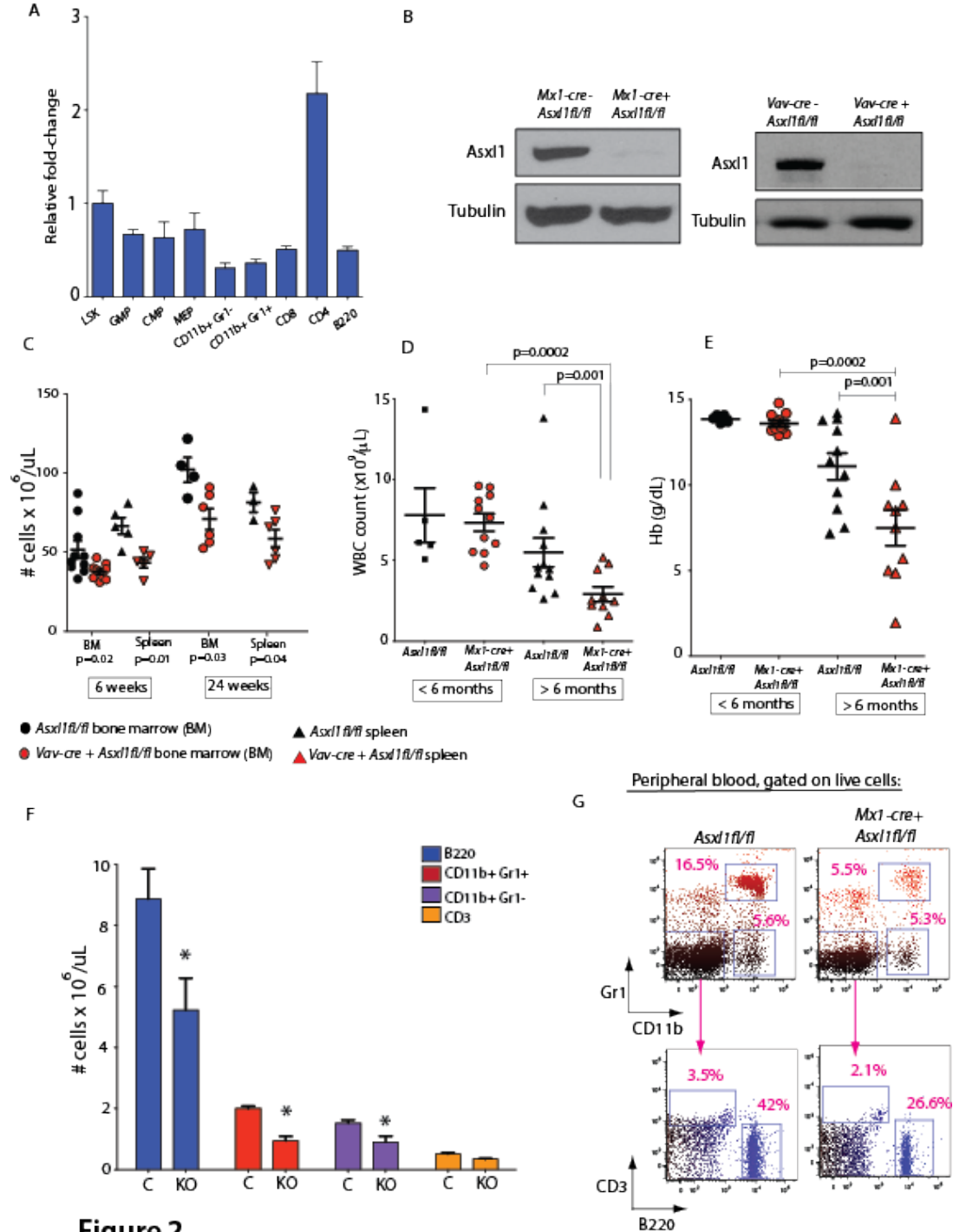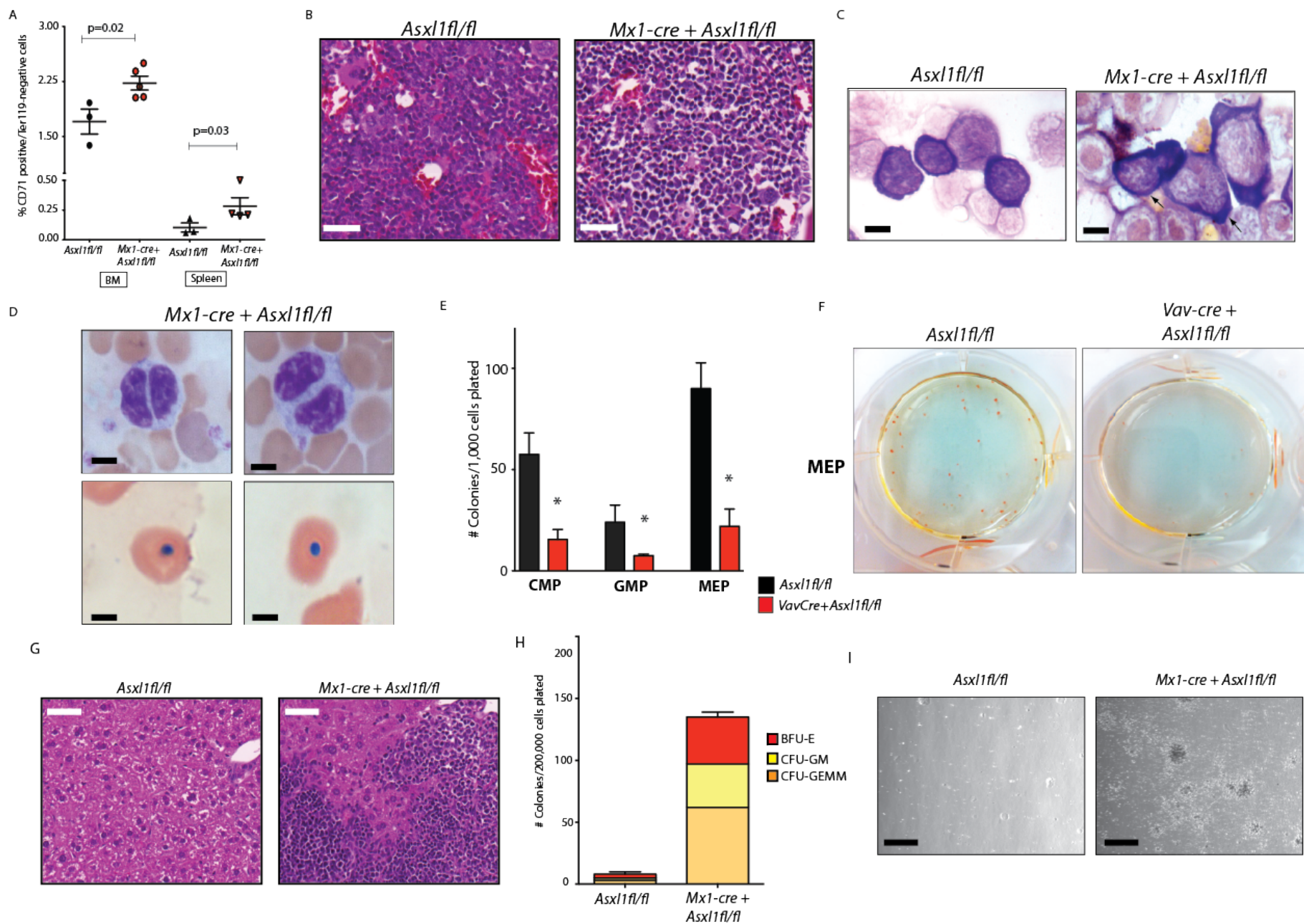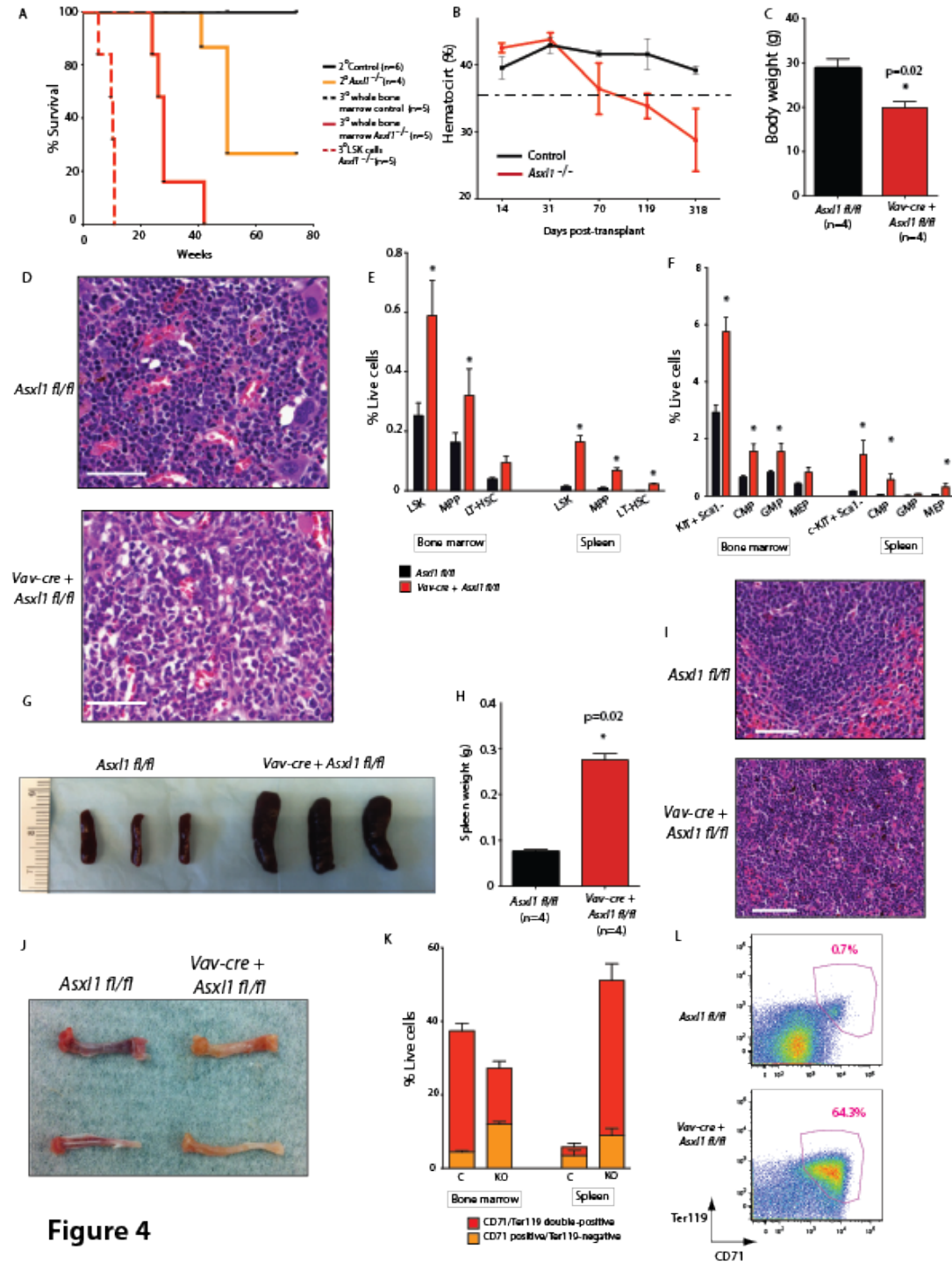
Figure 1

Figure 2

Figure 3

Figure 4

Figure 5

Figure 6

A

% Survival

Mx1-cre Asxl1 wildtype
Tet2 wildtype (n=5)
Mx1-cre Asxl1fl/fl (n=12)
Mx1-cre Tet2fl/fl (n=6)
Mx1-cre Asxl1fl/fl + Tet2fl/fl (n=10)

Weeks

B

WBC Count (x10^9/μL)

C   Asxl1 KO   Tet2 KO   Asxl1/Tet2 DKO

B220+   CD4+   CD11b+Gr1+
CD8+   CD11b+Gr1-

C

Hematocrit (%)

C   Asxl1 KO   Tet2 KO   Asxl1/Tet2 DKO

D

Total BM Cell number (x10^6)

C   Asxl1 KO   Tet2 KO   Asxl1/Tet2 DKO

E

Gated on Live, Lineage-negative cells

Control   Asxl1 KO   Tet2 KO   Asxl1/Tet2 DKO

6.5% 0.37%   7.5% 0.39%   9.3% 0.5%   11.4% 0.65%

Sca-1

c-KIT

F

Total Live Cell Number

C   Asxl1 KO   Tet2 KO   Asxl1/Tet2 DKO   C   Asxl1 KO   Tet2 KO   Asxl1/Tet2 DKO

LSK   Myeloid Progenitor

G

Control   Asxl1 KO

Tet2 KO   Asxl1/Tet2 DKO

H

Control   Asxl1 KO   Tet2 KO   Asxl1/Tet2 DKO

Figure 7

Figure 8

Figure 9